Design of a Domestic High Temperature Proton Exchange Membrane Fuel Cell Cogeneration System: Modelling and Optimisation

MYALELO VUYISA NOMNQA

Thesis submitted in fulfilment of the requirements for the degree

Doctor of Engineering: Chemical Engineering

in the Faculty of Engineering

at the Cape Peninsula University of Technology

Supervisor: Prof. Daniel Ikhu-Omoregbe

Co-Supervisor Mr. Ademola Rabiu

Cape Town

November 2017

Declaration

I, **Myalelo Vuyisa Nomnqa**, declare that the contents of this thesis represent my own unaided work and that the thesis has not previously been submitted for academic examination towards any qualification. Furthermore, it represents my own opinions and not necessarily those of the Cape Peninsula University of Technology.

Myalelo Vuyisa Nomnqa

November 2017

Abstract

Fuel cells are among power generation technologies that have been proven to reduce greenhouse gas emissions. They have the potential of being one of the most widely used technologies of the 21st century, replacing conventional technologies such as gas turbines in stationary power supplies, internal combustion engines in transport applications and the lithium-ion battery in portable power applications. This research project concentrates on the performance analysis of a micro-cogeneration system based on a high temperature-proton exchange membrane (HT-PEM) fuel cell through modelling and parametric analysis.

A model of a $1\,kW_e$ micro-cogeneration system that consists of a HT-PEM fuel cell, a methane steam reformer (MSR) reactor, a water-gas-shift (WGS) reactor, heat exchangers and an inverter was developed. The model is coded/implemented in gPROMS Model Builder, an equation oriented modelling platform. The models predictions for the HT-PEM fuel cell, MSR and WGS, and the whole system were validated against experimental and numerical results from literature. The validation showed that the HT-PEM fuel cell model was able to predict the performance of a $1\,kW_e$ fuel cell stack with an error of less than 6.4%.

The system model is firstly used in a thermodynamic analysis of the fuel processor for a methane steam reforming process and investigated in terms of carbon monoxide produced. The combustor fuel and equivalence ratios were shown to be critical decision variables to be considered in order to keep the carbon monoxide from the fuel processor at acceptable levels for the fuel cell stack.

For fuel cell systems to compete with or replace combustion-based systems, they should

offer the performance that can either better or match the system they replace. In the second part of this study, the micro-cogeneration system model is used in a parametric study with four decision variables (equivalence ratio, fuel flow rate, current density and fuel utilisation) to search the design space for a set of solutions that describe the system ability to reach performance targets for system's in the 1-5 kW_e range. The analysis revealed a set of possible solutions that present the optimal performance of the system (electrical efficiency of 42.7%, thermal efficiency of 47.2% and cogeneration efficiency of 90%) to be flow rate of $0.133\,kg\,h^{-1}$, a voltage of $0.54\,V$, fuel utilisation of 76%, combustion temperature of $960\,K$ and steam-to-carbon ratio of 3.5.

In the last section of this work, the system model is used in a case study to conduct an appraisal for the technical, environmental and economic viability of a system in a South African domestic-energy environment. Three operating strategies (continuous, day-night segmented and with restricted running time modes) were used to examine the system's performance. The results showed that using the fuel cell cogeneration system greatly reduces the carbon dioxide (CO_2) emission with the restricted running mode leading to a 62.4% reduction of the CO_2 emission compared to 59.7 % for the day-night segmented mode and 53.9% for the continuous mode. The economic analysis revealed that the system can be operated economically using any of the operating strategies. A payback period, based on net present value, was 8.4 years for continuous mode while for the day-night segmented and restricted running mode, it was 9.7 and 11.1 years, respectively.

Keywords: *HT-PEM, Fuel cell system, Micro-cogeneration system, Mathematical model, High temperature PEM fuel cell, Parametric analysis, Modelling and simulation, HT-PEMFC, Operating strategies, Combined-heat-and-power, CHP*

Acknowledgements

This Doctor of Engineering project was carried out between May 2012 and November 2016 at the Chemical Engineering department, Cape Peninsula University of Technology (CPUT).

Myalelo Vuyisa Nomnqa,
Cape Town, May 2017

Research Outputs

Research articles

1. **Myalelo Nomnqa**, Daniel Ikhu-Omoregbe, & Ademola Rabiu. 2016. Parametric Analysis of a High Temperature PEM Fuel Cell-Based Micro-Cogeneration System. *International Journal of Chemical Engineering*, vol. 2016, Article ID 4596251, 14 pages, 2016.

2. **Myalelo Nomnqa**, Daniel Ikhu-Omoregbe, & Ademola Rabiu. 2017. Performance evaluation of a HT-PEM fuel cell micro-cogeneration system for domestic application. *Energy Systems*.

Conference outputs

1. **M.V. Nomnqa**, D. Ikhu-Omoregbe & A. Rabiu. Effects of fuel processor combustion parameters on the performance of a 1kWel HT-PEM fuel cell-based CHP system. 5th International Conference of Fuel Cell and Hydrogen Technology (ICFCHT) 2015 . Kuala Lumpur, Malaysia, 1-3 September 2015. Paper no: AO 14.

2. **Myalelo Nomnqa**, Daniel Ikhu-Omoregbe & Ademola Rabiu. Model-based Analysis of a High Temperature Proton Exchange Membrane Fuel Cell Micro-Cogeneration System. 4th International Conference on Renewable Energy Research and Applications (ICRERA).Palermo, Italy. 22-25November 2015. Paper No: 256.

3. **Myalelo Nomnqa**, Ademola Rabiu, Daniel Ikhu-Omoregbe & Yusuf Isa. Modelling the Performance of a HT-PEMFC Stack under Different Operating Conditions. 20th

World Hydrogen Energy Conference (WHEC) 2014. 15-20 June Gwangju, Korea. Poster.

Other publications during candidacy that are not part of this thesis

1. Bujlo P, Pasupathi S, Ulleberg Ø, Scholta J, **Nomnqa MV**, Rabiu A & Pollet BG. 2013. Validation of an externally oil-cooled 1 kWel HT-PEMFC stack operating at various experimental conditions. *International Journal of Hydrogen Energy.*38(23): 9847-9855.

Contents

List of Tables

List of Figures

Nomenclature

Nomenclature

C^{Pt} Concentration on the catalyst surface   (mol m^{-3})

C^{ref} Reference concentration on the catalyst surface   (mol m^{-3})

$C_{dissolved}$ Equilibrium concentration   (mol m^{-3})

D_{ij}^{eff} Effective Binary diffusion coefficient   (m^2 s^{-1})

$D_{i,k}^{\mathrm{H_3PO_4}}$ Diffusion coefficient of hydrogen/oxygen in phosphoric acid   (m^2 s^{-1})

D_{ij} Binary diffusion coefficient   (m^2 s^{-1})

Ea Activation energy   (kJ mol^{-1})

F Faraday constant   (C mol^{-1})

LHV Lower heating value   (kJ kg^{-1})

M Molecular mass   (kg kmol^{-1})

N Molar flux   (kmol m^3)

P_{elec} Electrical power   (W)

Q_{th} Thermal power   (W)

R Gas constant   (8.314 J kmol^{-1} K^{-1})

S_{pt} Real platinum surface area   (m^2)

T Temperature   (K)

T_{ref} Reference temperature   (K)

V_{cell} Cell voltage   (V)

V_{ocv} Open circuit voltage   (V)

W Acid doping level   ($-$)

$\dot{m}$ Mass flow rate   (kmol h^{-1})

a Catalyst surface area   (m^2)

c Concentration   (mol m^{-3})

i_o Exchange current density   (A m^{-3})

i_o^{ref} Reference exchange current density (A m^{-3})

j current density (A m^{-2})

n No of electrons transferred $(-)$

p Pressure (Pa)

r Reaction rate $(\text{kmol kg}_{\text{cat}}^{-1})$

v Velocity (m s^{-1})

y Mole fraction $(-)$

Greek Symbols

α Transfer coefficient $(-)$

η_{act} Activation loss (V)

η_{cogen} Cogeneration efficiency $(\%)$

η_{elec} Electrical efficiency $(\%)$

η_{ohm} Ohmic loss (V)

η_{th} Thermal efficiency $(\%)$

γ Reaction order $(-)$

κ Proton conductivity (S m^{-1})

θ_{CO} Catalyst site coverage by carbon monoxide $(-)$

ε Porosity $(-)$

Abbriviations

AC	Alternating Current.
ATR	Autothermal Reforming.
BFDM	Backward Finite Difference Method.
BoP	Balance-of-Plant.
BP	Bipolar Plates.
CFD	Computational Fluid Dynamics.
CHP	Combined Heat and Power.
CL	Catalyst Layer.
DC	Direct Current.
DoE	Department of Energy.
DST	Department of Science and Technology.
EER	Emission Reduction Ratio.
EIS	Electrochemical Impedance Spectroscopy.
EQR	Equivalence Ratio.
FCCS	Fuel Cell Cogeneration System.
FEM	Finite Element Method.
FR	Fuel Ratio.
GDL	Gas Diffusion Layer.
GDP	Gross Domestic Product.
HEN	Heat Exchanger Network.
HFCT	Hydrogen and Fuel Cell Technology.
HT	High Temperature.
HT-PEMFC	High-Temperature Polymer Exchange Membrane Fuel Cell.
HySA	Hydrogen South Africa.
ICE	Internal Combustion Engine.
IPPFO	Ideal Physical Properties Foreign Object.
LHV	Low Heating Value.

LT	Low Temperature.
LT-PEMFC	Low-Temperature Polymer Exchange Membrane Fuel Cell.
MEA	Membrane Electrode Assembly.
MSR	Methane Steam Reformer.
MWh	Mega Watt Hour.
NOx	Oxides of Nitrogen.
NPV	Net Present Value.
NTU	Number of Transfer Units.
OCV	Open Circuit Voltage.
PBI	Polybenzimidazole.
PEM	Polymer Exchange Membrane.
PGM	Platinum Group Metals.
POX	Partial Oxidation.
PSE	Process System Enterprise.
Pt	Platinum.
RH	Relative Humidity.
SA	South Africa.
SCWG	Supercritical Water Gasification.
SE	Stirling Engine.
SOEC	Solid Oxide Electrolysis Cells.
SOFC	Solid Oxide Fuel Cells.
SOx	Sulphur Compounds.
SR	Steam Reforming.
US	United States.
VOCs	Volatile Organic Compounds.
WGS	Water Gas Shift.

Chapter 1

Introduction

1.1 Background

Nowadays, there are various signs which indicate that the continued use of fossil fuels and our lifestyle, with respect to energy utilisation and production, need to change. Excessive burning of fossil fuels such as oil, gas and coal over the last century has not gone by without noticeable effects. The problems are fuelled by the rapid increase in the demand of energy caused by an increase of the world's population. Inefficient use of fossil fuels as a primary energy vector is causing a serious environmental impact, changing our global climate and causing extreme weather phenomena to be more frequent and severe. Examples of change in global climate effects include shifting weather patterns that result in unpredictable rain patterns threatening food production, contamination of coastal freshwater reserves and flooding caused by rising sea levels.

Another change is an increase in pets and diseases that were limited to the tropical regions towards the poles as a result of the warming of the atmosphere (UNEP (United Nations Environmental Programme), 2012). Dara (2012) estimates that the current carbon-intensive economy and climate change are linked to about 4.9 million deaths worldwide with a loss of about 1.6% ($1.2 trillion) of the world's gross domestic product (GDP). Dara (2012) also states that deaths resulting from toxic air pollution, hunger and communicable diseases and about 90% of these deaths are recorded in developing countries.

These figures are expected to rise to 6 million deaths by 2030 if no action is taken to mitigate climate change.

Globally, there are various efforts under way to mitigate the effects of climate change in sectors like agriculture, energy, manufacturing, transport, construction and waste. These include, but not limited to, improving the efficiency of old equipment, changing consumer behaviour, promoting the use of renewable energy and new technologies, greener construction methods, recycling waste so on. In the energy sector, particular attention is being devoted to shifting away from fossil fuel to renewable/sustainable and low-carbon energy options. Hydrogen has been noted as a future alternative that can deliver energy in the sector which is of a high-quality and is clean.

The concept of hydrogen economy can be explained as a long-term effort to change the current energy system that is based on the burning of fossil fuel, to one which uses the energy of hydrogen in high-efficiency conversion technology such as fuel cells. Hydrogen is the most abundant element known, although it is not an energy source in itself, but rather an energy carrier that is bound up in many compounds such as water, natural gas, oil, coal and biomass (Blanchette, 2008). It is produced commercially by dozens of processes. One widely and least expensive process is steam reforming, in which hydrocarbon reacts with water to yield hydrogen. This process emits significant amounts of carbon dioxide (CO_2) into the atmosphere. However, when combined with carbon capture and sequestration technologies designed to reduce CO_2 emissions, it can produce ample fuel that can help curb global climate change (Marbán & Valdés-Solís, 2007). There are also other lesser carbon dioxide-emitting processes for producing hydrogen such as electrolysis and renewable energy sources (wind, solar and geothermal).

This research project focuses on the mitigation efforts in the domestic energy sector. Centralised power generation in utility plants and distribution to homes have been criticised due to the inefficient design. These plants lose some 50-70% of their energy as waste heat is released into the atmosphere as can be seen in power-plants cooling towers. A decentralised power-generation system, close to the consumption site - a household in this case - provides advantages over traditional centralised power plants. A decentralised power-generation system offers an opportunity to utilise the waste heat for the heating

household in a concept known as Cogeneration or Combined-Heat-and-Power. Moreover, decentralised power generation eliminates transmission losses associated with the delivery of power to the consumer from the utility plant.

Cogeneration is a widely-used concept in industry, to increase efficiency and reduce operational costs. It has also found application in small-scale power production for households where it is referred to as micro-cogeneration. Traditionally, micro-cogeneration systems are based on fuel combustion engines, which are known for being inefficient and polluting. Fuel cells are emerging as alternative replacements for these combustion-based technologies. Cogeneration systems based on fuel cells offer high efficiency, low emission and a decentralised power and heat supply for buildings and industries. These systems also offers reliability and availability and a significantly long-term reduction in the cost of energy and an overall increase in system efficiency because of the effective use of heat at the point of use (Larminie & Dicks, 2003; Barbir, 2012; Ren & Gao, 2010).

The purpose of this work is to investigate the feasibility of fuel cell micro-cogeneration systems for domestic application. Although some pre-commercial projects have demonstrated the practical feasibility of these systems, there are still some challenges related to part-load operation, optimal operating strategies and optimal design with respect to energy output, capital and operational costs. It is expected that fuel cell micro-cogeneration systems will reach full-scale commercialisation in the near future. For this to happen, the challenges mentioned above need to be addressed. Modelling, if properly formulated, provides a means of accelerated testing and design as compared to practical testing. In that regard, the current work will help analyse and understand the nature of these systems and recommend optimal process parameters and optimal design.

There is particular interest in South Africa (SA) in the Hydrogen and Fuel Cell Technology (HFCT) value chain. This is because of the Platinum Group Metals-based (PGM) catalyst used in fuel cell components, of which 75% known global PGM reserves are found in South Africa with an estimated value of R50 000 billion. This places South Africa in a strategic position to have greater participation in the fuel cell value chain. In this regard, the South African government established the Hydrogen South Africa (*HySA*) strategy under the Department of Science and Technology (DST). This is a 15-year research and development

strategy to develop, prototype and commercialise technologies and products, with the aim of achieving a 25% share of the global hydrogen and fuel cell market.

1.2 Research statement

South African's small-scale renewable and sustainable energy has been entirely focused on photovoltaic systems with no research that focuses on the application/use of a fuel cell system in the domestic built-environment. This project aims to evaluate prospects of utilising a grid-connected high temperature polymer membrane fuel cell-based (HT-PEMFC) micro-cogeneration system in a South African single family household in terms of a technical feasibility study.

1.3 Aims and objectives

The aim of this research work is to develop modelling tools for the design and evaluation of a HT-PEMFC-based micro-cogeneration system that is suited for residential application.

The specific objectives were to:-

- Develop a new system model in gPROMS ModelBuilder.

- Validate the system's subcomponents and integrated system models using previously reported experimental and numerical results.

- Analyse the characteristics of the systems subcomponents, using sensitivity analysis and parametric study.

- Evaluate the systems optimal operating condition, using a parameter shifting technique.

- Conduct a technical, environmental and economic appraisal of operating the system in a South African household.

1.4 Delineation

This study was only limited to the steady-state operation and did not include start-up and transient characteristics of the system. The models developed did not account for degradation of performance of the systems components. Validation of the fuel processor and system models has been limited to the data of the literature. All aspects of hydrogen safety have not been considered when evaluating the system's technical performance. Numerical optimisation of parameters was not considered.

1.5 Report layout

To provide the necessary background, Chapter 2 gives a comparative analysis of micro-cogeneration systems. Particular attention is focused on the operation, durability/life-time, heat-to-power ratio, emissions and performance. Then a summary of commercially available systems for each prime-mover is provided. The remainder of this chapter focuses on a PEM fuel cell-based micro-cogeneration system. The components of a system are discussed, including the fuel cell stack's operating characteristics, hydrogen production technology, thermal management and power conditioning.

Chapter 3 is a literature review chapter. It focuses on the modelling of the HT-PEM fuel cell, from single cell to system-level analysis. This chapter starts by providing the modelling basics and governing principles. This is followed by an in-depth review of literature on modelling single cells categorised by the spatial distributions within the cell. After that, a review of stack-level modelling is provided. Finally, system-level application of modelling is provided.

The remainder of this thesis focuses on the modelling application of a HT-PEM fuel cell micro-cogeneration system. In Chapter 4, a mathematical model of the system, including a fuel cell stack, fuel processor and balance-of-plant (BoP) components, is presented. The model is used to evaluate the system's performance when the fuel processor parameters are decision-variables. Chapter 5 utilises the model developed in Chapter 4 to evaluate the micro-cogeneration system viability against the technical targets set by the United

States (US) Department of Energy (DoE) for 2015.

Chapter 6 provides a case study for the application of the micro-cogeneration system in a South African domestic-energy environment. Different operating modes and power outputs are used to appraise the technical, environmental and economic viability of the system. Chapter 7 concludes the work by providing a summary of the conclusions drawn from the thesis. Recommendations for future work are also given in the chapter.

Chapter 2

Background

2.1 Cogeneration

Cogeneration is an old and well-established concept that dates back to the 1800s (Pehnt *et al.*, 2006). Today it has been employed on a large scale, mainly for applications in industry ,large commercial and institutional buildings (Kerr, 2008; Ghadimi *et al.*, 2014). Industrial applications with continuous processing and high-steam requirements have been very economical for cogeneration and account for the large share of cogeneration that is operational today (Darrow *et al.*, 2014). Cogeneration has also been employed in commercial buildings with a large hot water demand such as hospitals (Boukhanouf, 2011; Smith *et al.*, 2013), hotels and laundries (Szklo *et al.*, 2004). Institutional buildings such as universities, prisons, schools and residential buildings have also seen large-scale use of cogeneration (Boukhanouf, 2011).

Cogeneration is the simultaneous generation and utilisation of heat and power from a single fuel or energy source. It can be classified as a distributed energy resource that is strategically located at or near the point of energy use (on-site). Instead of purchasing electricity from the centralised power-generation utilities and burning fuel in an on-site boiler for thermal energy, cogeneration provides the user, industrial, commercial or domestic, with both energy requirements in a single energy-efficient step (Veerapen & Beerepoot, 2011).

In addition to this, power losses from transmission and distribution (T&D) networks are avoided (Pehnt *et al.*, 2006). This allows for greater improvement in overall fuel efficiency resulting in lower costs and CO_2 emissions. Since cogeneration systems are designed to meet the thermal demand of the energy user, they can be seen primarily as a source of energy and the electricity produced as a by-product. Four basic elements make up a cogeneration plant: a prime mover, an electricity generator, a heat recovery system and a control system (Darrow *et al.*, 2014). Cogeneration power plants can use different technologies and their sizes are in the range of 1 kW_e to over 500 kW_e.

2.2 Micro-cogeneration technologies

Micro-cogeneration can be defined as the combined production of electrical and thermal energy from a single primary energy source based on small conversion units below 10 kW_e (Shaneb *et al.*, 2011; Lee *et al.*, 2013; Maghanki *et al.*, 2013). The heat produced is used for space and water-heating inside the building (Blanchette, 2008; Ren & Gao, 2010) and, depending on the demand, the electricity produced is used within the building or fed into the public grid. Micro-cogeneration systems typically have (or are expected to have) a lifetime of ten to twenty years (Pehnt *et al.*, 2006). They are designed to achieve more than 75% overall efficiency. The efficiency gain from cogeneration varies, depending upon technologies and fuel/energy source(s) used and the heat and power generation system displaced. Although micro-cogeneration systems can operate as stand-alone units, they however need to be connected to the grid (Chamra & Mago, 2007). Grid connection is essential as the potential exists to import and export electricity when there is a low and high demand, respectively. A stand-alone operation could also result in large amounts of heat being vented into the atmosphere, due to the continuous electric-led operation(Arsalis *et al.*, 2012*b*).

A micro-cogeneration system can be categorised, based on the fuel conversion process, as the fuel-air combustion and direct electrochemical conversion (Pehnt *et al.*, 2006). In the combustion-based systems, a fuel-air mixture is combusted in a chamber producing heat and mechanical energy. The heat from the combustion is recovered for heating purposes and the mechanical energy is used to produce electricity. Two thermodynamic cycles

are used in the combustion-based systems, including the Sterling cycle (Sterling engine) and the Otto cycle (internal combustion engine). The alternative to the combustion process is electrochemical conversion of the fuel (chemical energy) to electricity (electrical energy). There are two types of electrochemical conversion technologies used for micro-cogeneration systems: the polymer electrolyte membrane fuel cell and the solid oxide fuel cell.The characteristics of the different micro-cogeneration systems are found in Table 2.1.

Table 2.1: Fuel cell cogeneration products (adapted from Elmer *et al.*, 2015)

	Internal Combustion engine	Sterling engine	Fuel cell
Power capacity (kWe)	1-10	1-9	0.7-5
Electrical efficiency (%)	15 -25	20	PEMFC 30-46 SOFC 40-60
Cogeneration efficiency (%)	90	95	95
Heat to power ratio	3	8	PEMFC - 2 SOFC 0.5 - 1
Fuel	Gas, biogas, liquid fuels	Gas, Biogas, Butane	Hydrocarbons
Noise	Loud	Fair	Quite
Durability	-	-	-
Part load ability	No	Yes	PEMFC Yes SOFC No
Maturity	High	Fair	Low

2.2.1   Internal combustion engines

The internal combustion (IC) engine technology is well established and mature having been in use and continuously developed for more than a century. Internal combustion engines are used in widespread of applications, including stationary power generation, transport and combined-heat-and-power systems. This is because they offer excellent fuel-conversion efficiencies, high power-to-weight ratios, good dynamic characteristics during varying load demands and are suitable for scaling down to small sizes (Mikalsen, 2011). Spark ignition (Otto-cycle) engines, similar to those used in vehicles, are used in cogeneration systems. In an internal combustion engine, a mixture of fuel, such as natural gas and air, are compressed in a cylinder. A spark plug is used to ignite this mixture. Upon

ignition, this gas expands and moves the piston, thus causing the crankshaft to rotate. The mechanical energy produced by this combustion is then used to drive a generator. The exhaust heat, as well as the heat from the lubricating air cooler and the jacket water cooler of the engine, are recovered using heat exchangers and then supplied to the heating system. The ICE heat recovery system can produce up to 160 °C hot water or 20 bar steam output (Frangopoulos & Nakos, 2006; Onovwiona & Ugursal, 2006). The typical system components of an ICE-based cogeneration system are shown in Figure 2.1 . The electrical and overall efficiencies reported for internal combustion engine-based cogeneration systems are in the range of 20-30% and 85-90%, respectively. Whilst the former varies with size, the latter is not affected by the size of the system (Veerapen & Beerepoot, 2011).
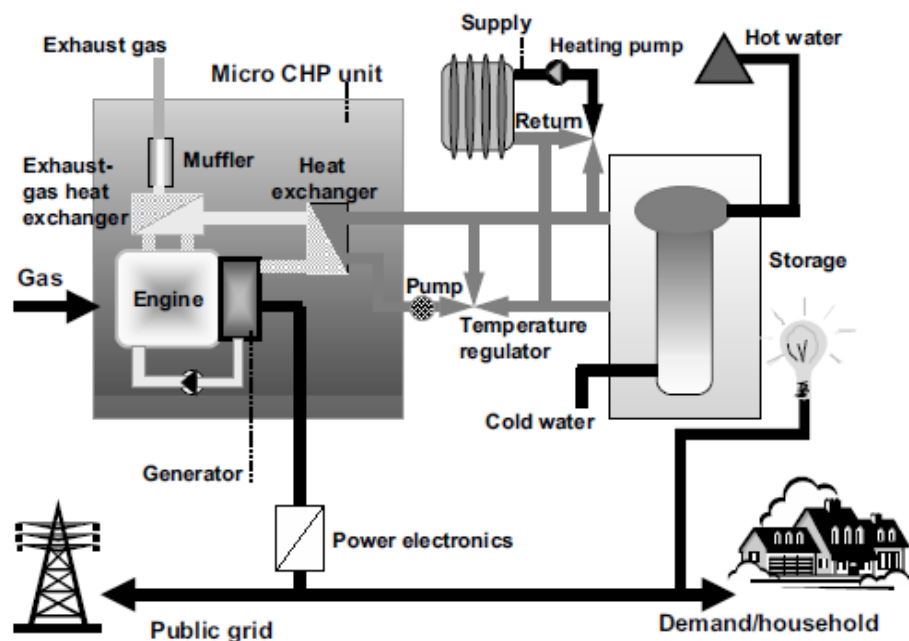
Figure 2.1: Schematic diagram of internal combustion engine cogeneration system (adapted from Pehnt *et al.*, 2006).

The primary emissions from internal combustion engines are carbon monoxide (CO), oxides of nitrogen (NOx) and volatile organic compounds (VOCs-unburned, non-methane hydrocarbons). Other pollutants, like sulphur compounds (SOx), are largely dependent on the type of fossil fuel (sulphur content) used. They are produced by burning fossil fuels in the presence of oxygen. NOx production is dependent on temperature, pressure, combustion chamber geometry and the air-fuel mixture of the engine (Mikalsen, 2011). To reduce the NOx emission levels, stoichiometric engines fitted with three-way catalytic converters are used.

2.2.2 Stirling engines

The Stirling engine (SE) is a type of combustion engine in which the combustion occurs in an external chamber using a Stirling thermodynamic cycle. The combustion process, which is the energy input to the engine, is separated from the working fluid. The heat supply in SE is from an external source. This allows the use of a wide range of energy source such as oil/gas (fossil fuels), biomass and solar (renewable) (Harrison & On, 2011). Cogeneration-based on Stirling systems with electrical power sizes ranging from 1 kW_e to 9 kW_e, are available on the market (Maghanki *et al.*, 2013). Figure 2.2 illustrates the basic components of a natural gas fuelled SE system. The major disadvantage of Stirling systems is their low electrical efficiency, which is in the range of 15-25% when fuelled with natural gas and as low as 15% when a solid fuel like biomass is used (Onovwiona & Ugursal, 2006; Conroy *et al.,* 2013). Overall efficiency higher than 80% has been reported and is expected to be higher than 95% in the near future (Veerapen & Beerepoot, 2011).
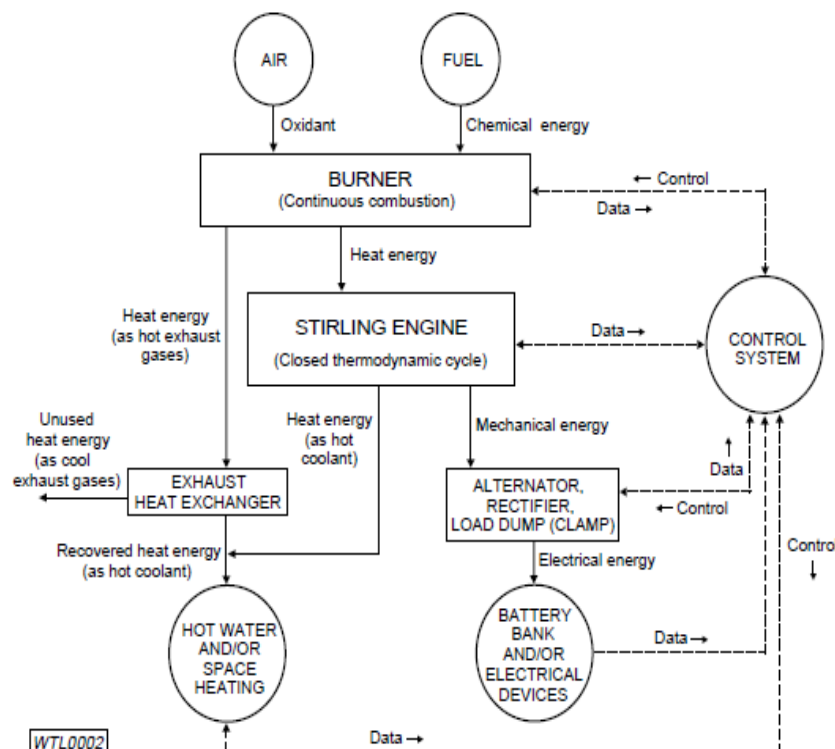
Figure 2.2: Schematic diagram of a Stirling engine cogeneration system (adapted from Harrison & On, 2011).

Compared to the IC engine systems, the SE systems have emissions (NOx) that are 10 times lower and exhibit good part-load performance characteristics (Kuhn *et al.*, 2008).

In addition, the degradation of component is minimized because the external combustion closed-cycle operational nature of SE restricts the exposure of the moving parts of the engine to the products of combustion. There are different heat-recovery sources in the SE-based micro cogeneration system and they mostly depend on the type of fuel used (Harrison & On, 2011). For instance, in a natural gas fuelled system, the sources of heat for heat recovery are the gas cooler, exhaust gas heat exchanger and, to a lesser extent, the cylinder walls and the lubricating oil (Harrison & On, 2011).

2.2.3 Fuel cells

Fuel cells are electrochemical devices that convert the chemical energy of a fuel directly into the direct current (DC) electricity and heat without combustion. A simplistic view of a fuel cell is a cross between a heat engine (chemical-to-heat generator) and a battery (chemical-to-electrical generator) (Hawkes *et al.*, 2009a). Typical components of a fuel cell micro-cogeneration system are shown in Figure 2.3. In the centre is the fuel cell stack, a set of individual cells stacked together to provide greater power.
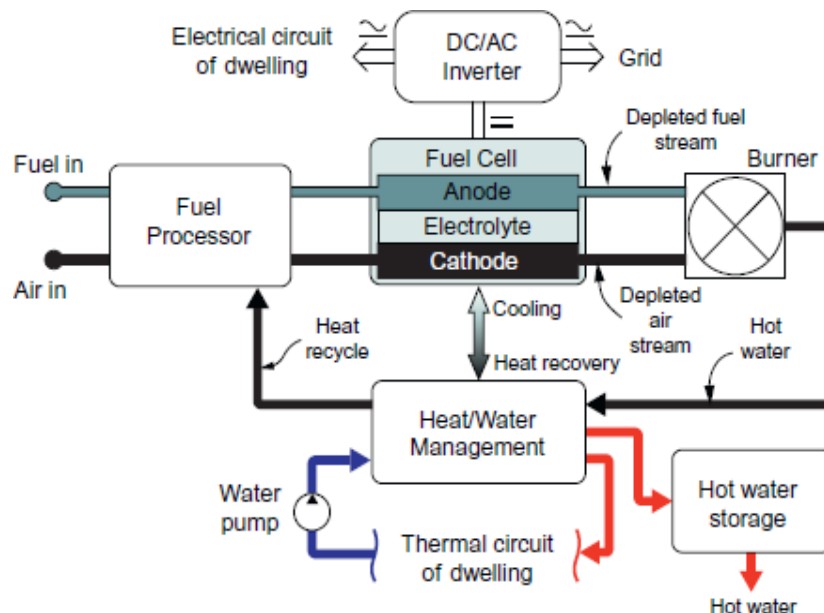
Figure 2.3: A schematic diagram of a fuel cell-based cogeneration system (adapted from Breeze, 2014).

The stack provides the main conversion of fuel into electricity and must be surrounded with several ancillary systems to form a complete cogeneration system. These are:

- A fuel processor to convert natural gas or other fuels into hydrogen;

- Heat recovery systems to produce hot water;

- An inverter and power conditioner to provide grid-synchronised AC;

- A backup gas boiler to meet peak heat demand;

- Control and safety systems.

There are many different types of fuel cell stacks that are being researched and developed. However, the solid oxide fuel cell and the polymer electrolyte membrane fuel cell are the most suitable for use in a micro-cogeneration system. Its products and prototypes have been deployed in large-scale field trials in Japan, Germany and South Korea (Ren & Gao, 2010; Staffell, 2015). Characteristics of the two fuel cell-based systems are compared in Table 2.2.

Table 2.2: Comparison between PEM fuel cell and SOFC system (adapted from Elmer *et al.*, 2015)

	SOFC	PEMFC
Operating Temp (°C)	500-1000	LT PEM - 30 to 100 HT-PEM - 120 to 200
Electrical efficiency (%)	40 - 60	30 - 46
Electrolyte	Stabilised zirconia ceramic matrix	Polymer membrane
Fuel	Natural gas or propane	H_2, hydrocarbon, reformate
Contaminants	Sulphur	Carbon monoxide
Advantages	High temperature enables internal reforming; no liquid electrolyte used; useful high temperature heat output can be used in another cycle	Quick start up time; can vary output quickly; compact; no corrosive fluid used
Disadvantages	long start up time; expensive heat resistant materials needed	expensive platinum catalysts required; limited level of CO allowed in reformate fuel

Since fuel cells systems do not involve combustion fuels in the generation of electricity, emissions from these systems are minimal. The emissions are primarily from the fuel-processing subsystem. The anode-off gas which, depending on the fuel, contains hydrogen, carbon monoxide and VOCs, is oxidised in a catalytic burner to provide the heat required

for the reforming reactor. Pollutants, such as oxides of sulphur, are normally eliminated from the system prior to the reforming step.

2.2.3.1   Polymer electrolyte membrane fuel cells

Of all types of fuel cells, polymer electrolyte membrane (PEM) fuel cells are the most popular and most widely researched and developed. The fuel used in a PEM fuel cell can either be directly fed into the fuel cell, or sent to a reformer to produce pure hydrogen, which is then fed to the fuel cell. PEM fuel cell systems are available from a few kilowatts up to 250 kilowatts (Larminie & Dicks, 2003).

There are two types of PEM fuel cells: the low-temperature (LT) and high-temperature (HT) PEM fuel cells. The low-temperature PEM operates between 30-80 °C and the high-temperature PEM operates between 120-200 °C. The main difference in the components of the two types of fuel cells is the electrolyte used. The low-temperature PEMFC uses a perfluorinated sulfonic acid membrane and the high-temperature PEM uses acid-doped polybenzimidazole (PBI) membranes as the electrolyte. PEM fuel cells were primarily used for automotive applications, but are now strong candidates for small-scale distributed stationary power generation and portable power applications (Crawley, 2006).

2.2.3.2   Solid oxide fuel cells

Solid Oxide fuel cells (SOFC) are made entirely of solid materials and are simpler in design than other fuel cell technologies. They are classified as high-temperature fuel cells operating at between 600-1000 °C. The high-temperature operation means that there is no requirement of precious metal catalysis and allows for a variety of hydrocarbon fuels to be used. Operating at high temperatures also supplies the heat required for fuel reforming, thus eliminating the need for an external reformer to produce H_2.

The two main configurations of SOFCs are tubular and planar (flat). Planner designs are similar to other fuel cell designs. The reactants flow through channels in the cathode and anode. In tubular designs the inside of the tube is the cathode where air is supplied

and the other components are built around the tube (Andújar & Segura, 2009). During operation, air enters the cathode, undergoes electrode reaction and oxygen ions migrate through the electrolyte to the anode where hydrogen oxidation occurs. SOFCs are more tolerant to impurities in fuel and can operate with CO and H_2 directly in the anode (Adam *et al.*, 2013).Unconventional fuels such as biomass and coal-derived syngas may also be used. SOFC cogeneration systems offer efficiencies of up to 80% (Crawley, 2007).

2.2.4 Heat-to-power-ratio

The heat-to-power ratio of a micro-generation system plays an important role in deciding which type of system is to be used, as it affects the overall system efficiency, costs and carbon savings (Liso *et al.*, 2011). The electrical power output is the key factor in terms of the overall CO_2 and cost savings. An increase in the electrical power output of the system results in increased carbon savings for a given energy input. The internal combustion engine and the Stirling engine systems typically have higher heat-to-power ratios in the range of 3:1 to 2:1 and 4:1 respectively (Guy & Sykes, 2007). As a result, they are designed to meet the full household heat demand using a heat-led operating strategy. Fuel cell-based systems, on the other hand, have relatively low heat-to-power ratios (0.6 - 2:1) (Ang *et al.*, 2010). The lower heat-to-power ratio allows for an electrically-led operating mode that meets the electrical demand with the heat providing a small part of the overall heat demand (Guy & Sykes, 2007). A supplementary boiler is usually installed so as to meet the remainder of the heat demand. This type of operation is economically beneficial when there is a low demand of heat, such as in the summer season (Hawkes *et al.*, 2009b).

2.2.5 Durability/ Lifetime

The requirement for a long life-time relates to the very long operating periods required of stationary heating systems (typically around 20 000 - 30 000 hours for the typical 10-year life expectancy of a central-heating boiler). As far as service intervals are concerned, it is not just the cost of the service, but the frequency and intrusiveness of a service that is important (Avasarala & Haldar, 2013). Cogeneration systems generally run under stable

conditions, normally at constant load and over long periods of time. This presents an advantage in terms of maintenance, wear rates and reliability compared to systems which operate under constantly varying load demands with frequent start/stop cycles such as automotive applications (Veerapen & Beerepoot, 2011).

The internal combustion engine, being a mature and well-tested technology, is generally reliable, but it does, however, require regular maintenance and results in regular scheduled outages. The recommended maintenance intervals are typically every 3500-4000 h for natural gas fuelled engines; 2700 h for operating on heated oil; 1400 h for biodiesel operation; and 750-1000 h for engines running on vegetable oils (Thomas, 2008). This includes the changing of lubrication oil, filters, engine coolant, spark plugs, and so on.

Stirling engines have sealed operating chambers resulting in low wear with long maintenance intervals (Elmer *et al.*, 2015). The service interval of engines with a capacity less than 20 kW is 5000-8000 h, which is long when compared to the ICE of the same range. The longer service intervals considerably reduce the operating costs compared with internal combustion engines. The elimination of mechanical contact, friction and wear results in no mechanical maintenance during the 10-year lifetime (Onovwiona *et al.*, 2007).

The operating lifetime is an important metric for fuel cell cogeneration systems, since a long lifetime is needed to realise the expected utility savings and offset high equipment and installation costs (Spendelow *et al.*, 2012). For acceptance to customers, a target of 60,000 operating hours in 2020, corresponding with a lifetime of around 10 years at 6,000 operating hours per year, has been set by the US Department of Energy (DOE) (Spendelow *et al.*, 2012). Staffell (2010), reports that both PEMFC and SOFC stacks lose power at a rate of up to 5% per thousand hours, while current targets of net power degradation of less than 0.3% per thousand hours has been set. The typical maintenance cost of fuel cell-based systems include the replacement parts and material such as air and fuel filters, reformer igniter, water treatment beds, electronic components and consumables such as sulphur-adsorbent bed catalysts and nitrogen for purging, while a major service includes catalyst replacement (5 years), and stack replacement (5 to 10 years) (Veerapen & Beerepoot, 2011).

2.2.6 Commercialisation

There are a number of IC engine-based cogeneration systems available in the market. The specific costs of these systems range from between 2200-5500 US\$ /kW$_e$ when the power is more than 2 kW$_e$. The Japanese Honda Ecowill, shown in Figure 2.4, was the worlds first mass-market micro-cogeneration unit in 2003 (Angrisani *et al.*, 2012; Tanaka *et al.*, 2011). The unit is designed for a single family household application and has a 1 kW electrical and 3 kW thermal output with 92% overall efficiency. This unit was successful in creating a new market for domestic cogeneration systems with over 100,000 units (cumulative) sold in the period 2003-2010 (Carter *et al.*, 2012). After the success of this product in Japan, it was introduced to the American market in 2006.

Figure 2.4: Honda ECOWILL 1kWe unit (adapted from Tanaka *et al.*, 2011).

Different micro-cogeneration systems, based on the Stirling engine, are available on the market. One such is the WhisperGen shown in Figure 2.5, produced by a New Zealand company. It is based on a four-cylinder Stirling-cycle that heats nitrogen gas pressurised at 28 bar, producing 0.75 kW and 5 kW electrical power and thermal energy in the process. The system operates on kerosene or diesel fuels.

Figure 2.5: 1 kW WispherGen cogeneration system (adapted from Elmer *et al.*, 2015).

By 2012, the fuel cell-based micro-cogeneration outsold the conventional engine-based system for the first time, accounting for 64% of global annual sales. This was particularly as a result of two large-scale demonstration projects, the Japanese Ene.Farm (Carter *et al.*, 2012) and the German Callux (Ren & Gao, 2010; Staffell & Green, 2013) schemes. The Japanese Ene.Farm scheme was launched in 2009 and saw around 50,000 units installed by 2013. Through research development efforts in recent years, the fuel cell cogeneration systems used in the Ene.Farm scheme have gained an increase in efficiency and durability, while a lower cost and reduction in system size has been achieved.

Cogeneration efficiency of 95% has been reported for PEM fuel cell models with an electrical power output of 700-750W. Financial incentives from government have led to a reduced cost of up to 25% of the normal unit cost. The German Callux project is the second biggest demonstration project, where 350 units were installed from September 2008

to the end of 2015. The experience from the Callux project has been shared with the
Ene.Field, a Europe-wide micro-cogeneration field-demonstration project. Ene.Field is a
project with 27 partners, which includes nine European manufactures and aims to instal
around 1000 fuel cell systems in 12 member states by 2017 (Ren & Gao, 2010).

Figure 2.6 shows an Ene.Farm 700 W_e system based on a LT-PEM fuel cell manufactured
by Panasonic. The unit has been available in the market since 2011 (Elmer *et al.*, 2015;
Napoli *et al.*, 2015). It consists of a PEMFC, a fuel processor, thermal storage tank,
an auxiliary boiler and BoP components. Panasonic states that the system can reduce
the primary energy consumption by 35% and CO emission by 48% for a single-house
household. The company has achieved a durability of 40 000 hours of start/stop operation
and 70 000 hours of operation (Napoli *et al.*, 2015) at the rated cogeneration efficiency of
95%.
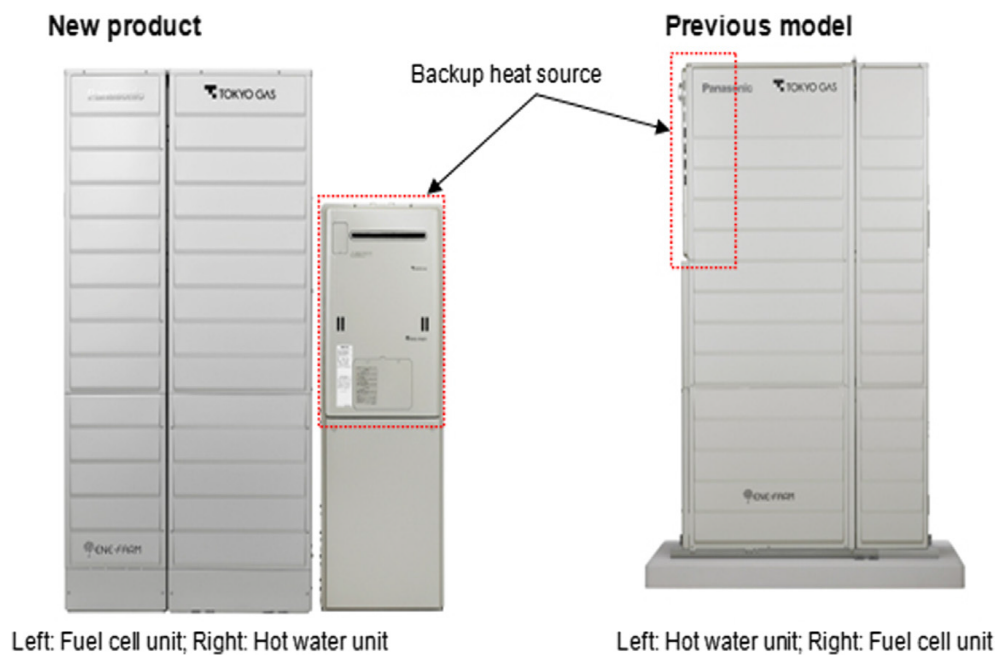
Figure 2.6: Ene.Farm Panasonic PEM fuel cell unit (adapted from Carter *et al.*, 2012).

In South Africa, the hydrogen and fuel cell technology programme was launched in 2008.
This is a 15-year initiative by the government under the banner of Hydrogen South Africa
(HySA). Its main objectives are to develop hydrogen and fuel cell components, system
and products. One of the technological focuses of the programme is the development of
a HT-PEM fuel cell-based cogeneration system in the 1-2 kW_e range. The first South

African prototype testing of the cogeneration system and validation was scheduled for 2015 with trials in the residential sector expected to follow (Pollet *et al.*, 2014). This target has however not been achieved and this research work serves as a means towards the attainment of this goal by using models to evaluate the performance of a cogeneration system in a South African residential sector.

2.3 PEM fuel cell-based micro-cogeneration

2.3.1 Fuel cell stack

2.3.1.1 Basic principle

A fuel cell is an electrochemical reactor that converts the chemical energy of a fuel directly into the direct current (DC) electricity by oxidising a fuel. Fuel cells are similar to batteries in that they both produce DC through an electrochemical process without the direct combustion of a fuel. However, whereas a battery delivers power from a finite amount of stored energy, fuel cells can operate indefinitely provided that a fuel source is continuously supplied. At the heart of the fuel cell is an electrolyte sandwiched between two porous electrodes, a positive electrode (anode) and a negative electrode (cathode). The combination of the three layers is called the membrane electrode assembly (MEA). The operating principle of a PEM fuel cell and the different layers of the MEA are shown in Figure 2.7.

A hydrogen-rich fuel is fed continuously into the anode where the hydrogen is oxidised into protons and electrons in a catalytic reaction. The protons diffuse through the electrolyte to the cathode. The electrons travel through the external circuit where they produce electricity and complete the circuit by travelling to the cathode. At the cathode, the electrons and hydrogen ions (protons) combine with oxygen to form water and heat.

The electrochemical reactions occurring in the PEM fuel cell at each electrode are:
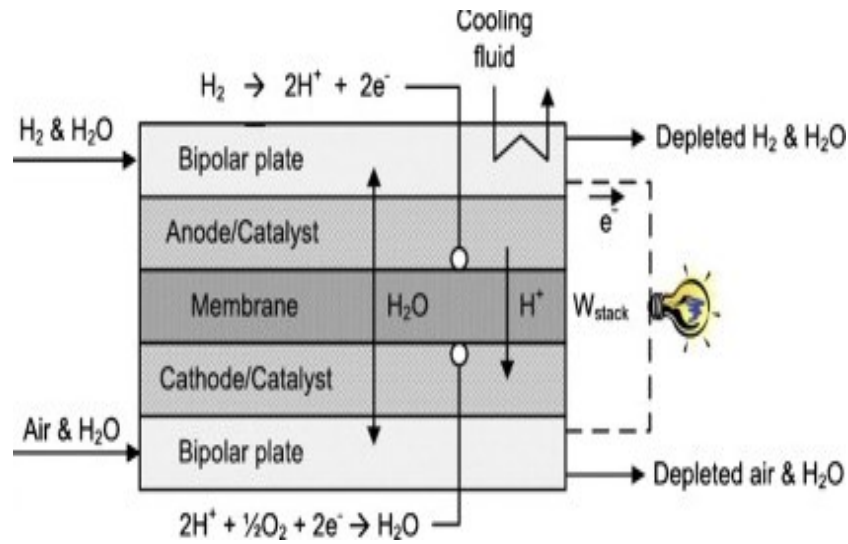
Figure 2.7: PEM fuel cell operating principle (adapted from Ang *et al.*, 2011).

At the Anode:

$$\mathrm{H_2} \longrightarrow 2\mathrm{H^+} + 2e^- \tag{2.1}$$

At the Cathode:

$$\frac{1}{2}\mathrm{O_2} + 2\mathrm{H^+} + 2e^- \longrightarrow \mathrm{H_2O} \tag{2.2}$$

Overall:

$$\mathrm{H_2} + \frac{1}{2}\mathrm{O_2} \longleftrightarrow \mathrm{H_2O} + Heat \tag{2.3}$$

2.3.1.2 Performance

The steady-state performance of a fuel cell is measured using the voltage (V) and power (W) versus current (A m^{-2}) as shown in Figure 2.8 . With reference to the voltage, it can be seen that the operating voltage decreases as the current density is increased. This decrease in the voltage is a result of voltage losses within the cell (Barbir, 2012). These losses include the initial drop (activation losses) caused by sluggish electrode kinetics, particularly the oxygen reduction reaction in the cathode. In Figure 2.8a, this can be seen as the drop from point 'A' to 'B'.

The second voltage loss from point 'B' to 'D' is mainly due to two forms of resistance in the cell: the resistance of the flow of electrons through the electrode and the resistance of the flow of ions through the electrolyte. This linear drop in performance obeys Ohms law of resistance and is referred to as ohmic polarisation. The ionic resistance is mainly
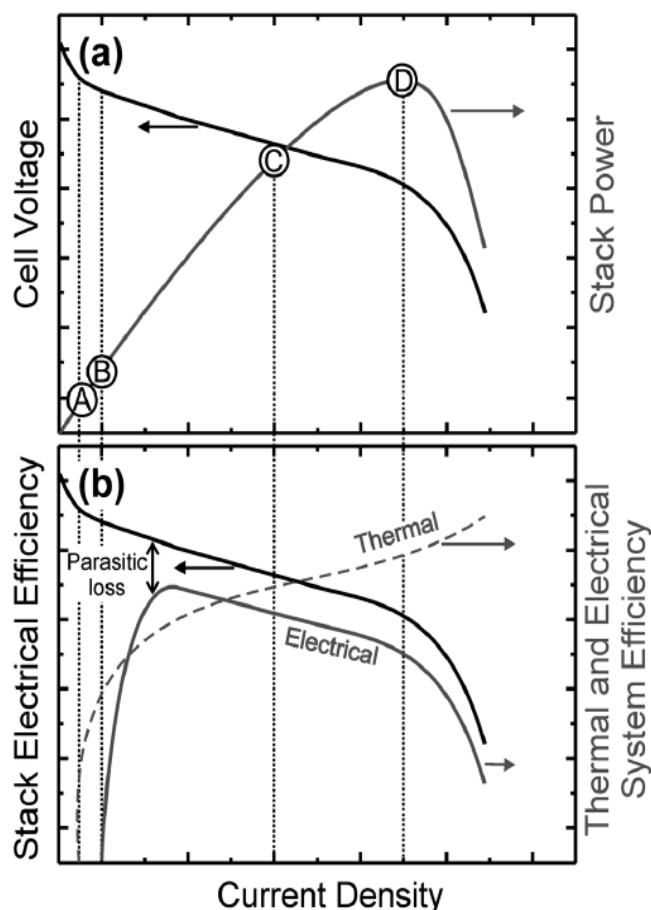
Figure 2.8: Operating range of fuel cell cogeneration system: (a) stack voltage and power and (b) electrical and thermal efficiency (adapted from Hawkes *et al.*, 2009b).

influenced by the conductivity of the electrolyte and the electrical resistance by the con-
ductivity of the electrode. The last rapid voltage drop in the performance curve is due
to the mass transport limitations in the fuel cell. This arises when the reactants in the
catalyst layers are consumed faster than they are supplied, thus causing a concentration
gradient. The power output of the fuel cell initially increases with current density until a
maximum, point 'D', is reached. Point 'C' is the nominal operating point which is about
2/3 to 3/4 of the open circuit voltage (Hawkes *et al.*, 2009b). The correlation between
the system efficiency (electrical and thermal) and electrical power load is shown in Figure
2.8b.

Although fuel cells have higher efficiencies at low electrical load compared to other cogen-
eration system prime movers, this can be reduced by the parasitic load that is required
to run other system components such as sensors, actuators and control systems. There-
fore, operating at a higher electrical load demand can reduce this degradation, since these
components require constant electrical supply. At point 'B', the parasitic load equals the

power delivered by the fuel cell and the system therefore has zero efficiency. From Figure 2.8b, it can be seen that the electrical efficiency decreases and the thermal efficiency increases with the current density increase (electrical load).

2.3.1.3 Thermal management

Owing to the fact that fuel cells generate heat when operational, this heat therefore needs to be removed for a steady-temperature operation. Thermal management is an important consideration in the design and operation of a PEMFC stack for the maintenance of a uniform temperature throughout the stack (Reddy *et al.*, 2014). If the heat is not removed it may lead to non-uniform temperature distributions which cause variations in the electrochemical reactions (Reddy & Jayanti, 2012). In addition, non-uniform temperature results in local hot spots which may lead to the damage of the structural components. The cooling methods employed for PEMFC stacks include: cooling with increased cathode air supply (Yu & Jung, 2010), cooling with separate air flow (Baek *et al.*, 2011), cooling with heat spreaders (edge cooling) (Choi *et al.*, 2008), cooling with liquid (water or antifreeze coolant) and cooling with phase change (Zhang & Kandlikar, 2012). Each of these methods has its own disadvantages as they influence the volume and mass of the stack, as well as the parasitic power utilisation. A nearly uniform temperature distribution can be obtained by using a large flow rate of coolant which circulates through the cooling plate (Choi *et al.*, 2008). However, having a separate coolant adds to the complexity of the system, increasing the operational cost and the high parasitic power consumption decreases the overall efficiency of the system.

2.3.2 Hydrogen production

Theoretically, any substance that is capable of chemical oxidation can be used as fuel in the anode of a fuel cell (Ang *et al.*, 2012). Hydrogen is the most abundant element on earth; however, it is not found present in its molecular form, but rather in chemical compounds such as water, hydrocarbons and biomass. For hydrogen fuel cell systems, H_2-rich gas may be produced from these fuel sources and then stored as part of the system. Hy-

drogen storage does, however, require a lot of space even when hydrogen is compressed to very high pressures or even liquefied (Dutta, 2014). By making hydrogen generation part of a fuel cell system, conventional hydrocarbon fuels such as methanol (portable power applications), natural gas (stationary application) and gasoline (transportation application) may be used. Fuel-processing technologies convert these hydrogen-carrying compounds into a hydrogen-rich gas stream using thermal-chemical, electrical and biological energy (Dincer & Acar, 2015). This section gives a brief description of hydrogen-production methods for fuel cell systems. These are classified based on the type of primary fuel source as hydrocarbon reforming, H_2 from biomass and H_2 from water. This is not meant to be a thorough review of hydrogen-production methods; that can be found elsewhere (Holladay *et al.*, 2009; Dincer & Rosen, 2011; Dutta, 2014; Dincer & Acar, 2015) .

2.3.2.1 Hydrocarbon reforming

Steam reforming (SR), partial oxidation (POX) and autothermal reforming (ATR) are three main fossil fuel-reforming technologies for producing hydrogen. The reforming process produces a reformate gas stream composed primarily of hydrogen, carbon monoxide and carbon dioxide (Dincer & Acar, 2015). Steam reforming is endothermic and requires an external heat source but, unlike the POX and ATR, it does not require oxygen to drive the reactions (Kolb, 2008; Kolb, 2013). In partial oxidation, hydrocarbons are reacted with less than the stoichiometric amount of oxygen to produce hydrogen. POX is more tolerant to sulphur compared to steam reforming and autothermal reforming and no catalyst is required for the reactions to proceed.

Autothermal reforming is a combination of both the steam reforming and POX. It consists of a thermal zone where POX is used to generate the heat needed to drive the downstream steam-reforming reactions in a catalytic zone (Krumpelt *et al.*, 2002). Autothermal reforming and partial oxidation does not need an external heat source as they are both thermally neutral and exothermic (Kolb, 2008). Since these processes require pure oxygen feed, they are more complex and costly than steam reforming due to the additional oxygen separation units. Compared to other fossil fuel-reforming technologies, steam reforming (particularly methane-steam reforming) is the least expensive and most

common method to produce hydrogen. Since all three processes produce large amounts of carbon monoxide, one or more water-gas shift (WGS) reactors are used, typically a low and high-temperature WGS reactor, to reduce the carbon monoxide in the reformate gas to amounts that are tolerable for PEM fuel cell operation.

2.3.2.2 Hydrogen from biomass

Hydrogen rich gas can be produced from biomass-derived fuels via two routes, namely, thermo-chemical conversion and bio-chemical/biological conversion. The choice of the process is influenced by the type and quantity of the biomass feedstock (Kalinci *et al.*, 2009; Tanksale *et al.*, 2010; Chaubey *et al.*, 2013). Bio-renewable feedstock can also be used to produce hydrogen through thermo-chemical conversion processes such as gasification, pyrolysis, steam reforming of bio-oils and supercritical water gasification (SCWG) (Saxena *et al.*, 2008; Parthasarathy & Narayanan, 2014; Udomsirichakorn & Salam, 2014). High overall efficiencies (thermal to hydrogen) of up to 50% have been reported for thermo-chemical conversion processes (Balat & Kirtay, 2010). One of the major disadvantages of these thermo-chemical processes is the formation of char and tar when biomass is decomposed (Saxena *et al.*, 2008). Biological biomass conversion can be categorised as fermentative hydrogen production, biological water-gas shift and photosynthesis process (Nissilä *et al.*, 2014; Singh & Wahid, 2015). In fermentative processes, anaerobic (dark fermentation) and photoheterotrophic (light fermentation) using carbohydrate-rich biomass as a renewable resource are used. Solar energy together with phototropic organisms, such as purple bacteria, green bacteria, cyanobacteria and algae, are used in the photosynthesis processes to produce hydrogen (Kalinci *et al.*, 2009).

2.3.2.3 Hydrogen from water

Electrolysis is the decomposition of water into hydrogen and oxygen by driving an electric current through the electrolyte. The three electrolyser technologies used for water electrolysis are alkaline, polymer membrane (PEM) and solid oxide electrolysis cells (SOEC). The electrolyser technologies can produce high-purity hydrogen with reported efficiencies

in the order of 65-85% (Ngoh & Njomo, 2012). Among these, the alkaline electrolysers are the most mature technology and have been in use since the 1920s (Ngoh & Njomo, 2012) . The electrodes are commonly made of nickel-coated steel, while the electrolyte is an aqueous solution containing potassium hydroxide or sodium hydroxide. The high-temperature (500-800 °C) operation of SOEC results in a decrease in the electrode over-potentials. This increases efficiency especially if the electricity is sourced from a renewable source such as solar cells or nuclear energy (Holladay et $al.$, 2009).

Thermochemical water-slitting uses heat to decompose water into hydrogen and oxygen through intermediate reactions at high temperatures (450-1000 °C) (Rosen, 2010; Wang et $al.$, 2014a). Highly endothermic reactions of thermochemical cycles require heat sources that are integrated into these cycles. Nuclear and solar systems have demonstrated to be suitable low-carbon heat sources for thermochemical hydrogen-production (Bolat & Thiel, 2014). All the chemicals used in the thermochemical cycle are recycled, except water, because it is the material source for the hydrogen. Typically, three process steps are involved in the cycle: hydrogen production, oxygen production and materials regeneration (Rosen, 2010; Varsano et $al.$, 2014; Zamfirescu & Dincer, 2014). Brown et $al.$ (2002) reviewed the work done in nuclear-based thermochemical cycles and they identified the most promising cycles in terms of efficiency, cost effectiveness and large-scale production of hydrogen. The sulphur-iodine (S-I) and the UT-3 cycles were identified as the most promising technologies. Some of the advantages of thermochemical water-splitting cycles are: (i) there is no need for the O_2-H_2 separation membranes; (ii) there is a reasonable temperature requirement range of 600-1200 K; and (iii) there is a zero or low electrical energy requirement (Rosen, 2010).

2.3.3   Fuel oxidant

In stationary fuel cell systems, oxygen from the atmosphere air is normally used as the fuel oxidant since it is readily available. The oxygen content in air is 20.95% by volume, which leads to about 50mV degradation in the fuel cell voltage. This small voltage loss is overset by the requirements of oxygen storage which will be required if pure oxygen is stored as part of the system (Barbir, 2012). Since micro-cogeneration systems operate at

low pressures, the air is supplied using a blower or a fan. In any case, a fan or a blower is run by an electric motor that requires electrical power and thus represents power loss or parasitic load.

2.3.4 Power electronics

The power produced by the fuel cell stack is of a low voltage, typically around 20-40 V for a 1 kW$_e$ system. Since it is produced as direct current (DC), an inverter and power-conditioning unit is used to convert it into alternating current (AC) suitable for use in electrical appliances and exporting to the grid. The fuel cell stack also provides electrical power to run system components such as pumps, blowers, fans and instrumentation equipment. The inverters available for this application have the efficiency of 85-95% for micro-cogeneration systems. The power-conditioning unit also provides voltage regulation due to the tendency of voltage swing associated with the fuel stack (Larminie & Dicks, 2003).

2.4 Summary

This chapter provided the background to different micro-cogeneration technologies which are categorised by the prime mover in the power range of 0.5-10 kW$_e$, including the internal combustion engine, Sterling engine and fuel cells. The micro-cogeneration systems are compared according to their operational characteristics, environmental emissions and durability. The advantages of fuel cell-based systems compared to combustion-based systems, such as high efficiency, low noise levels and reduced green house gas emissions are highlighted. For each prime mover technology, a review of a commercially available product was provided.

The following chapter provides an in-depth review of the literature on modelling of HT-PEM fuel cell, including a single cell, stack-level and system-level modelling.

Chapter 3

Modelling of HT-PEM Fuel Cells and Systems

Over the past two decades, modelling and simulation have been extensively used to investigate the performance of fuel cells. This use is motivated by the complexity of the fuel cell operation in which some of the details can be difficult or even impossible to measure in-situ, such as the distribution of temperature, reactant and current in the fuel cell individual components (Barbir, 2012; Siegel, 2008). As such, fuel-cell modelling provides a less expensive and faster alternative to laboratory trials (Spiegel, 2008), thus reducing the financial burden and timescales associated with such trails. Properly formulated fuel cell models provide insight into the performance of a fuel cell system and how the performance can be influenced.

Modelling is normally initiated early into fuel cell development because it helps to down select test scenarios that enable the analysis of feasibility, reliability, profitability and safety in the design phase to ensure that a design works under a wide range of conditions (Siegel, 2008). In order for a fuel cell model to be a useful design tool, it should be robust, accurate and be able to provide usable answers quickly (Barbir, 2012). A good model should be able to predict the performance under a wide range of fuel cell operating conditions. This chapter reviews literature on HT-PEM fuel cell modelling from single cell models to systems-level model applications.

3.1 Characteristics of fuel cell models

Since the high-temperature PEM fuel cell's structural components, except for the electrolyte, are the same as that of a low-temperature PEM fuel cell, the modelling is similar and thus the HT-PEMFC modelling can be characterised in a similar way as LT-PEMFC. Similarly to Siegel (2008), Haraldsson & Wipke (2004) and Ang *et al.* (2011), the key modelling features are summarised in Table 3.1 and are discussed below.

Table 3.1: Characteristics of HT-PEMFC fuel cell models

Category	Level
System boundary	cell, stack, system
Approach	physical, empirical, semi-empirical
State	steady state, transient
Spital dimension	lumped, 1-D, 2-D, 3-D
	Electrochemistry, transport processes,
	thermodynamics, catalysis, fluid dynamics
Complexity	thermal analyses, gas channel design
	cooling channel and manifold design, impedance spectroscopy
	structural and mechanical analysis

3.1.1 System boundary

Depending on the simulation application and objective, the system boundary defines the area of interest in the model. The system boundary in HT-PEMFC modelling includes: the cell level (which includes models that consider specific components of a fuel cell such as the membrane or the electrodes, or an entire fuel cell), the stack-level with individual fuel cells assembled in a stack and, finally, the system level consisting of a fuel cell stack and auxiliary components or balance-of-plant.

3.1.2 Approach

The fuel cell modelling approaches in literature are classified into three main categories: theoretical/physical, semi-empirical and empirical. Theoretical cell models are based on electro-chemistry and physics that govern a particular domain of interest in the fuel cell (Cheddie & Munroe, 2005; Siegel, 2008). Theoretical are constructed by using a mixture of partial differential and algebraic equations that are solved numerically. Theoretical models provide insight into complex, localized phenomena occurring in a particular region, such as catalyst agglomerates, triple phase boundary etc. As their development is laborious, commercial software with dedicated fuel cell modules, such as Ansys Fluent, COMSOL Multiphysics, FemLab, STAR-CD, are normally used to develop and simulate the models.

Empirical models are employed when the physical phenomena are difficult to model or the theory governing the phenomena is not well understood (Cheddie & Munroe, 2005). They are developed based entirely on experimental data. Their predictive outputs match the experimental values almost exactly (Haraldsson & Wipke, 2004). These models are only valid for the specific fuel cell or stack for which the experimental data was obtained (Haraldsson & Wipke, 2004). For a model to be useful for different fuel cell stack performance, the coefficients used in the equations need to be re-evaluated or modified. Empirical models are useful for making quick predictions and provide a fast start into fuel cell modelling (Ang *et al.*, 2011). Semi-empirical modelling combines theoretically derived differential and algebraic equations with empirically determined relationships. They contain more detail than empirical models, but are solved more quickly than physical models.

3.1.3 State

The state of a model is either steady-state or transient (dynamic) and is determined by the simulation objective of the model. Steady-state models appear more in literature and are often used to perform parametric studies using one operating point at a time (Asl *et al.*, 2010; Chanpeng & Khunatorn, 2011; Ziogou *et al.*, 2011; Meidanshahi & Karimi, 2012; Tiss *et al.*, 2013). Transient models are used to predict the performance of the

fuel cell/system when there is a step change in operating parameters. They can be used for start-up (Jia *et al.*, 2015; Petrone *et al.*, 2015; Saygili *et al.*, 2015) and shut-down procedures, analysing the influence of various components on flows during a drive cycle (Candusso *et al.*, 2006) and optimisation of the response-time on load changes (Chen *et al.*, 2013). Furthermore, transient models are also needed for designing control systems to control the fuel cell's terminal electrical quantities as desired. Transient models are also vital for the study of degradation phenomena, characterised by a short and long timespan, for example CO-poisoning and carbon Pt dissolution respectively (Jia *et al.*, 2015).

3.1.4 Spatial dimension and complexity/details

The choice of spatial dimension of a model depends on its application and domain of interest. The simplest model for fuel cell analysis is a lumped model, which provides the current-voltage characteristics for the entire operating region. This type of model is usually employed for system analysis because of its simplicity and low computational requirements. Spatially distributed models are preferable when local characteristics within the fuel cell are of importance. When examining modelling phenomena, like mass and energy transport, electrochemical, gas channel design etcetera, one, two or three dimensions may be considered. Since the spatial variations are taken into account, the models offer a more realistic view of certain phenomena in a fuel cell. Compared to lumped models, spatially distributed models are quite complex and require long computational times.

3.2 Modelling review

The cell-level system-boundary considered in HT-PEM fuel cell modelling is depicted in Figure 3.1, showing each domain (components) within the single cell to be considered when a model is developed. Each of the components has quite unique characteristics and the physical processes occurring at one component influence the ones that occur at the next component. A concise overview of the characteristics of each component is given first, followed by the cell level governing equations applicable to modelling. The porous regions
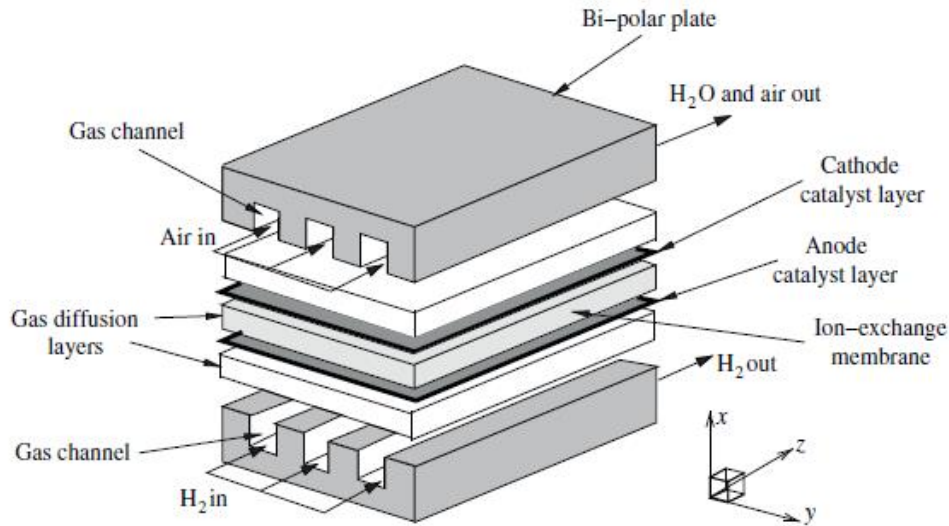
Figure 3.1: The structure of a typical PEM fuel cell (adapted from Shah *et al.*, 2011).

within a HT-PEMFC which include the gas-diffusion layer (GDL) and catalyst layer, play an important role of mechanical support and reactant gas and electrons distribution over the electrode while removing the product water from the electrode to the flow channel. The GDL links the catalyst layer electronically and gives structural support to the catalyst layer (El-kharouf & Pollet, 2012; Chandan *et al.*, 2013).

As it is an electrical conducting medium, it serves as an electron conductor from the catalyst layer to the bipolar plate. A typical GDL is Toray TGP-H-060 carbon-fibre paper (Frey & Linardi, 2004), which has a porosity of 0.78, a density of $2045\,\mathrm{kgm}^{-3}$ (Park *et al.*, 2015) and a mean pore diameter of $23\,\mu$m (Chandan *et al.*, 2013). The catalyst layers (CL) are complex structures made of precious-metal catalysts like platinum (Pt) or Pt-alloy nanoparticles supported on porous carbon, ionomer and pores. Their purpose is to promote the reduction (cathode) or oxidation (anode) reactions occurring at points of simultaneous contact between the metal catalyst, the carbon support and the electrolyte. The complex structure provides pathways for the transport of reactant and product species, electrons and protons to the reaction sites. As a result of the interplay of multiphysics at a multiple-length scale, all within a layer of micron-level thickness, the catalyst layers are the most complex of all the components to study, either experimentally or numerically, within a HT-PEMFC (Shah *et al.*, 2011). Optimisation of the catalyst layers attracts a lot of attention because of the significant expense of precious metals used and the hope of increasing the effective utilisation of fuels and durability (Kocha,

2011).

Gas channels or flow fields distribute reactant and product gases for anode and cathode GDL, acting as a current collector and mechanical reinforcement of the cell. Traditionally, graphite plates have been used in fuel cells owing to their chemical stability and high electrical conductivity (Barbir, 2012). However, metallic plates are considered superior alternatives to graphite plates due to the reduction in cost, increased volumetric power density and higher mechanical strength (Li & Sabir, 2005; Tawfik *et al.*, 2007; Taherian, 2014). One other important feature is the layout or topology of the flow-field structure, which ultimately directs the quality of the gas distribution into and across the cell area. Owing to the water formed in HT-PEMFC being in vapour form, the design and shape of the flow field is not limited, designs vary from multiple serpentine to parallel channels, to metal foams or meshes and to interdigitated designs (Barbir, 2012).

3.2.1 Governing equations

All physical phenomena within the HT-PEM fuel cell can be presented by solving conservation equations for mass, momentum, energy, species and current transport (Barbir, 2012). In addition to the conservation equations, specific relations such as Fick's law of diffusion, Stefan-Maxwell multi-species diffusion, Fourier's law for the conduction of heat, Darcy's equation for fluid flow in porous media, the Bulter-Volmer equation for electrical current and potential relationship may be used as applicable in each specific region within the fuel cell. Due to the complexity of these relations, assumptions are necessary so as to simplify the model. Assumptions used in fuel cell modelling depend entirely on the application of the model.

3.2.1.1 Conservation of mass

A general species conservation law is applied to account for the conservation of mass for all the gas species in the domains of a fuel cell. This can be written in terms of the partial pressure of gas, c-concentration of solution, x-mole fraction of a particular species, or ρ-density of fluid (Barbir, 2012).

$$\frac{\partial \varepsilon \rho x_i}{\partial t} + \nabla \cdot (v \varepsilon \rho x_i) = \nabla \cdot (\rho D_i^{eff} \nabla x_i) + S_i \tag{3.1}$$

where x_i is the mass fraction of species i, D_i is a diffusion coefficient and the superscript eff is used to denote an effective diffusion. The first term in the above equation accounts for change in the number of species within a control volume over time (accumulation term). The second term accounts for the material that enters and leaves a control volume by mass transport (advection term). The source terms S_i in the species conservation accounts for mass that is generated or consumed due to electrochemical reactions and is written as (Barbir, 2012):

$$S_i = j_k \frac{M_i}{n_k F} \tag{3.2}$$

in which j_k is the transfer current density, M_i is the molecular mass of species i, F is Faradays constant and n_k is the number of electrons transferred in the relevant half-cell reaction: anode (k = a) and cathode (k = c).

The binary interactions among the species in a multi-component mixture are accounted for using Stefan-Maxwell equations (Barbir, 2012):

$$\nabla x_i = RT \sum \frac{x_i N_j - x_j N_i}{p D_{ij}^{eff}} \tag{3.3}$$

where x_i is a mole fraction species i, and D_{ij}^{eff} is the effective binary diffusion coefficient between species i and j, and N_i is the superficial flux of species i averaged over a differential volume.

3.2.1.2 Conservation of thermal energy

The electrochemical reactions occurring in the cathode of a HT-PEM fuel cell release heat energy that is conducted by the components of the fuel cell and rejected either into cool-

ing plates/channels or into the external environment. An increase in local temperature is experienced due to the heat energy released and this affects local properties such as diffusion coefficients, currents densities, etcetera. The same conservation of energy equation is applicable to all layers of the HT-PEMFC with the same general transport properties and only the source terms vary (Barbir, 2012).

$$(\rho c_p)_{eff} \left(\frac{\partial T}{\partial t} + v \cdot \nabla T \right) = \nabla \cdot (k_{eff} \nabla T) + \sum Q \tag{3.4}$$

In the above expression, the term on the left-hand side represents the accumulation and convective transport of enthalpy, where C_p is the heat capacity, ρ is the density and T is the temperature. The first term on the right represents heat transport due to conduction, where k is the thermal conductivity. The second term represents the heat-source terms. There are two heat-source terms in the energy equation due to electrochemical reactions in the catalyst layer, that is, reversible and irreversible. The reversible heating is due to the Peltier effect and can be expressed in the form $Qrev = (T\Delta S)j/nF$, where ΔS is the entropy change for the relevant half-cell reaction. The irreversible heat is released due to activation over-potential and can be written as $Qirrev = j\eta$. Ohmic (Joule) heating in the electronic and ionic phase also results in irreversible heat generation which may be expressed as (Barbir, 2012):

$$Q_{ohm} = \sigma_s \left(\nabla \phi_s \right)^2 + \sigma_e \left(\nabla \phi_e \right)^2 \tag{3.5}$$

Effective terms are employed to account for the assumption of the thermal equilibrium of gas and the solid phase The effective thermal conductivity is expressed in terms of resistances (Barbir, 2012):

$$k_{eff} = -2k_s + \left[\frac{\varepsilon}{2k_s + k} + \frac{1 - \varepsilon}{3k_s} \right]^{-1} \tag{3.6}$$

where ε is the porosity of the domain and k_s and k represent the thermal conductivity

of the solid and gas phases, respectively. The effective density and specific heat are calculated as (Barbir, 2012):

$$(\rho cp)_{eff} = (1 - \varepsilon)\rho_s c_{p,s} + \varepsilon \rho c_p \tag{3.7}$$

3.2.1.3 Conservation of charge

The transport of charge occurs in the electrode catalyst layers, and the conservation of total electronic and ionic charges demands that for both the anode and cathode, the currents generated are equal $S_{\phi e} = S_{\phi s}$, where $S_{\phi e}$ and $S_{\phi s}$ are electronic and ionic currents, respectively (Shah *et al.*, 2011). The conservation of charge is governed by Ohms Law (Shah *et al.*, 2011):

$$\nabla \cdot (\kappa_s \nabla \phi_s) = S_{\phi s} \tag{3.8}$$

$$\nabla \cdot (\kappa_e \nabla \phi_e) = S_{\phi e} \tag{3.9}$$

where κ_s and κ_e are the effective ionic and electronic conductivities, ϕ_e and ϕ_s represent the electronic and ionic potentials, respectively. The conductivity κ_s of the acid-doped PBI membrane is assumed to follow a semi-empirical form and is a function of temperature and acid-doping level (W) (Cheddie & Munroe, 2007):

$$\kappa_s = \frac{100}{T} exp \left[8.0129 - \frac{2605.6 - 70.1W}{T} \right] \tag{3.10}$$

3.2.1.4 Reaction kinetics

The chemical reactions occurring at the electrodes are complex and not understood entirely. At the anode, H_2 is oxidised while at the cathode, O_2 is reduced over a noble metal catalyst. These reactions occur in either a four-electron path or through a series of two-electron pathways (Qingfeng *et al.*, 2001; Shah *et al.*, 2011; Avasarala & Haldar, 2013).

The transfer current densities for the two reactions are presented by the Bulter-Volmer equation, which can be expressed as (Barbir, 2012):

$$j_k = j_{o,k} \left[exp \left(\frac{-\alpha_{Rd,k}F}{RT} \eta_k \right) - exp \left(\frac{\alpha_{Ox,k}F}{RT} \eta_k \right) \right] \tag{3.11}$$

In the above equation j_o represents the exchange current density, α the transfer coefficient and η the activation over-potential. The exchange current density can be approximated by (Barbir, 2012):

$$j_{o,k} = i_o^{ref} a_k L_k \left(\frac{C_i}{C_i^{ref}} \right)^\gamma exp \left[-\frac{Ea_k}{RT} \left(1 - \frac{T}{T_{ref}} \right) \right] \tag{3.12}$$

Where Ea is the activation energy, γ is the reaction order. The i_o^{ref} is the reference exchange current density measured at reference concentration on the catalyst surface C_i^{ref} and reference temperature T_{ref}; a is the available catalyst specific area and L is the catalyst loading, with their product being a dimensionless parameter known as the roughness factor.

3.2.1.5 Equivalent-circuit models

Equivalent circuit models are normally used in the design and analysis of fuel cell stacks and systems with minimal computational requirements. In this approach, the cell voltage is determined by subtracting the voltage losses (over-potential) from the theoretical open circuit voltage (OCV). The cell voltage can be determined from (Shah *et al.*, 2011):

$$V_{cell} = V_{ocv} - V_{act} - V_{ohm} - V_{conc} \tag{3.13}$$

where V_{ocv} is the theoretical open-circuit voltage which is obtained from Nernst's equation and is a function of temperature and reactant concentration (Shah *et al.*, 2011). V_{act} is the activation voltage loss and can be obtained from the Bulter-Volmer or Tafel equations. The ohmic voltage loss V_{ohm} is determined using Ohm's Law and is a function of tem-

perature and acid-doping level. V_{conc} represents the concentration voltage loss, which is determined by introducing a limiting current density in the equivalent circuit model.

3.3   Overview of single cell models

The equations in the previous section, when used to model the characteristics of a single cell, are applied to the computational domain shown in Figure 3.2. They are solved using th finite difference method, finite volume or finite element methods (Barbir, 2012). Associated boundary conditions must include initial, continuity, boundary and external conditions.
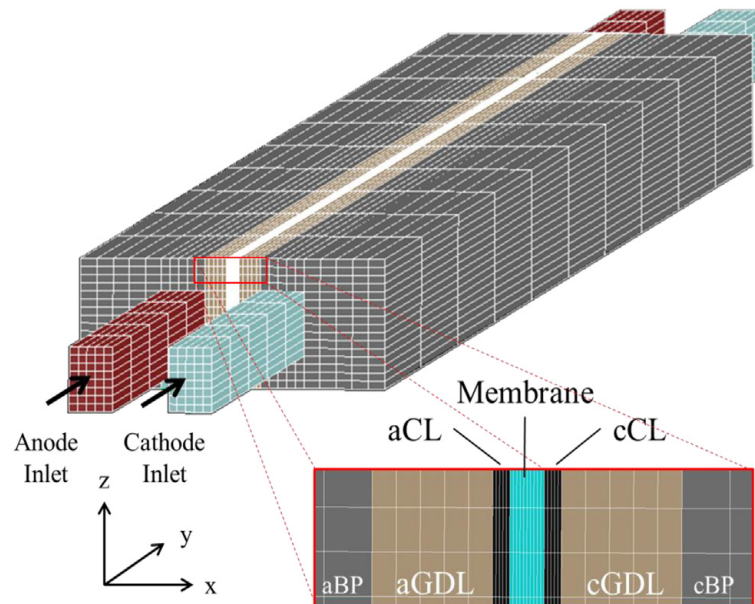
Figure 3.2: Typical modelling domain of a single cell (adapted from Siegel, 2008).

3.3.1   Lumped models

Korsgaard *et al.* (2006) present a semi-empirical model to express the polarisation of a fuel cell. In their work, they assume the anode polarisation is negligible for pure hydrogen operation and they derive linear regressions for diffusive resistance levels, ohmic resistance, charge transfer and an exponential regression for exchange current density. The authors present experimental results showing the performance effects related to cathode stoichiometric ratio versus temperature and the synthesis gas influence on anode polarisation.

Their experimental results show that CO-surface coverage is highly dependent on temperature. This could, however, not be predicted by their model as it neglected the anode polarisation (Korsgaard *et al.*, 2006). The modelling results indicate that the total ohmic losses were three times what the resistance of the membrane itself would predict, which they believed to be realistic. Pohl *et al.* (2015) employed an empirical electrochemical impedance spectroscopy model to simulate integrated short-term and long-term accelerated lifetime testing. In this work, the authors study the degradation on the open-circuit voltage over a simulated period of 35 days. The degradation effect was modelled with an empirical approach, depicting the hydrogen crossover and increasing charge transfer resistance.

3.3.2   One-dimensional models

One dimensional (1-D) models are solved in the x-direction (through-the-MEA), shown in Figure 3.2. 1-D models can be employed to analyse fluxes, concentration, temperatures, catalyst layer electrical potentials and the electrolyte for given boundary conditions in the channel. The model presented by Cheddie and Munroe (2006) is one-dimensional through the thickness of the MEA model. The authors studied how the cell behaves when air and oxygen are supplied as oxidants. They showed that the performance increased significantly by increasing conductivity from 1.87 S m^{-1} to 9.6 S m^{-1}. However when the conductivity was increased from 9.6 S m^{-1} to 17 S m^{-1} there was no significant change in the performance of the cell.

Scott *et al.* (2007) presented a steady-state, isothermal and one-dimensional model that accounted for 1-D electrode potential and reactant partial pressure distributions. The model was used to simulate effects of catalyst-loading and platinum-to-carbon ratio on the cell performance. Kim *et al.* (2014) presented a 1-D model of a fuel cell coupled with a semi-empirical degradation model. Increasing temperature was shown to result in increased average cell. However, on the other hand, the lifetime decreased by a factor of approximately 15 when the operating temperature was increased from 150 °C to 190 °C.

In a recent study, Lang *et al.* (2015) investigated the MEA degradation using a semi-empirical method. In their work, the authors developed a model for a HT-PEMFC and validated it using degradation data of long-term operations reported in the literature. The effects the of operating temperature, phosphoric acid-doping level and inlet-gas pressures on the degradation of the MEA were analysed. Their results suggest a trade-off between the fuel cell life-time and average performance of the MEA when the operating temperature is changed (Lang *et al.*, 2015).

3.3.3 Two-dimensional models

Two dimensional (2-D) models can be considered as an extension of 1-D models, to improve the understanding of local phenomena within a fuel cell due to the spatial variation used. The models can be implemented in the through-the-MEA (*x-z*) or along-the-channel (*y-z*) directions shown in Figure 3.2. Like in 1-D models, the through-the-MEA model is used to analyse fluxes, heat and mass transfer, concentrations in the catalyst and gas diffusion layers (Siegel, 2008). The models also take into account the effects of the bipolar plate and gas channels. Along-the-channel models are used to analyse change in species concentration and pressure drops along the gas channel.

Cheddie and Munroe (2007) extended their previous work (Cheddie & Munroe, 2006) into a two-dimensional, two-phase model. Simulation results show how the cell performance varies with acid-doping level, catalyst activity, dissolved gases in the electrolyte and absorption of phosphoric acid ions onto the catalyst sites. Sousa *et al.* (2010*b*) presented a two-dimensional agglomerate along-the-channel model. Results presented included the comparison of effects of porous media when air and heliox (mixture of oxygen and helium) were used as oxidants. They also presented the effects on cell performance when a reformate fuel was used, H_3PO_4 loading and gas-channel effects.

To predict the influence of the electrode double layer during a step change in potential, Sousa *et al.* (2010*a*) developed a two-dimensional model of a PBI-based PEMFC. The model predicted a current overshoot when the step change was induced, caused by the delay in the change in oxygen concentration. The authors showed that by increasing the

double-layer capacitance, the current density moved smoothly to the steady-state value without an overshoot (Sousa *et al.*, 2010*a*). Shamardina *et al.* (2010) presented an analytical pseudo 2-D, steady-state and isothermal model that accounts for the crossover of reactant gases through the membrane, to conduct a parametric study of operating conditions. Bergmann *et al.* (2010) presented a transient model to account for CO-poisoning effects in a HT-PEM fuel cell. The model was used to evaluate gas flows in the electrode and to evaluate the electro-chemistry of CO adsorption/desorption and electro oxidation on the catalyst surface. The dynamics of CO effects on the fuel cell were simulated by introducing a pulse in the anode electrode.

A two-dimensional isothermal model is presented in Sohn *et al.* (2011). The model is used to investigate the convective and diffusive transport phenomena in a HT-PEMFC with a straight flow-channel configuration. Bezmalinović *et al.* (2014) quantified the water vapour transport across the MEA during the cell operation. Their results indicate the water vapour partial pressure at the anode outlet exceeds that at the cathode exit, suggesting that there is a reversal in the water vapour transport from the anode to the cathode along the channel (Bezmalinović *et al.*, 2014). This lowers the hydrogen concentration at the outlet which, in turn, results in cell performance (Bezmalinović *et al.*, 2014).

Shamardina *et al.* (2014) also developed a pseudo 2-D to analyse the electrochemical impedance spectra of the cell in both potentiostatic and galvanostatic modes at different potentials and oxygen-flow velocities, current-interrupt results and step changes of the cell potential. Sun *et al.* (2015) presented a 2-D single-phase MEA model of an ab-PBI membrane-based HT-PEM fuel cell. The model accounts for the species, flow, energy and current density in the anode, cathode and ab-PBI membrane. The model was used to analyse effects of temperature, GDL porosity and thickness on the cell current density. The results presented showed that the cell performance increases when the operating temperature and GDL porosity is increased and when the GDL thickness is decreased. This increase in performance, the authors explain, is a result of increased mass transport in the electrode (Sun *et al.*, 2015).

3.3.4 Three-dimensional models

Three-dimensional (3-D) models are implemented in the *x-y-z* domain shown in Figure 3.2. They are a combination of the two types of 2-D models, that is, through-the-MEA (*x-z*) and along-the-channel (*y-z*). Their use is best suited when the overall behaviour of the fuel cell is of interest. As a result of the advances made in modelling a LT-PEM fuel cell, there are many studies that utilise 3-D models of HT-PEM fuel cells to investigate their performance. 3-D models are used to study the detailed characteristics of a fuel cell such as designs, durability, electro-chemistry and operational characteristics.

Peng and Lee (2006) presented a 3-D model model that includes mass, momentum, energy, species and charge transport in the PEM fuel cell. The electron transport equations were solved in the catalyst layer and current collector. The effects of temperature on the average current density, oxygen molar concentration and local electrode were investigated. They found that these decreased along-the-channel and the decrease is influenced by the decrease of reactants along-the-channel .

The model presented by Jiao and Li (2010) is a 3-D along-the-channel to investigate the effects of temperature, doping level and relative humidity (RH) in the cell performance. Their results showed that by increasing the doping level, temperature and pressure have a significant improvement on cell performance. However, they caution that the thermal sensitivity of the PBI membrane decreases with an increase of both temperature and doping level, and thus the maximum allowable temperature and doping level should not be exceeded (Jiao & Li, 2010).

Lobato *et al.* (2010) applied a 3-D model on a fuel cell with a 50 cm^2 active area to study three different flow-channel geometries: 4-step serpentine, parallel and pin-type. Well-defined current density profiles for each geometry are predicted by the model. They explain this as being influenced by the way reactants are spread over the surface of the electrode. The serpentine and pin-type flow-channels were reported to have a similar performance, which was higher than that of a parallel flow-channel geometry. Su *et al.* (2010) investigated the effects of operating conditions including the inlet gas temperature, system pressure and inlet gas-flow rate on fuel cell performance. An increase in these

operating conditions was shown to result in improved fuel cell performance.

Barelli *et al.* (2011) conducted a parametric study to investigate the influence of operating parameters such as temperature, pressure, relative humidity and CO content, using a semi-empirical model. Úbeda *et al.* (2012) presented a parameter estimation procedure from experimental polarisation curves for validation of a HT-PEMFC fuel cell using a 3-D model. The procedure consisted of adjusting the model results by region (activation, ohmic and concentration). The model was shown to exhibit a high sensitivity to kinetic parameters, followed by the ionic and electronic conductivities. The cell potential dependence on cell temperature was again shown by the study conducted by Park & Min (2012). In this work the authors develop a quasi-3-D model of a HT-PEMFC that takes into account the conservation of mass and energy, and electrochemical reactions. A delay response of 10s for the cell temperature to reach a steady-state was observed when a step change in the current density was induced. This was slightly more significant compared to the 0.1s delay due to oxygen depletion (Park & Min, 2012).

Durability of a HT-PEMFC is one of the critical factors to be considered in its commercialisation and thus it has been studied thoroughly in the literature. In general, the degradation of key fuel cell components, such as the gas diffusion layer (GDL), catalyst layer (CL), membrane and bipolar plates (BP), can be broadly categorised into chemical and mechanical degradations. Chemical degradation is mainly observed in the CL and membrane, whereas all the cell components are subject to mechanical degradation (Chippar & Ju, 2013; Chippar *et al.*, 2013; Oh *et al.*, 2014). In their work, Chippar *et al.* (2013) investigated the effects of GDL compression/intrusion on the performance of a straight channel fuel cell using a combined finite-element method (FEM)/computational fluid-dynamics (CFD) methodology. To analyse the cell deformation characteristics, 3-D FEM simulations are conducted under various displacement clamping. Subsequently, the CFD model is applied to the deformed cell geometry to investigate the electrochemical and transport processes during cell operation. The maximum stress is shown to occur near the edge of the ribs, which results in the increased non-uniformity of the current density distributions and reduced performance (Chippar *et al.*, 2013).

Jiao *et al.* (2013) compared the combined effect of the flow-field channel design (interdigitated, serpentine and parallel) and carbon monoxide poisoning on cell performance. For pure hydrogen operation, cell performance was highest with interdigitated design, while the serpentine showed better performance than the parallel flow field. Since the interdigitated, serpentine channel design facilitates better mass transport to the catalyst layer, the performance degradation caused by CO was reported to be more for this design than that of a parallel channel design. Chippar and Ju (2013) extended their earlier work to include the reactant crossover effects (mixed potential at the cathode CL and the hydrogen/oxygen catalytic combustion at the anode CL) on the cell performance. Their results indicated that fresh PBI and a moderately degraded membrane gas crossover had a negligible influence on cell performance, while for severely degraded membranes, effects had been observed.

In the work of Wang *et al.* (2014b), a 3-D physical model is employed to investigate the start-up process using four different strategies (cooling-channel heating, gas-channel heating, combined-gas channel and reaction heating, and combined cooling-channel and reaction heating). The cooling-channel heating is reported to be faster than the gas-channel heating for gas-flow rates lower than 1 L/min. The combined heating methods were reported to lead to faster start-up than the ones without reaction heating. The combined cooling-channel and reaction-heating method was shown to be the most effective as the combined-gas channel and reaction heating resulted in the upper limit of the temperature being exceeded (Wang *et al.*, 2014b).

Yin *et al.* (2014) numerically examined the performance of a HT-PEMFC with a sulfonated polybenzimidazole membrane. Their results indicated that high levels of phosphoric acid-doping, high pressure and temperature result in increased performance. The electrochemical reaction rates under the ribs of the bipolar plates were shown to be larger than the values under the flow channels. The authors concluded that this indicates the importance and dominance of the charge transport over the mass transport.

The effect of carbon monoxide on the performance of a HT-PEMFC was investigated by Oh *et al.* (2014) and Oh and Ju (2015). A 3-D model that accounts for the adsorption/desorption processes of CO and hydrogen on the anode catalysts was employed to

simulate the performance at different operating temperatures and CO levels in the anode feed. Similar results show the performance was affected by the operating temperature. At lower temperatures, cell performance was decreased, indicating stronger CO adsorption in the anode catalyst. Rasheed and Chan (2015) have considered the dynamics of CO poisoning in the anode under a specific rate of temperature increase during the warm-up process. A parametric study was employed to investigate the performance of the cell effects of the temperature increase rate, initial start-up temperature, CO volume fraction and extracted current density on the anode over-potential and the cell voltage. The authors found that in order to avoid premature shut-down of the fuel cell, the extracted current density, CO level and the temperature increase rate must be reduced.

Salomov *et al.* (2015) investigated the effects of the catalyst particle distribution on the reactant gas dynamics, electro-chemistry and subsequently the performance of a single cell. In their study, a 3-D macroscopic MEA model was employed to propose a mitigation strategy for cell performance degradation due to phosphoric acid loss and reactant crossover. The model showed a stress reduction of up to four times when the strategy was used and this came at a cost of 9% efficiency reduction (Salomov *et al.*, 2015).

3.4 Stack models overview

A fuel cell stack consist of a single cell repeat units stacked together with cooling channel cells. There are different approaches to developing fuel cell stack models, each depending on the modelling goal. There is a zero-dimensional (lumped) modelling approach that describes the stack voltage and current characteristics without spatial resolution. This approach is usually used for system-level simulations and only focuses on the overall performance of the stack. The second approach is a detailed model of a single cell and the stack behaviour obtained by multiplying the number of cells. The third approach is the most demanding in terms of computation requirements. It involves the explicit modelling of each single cell which are then coupled together to yield the full stack characteristics (Kvesić *et al.*, 2012).

The typical PEM fuel cell stack system's boundary, considered when modelling the stack, is shown in Figure 3.3. The stack models found in literature for a HT-PEM fuel cell vary considerably in size; from a short stack the size of 50 cm^2 that produce a few watts of electricity to stacks that can produce up to 1kW of electricity.
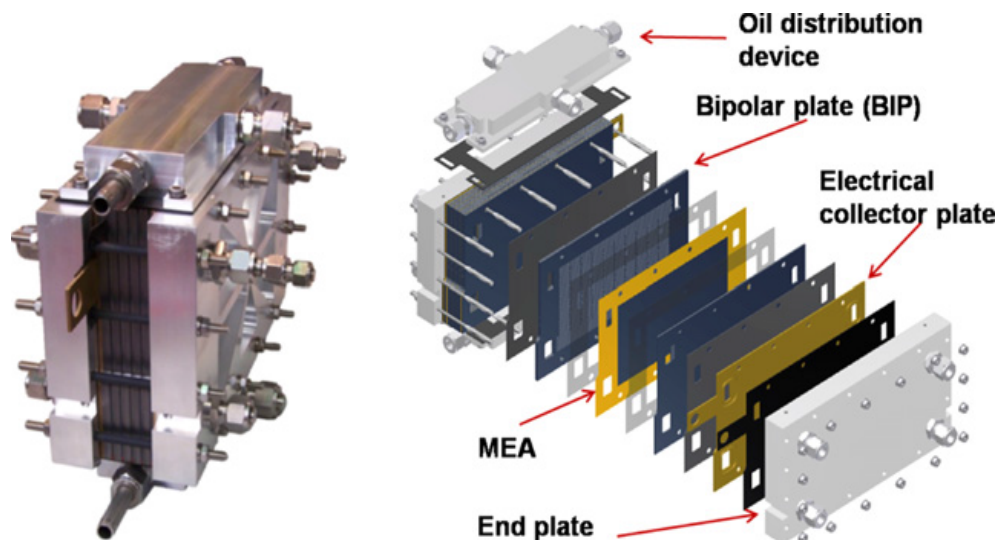
Figure 3.3: System boundary considered when modelling a HT-PEM fuel stack: (a) assembled stack and (b) an exploded view of the stack (adapted from Kvesić *et al.*, 2012).

Andreasen and Kær (2008) used electrochemical impedance spectroscopy (EIS) of a single cell to develop an impedance model for a fuel cell stack. The stack impedance depends on the impedance of each cell in the stack. They predicted the stack impedance using equivalent circuit models for each single cell at different temperatures. Reddy and Jayanti (2012) numerically examined heat-removal strategies of a 1 kW$_e$ stack suitable for transport application. Their study indicated a combination of excess stoichiometric factor and forced draft appeared to provide the optimal strategy for thermal management of the stack, keeping temperature variation across the stack within 20 K.

Kvesić *et al.* (2012) employed a 3-D fuel stack model to investigated the influence of the anode, cathode and coolant flow configuration on performance in the form of local current density and temperature distributions inside the stack. Their results indicate the flow configuration has a significant effect on the current density homogenisation when operating at a low anode stoichiometry. The optimum configuration was found to be a counter-flow of anode and cathode with a co-flow of anode and coolant (Kvesić *et al.*, 2012). The thermal management of stack in the 1-10 kW$_e$ range was investigated by

Reddy *et al.* (2014). The authors reported that for stacks in the 1-5 kW_e range, the temperature variation over the cell can be kept within 40 K by circulation of cathode air through the cooling channels (10 times stoichiometric factor), while for stacks larger than 5 kW_e, using a separate cooling liquid can keep the variations within 20 K. Rasheed *et al.* (2014) showed that the time to bring a 1 kW_e fuel cell stack from room temperature to an operating temperature of 180 °C can be reduced by using a heating strategy where constant current is drawn from the stack and heat is supplied through the end plates.

3.5 System-models overview

High-temperature proton exchange membrane fuel cells are being researched for application in stationary systems. This section reviews the modelling work done on system applications based on HT-PEM fuel. Modelling aspects of a HT-PEM fuel cell are mainly geared towards research and development of micro-cogeneration systems. Figure 3.4 shows a schematic representation of a micro-cogeneration system, illustrating the unit operations that are considered when developing a system model. Modelling work on at the systems level includes investigations of operating parameters, different fuel processor types, operating strategies and optimisation. The following is a summary of these studies.
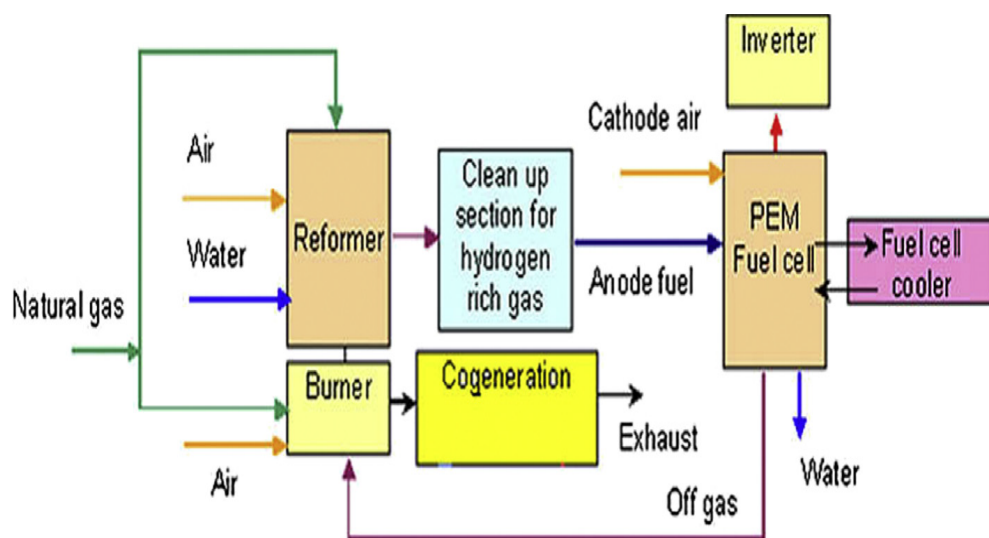
Figure 3.4: A typical schematic diagram of the components considered in system-level modelling (adopted from Ersöz & Sayar, 2015).

The model presented by Authayanun *et al.* (2010) is used to study the performance of a glycerol reformer coupled with a HT-PEMFC stack. The performance of a glycerol steam-reforming process is analysed based on a thermodynamic study in terms of carbon formation boundary, fuel consumption and product distribution. A comparison between the use of glycerol and methane for hydrogen production is also conducted. Perna *et al.* (2011) demonstrated the use of an LPG reformer coupled with a membrane shift reactor in a 5 kW$_e$ system. A sensitivity analysis showed the reforming pressure to be a crucial parameter as it influences the reformer conversion and hydrogen permeation through the membrane shift reactor.

Authayanun *et al.* (2012) observed an increase in cell voltage loss at high current densities at high reforming temperatures and low steam-carbon-ratios for a stack integrated with a glycerol reformer. The authors identified a 17% increase in the CO concentration along-the-channel of the anode as a plausible cause of this voltage loss. The overall system efficiency was shown not to be greatly affected by the S/C at low current densities. High S/C, however, was beneficial at high current densities. This was as a result of the low effect of CO at low current densities and the high energy required for additional steam at high S/C (Authayanun *et al.*, 2012).

Authayanun *et al.* (2013a) conducted a comparative study of a 3 kW$_e$ cogeneration system based on HT-PEM and LT-PEM fuel cells fed with pure hydrogen and using a reformate gas from a glycerol reformer. The LT-PEM system showed a higher performance for pure hydrogen operation, while the HT-PEM system exhibited better performance for a reformate operation at full load. A methanol fuel-based HT-PEM system in the 1 kW$_e$ power class was developed by Romero-Pascual and Soler (2014). The 65-cell stack, operating at 150 °C and hydrogen utilisation factor 0.9, needed a total methanol flow of 23.8 mol/h to reach 1 kW$_e$ power output. An electrical efficiency in the system of 24% and cogeneration efficiency over 87% was obtained. Samsun *et al.* (2014) analysed the use of a HT-PEM system operating with kerosene and diesel for use as an auxiliary power unit. The authors observed that in order to compensate for the parasitic losses in a 5 kW$_e$ net power output, the fuel consumption increased for both types of fuels used. For the kerosene operation, the gross power output was 5.65 kW$_e$ when the power-conditioning unit was included and 5.35 kW$_e$ when it was not included.

Arsalis *et al.* (2011*b*) investigated the influence of the steam-to-carbon ratio, fuel cell operating temperature and hydrogen stoichiometry on the cogeneration efficiency. The study was conducted in a form of sensitivity analysis where one variable is changed whilst keeping the rest of the system variables the same. It was reported that the considered parameters have a positive effect on the system performance when they are increased. However, the optimal values chosen were based on some of the system constraints such as the exhaust temperature of the flue gas leaving the system.

Arsalis *et al.* (2011*a*) and Zuliani and Taccani (2012) investigated partial load performance of a 1 kW_e HT-PEMFC cogeneration system with similar results, showing that efficiency increased with partial loads. Both studies showed that the system's BoP components do not have a significant effect on the system performance when the load is reduced. For instance, Zuliani and Taccani (2012) showed that the BOP requirement is reduced from 116 W_e to 54 W_e when the load demand is reduced from full-load to half-load. The parametric study, performed by Arsalis *et al.* (2012*b*) analysed the system performance of a 100 kW_e HT-PEM stack coupled with an absorption chiller subsystem for application in a commercial ship with electricity and cooling demands. The system performance is investigated using a double-effect water-lithium-bromide absorption chiller and a single-effect ammonia-water absorption chiller subsystem. The system is reported to be able to satisfy the cooling load in the form of chilled water at 5-10 °C from the lithium-bromide absorption chiller, while the cooling load was satisfied by the water-lithium-bromide chiller in the form of brine or glycol water at 60 to 0 °C.

Reddy and Jayanti (2012) have demonstrated the potential of coupling a 1 kW_e stack with a metal-hydride hydrogen storage system. The possibility of using cathode air to act as a coolant of the cell as well as the supplier of the heat required for hydrogen desorption from a sodium alanate-based hydrogen storage system was investigated. It was reported that, with a cathode air-flow rate seven times in excess of the stoichiometric requirement, it is possible to meet the triple requirement of (i) supplying preheated cathode air, (ii) maintaining uniform stack temperature and (iii) supplying the heat required for desorption of the required amount of H_2 (Reddy & Jayanti, 2012).

Similar results were shown by Jannelli *et al.* (2013) when they compared three cogeneration systems based on different electrolytes with a maximum power output of 2.5 kW$_e$. Three stack technologies were used in this study: a Nafion membrane stack-based system operating at 60 °C, a PBI stack system operating at 160 °C and a stack that is based on an aromatic polymer-pyridine membrane stack operating at 180 °C. The results indicated that the HT-PEM systems had electrical and cogeneration efficiencies of 40% and 78% respectively, while the LT-PEM system exhibited higher thermal recovery efficiencies.

The fact that fuel cell systems do not always operate at design points, such as when there is less demand for electrical energy, some authors have studied off-design performances. Najafi *et al.* (2015a) have developed a model for a CHP plant model composed of a fuel-processing subsystem, HT-PEM stack and auxiliary components to meet demand for two thermal users. The electrical and thermal performance of the plant are studied by conducting a parametric study of the fuel processor and stack design parameters. The results presented show that the electrical efficiency can be increased from 21.18% to 29.21% and primary saving index from 6.07% to 17.50% when an LT-PEM stack is replaced by a HT-PEM stack in an existing 30 kW$_e$ cogeneration system.

Using a genetic algorithm optimisation technique, Arsalis *et al.* (2012*a*) have maximised the net electrical power output of a cogeneration system, with respect to steam-to-carbon ratio, hydrogen stoichiometry, reformer number of tubes, reformer length, shift reactor length, combustor output temperature, reformer and WGS shift reactor inlet temperatures and fuel pre-heater flue gas inlet temperature. The optimisation procedure was able to reach a maximum (20.1%) increase in the objective function after 508 generations.

Rabiu *et al.* (2012) reported on the application of heat-integration technique to optimise the heat exchanger network of a 2 kW$_e$ system. The optimisation of heat exchanger network showed that a 5% increase in the system efficiency can be achieved without the need for external cooling utilities. Arsalis *et al.* (2013) investigated how a micro-CHP system can be optimised using two techniques: pinch analysis for the maximisation of electrical efficiency and mixed-integer nonlinear programming for the minimisation of heat exchanger network's (HEN) annual costs. The authors show that the combination of these two techniques can lead to a minimised HEN annual cost of $8,147/year without

a reduction in electrical efficiency.

Najafi *et al.* (2015b) implement two operating strategies for the mitigation of electrical and thermal power and the decay of related efficiencies in the first 15,000 hours of plant operation. The first strategy is partialisation, where the fuel fed to the system is reduced, thus keeping the thermal power generated at an acceptable range. The second is the recovery strategy in which the fuel supplied to the system is gradually increased so as to suppress the reduction in the power produced. Their results indicate that whilst the recovery strategy leads to higher electrical power generated, it also gives the lowest overall electrical efficiency when compared to the partialisation strategy and normal operation (Najafi *et al.*, 2015b). The model presented by Arsalis *et al.* (2015) proposes a grid-connected heat-pump-assisted residential CHP system. The model is used to investigate the load variation from full load to quarter load demand and optimised in terms of operating thermo-physical parameters for every different load.

3.6 Summary

This chapter reviews the modelling techniques currently employed in HT-PEM fuel cell single cells, stacks and systems analysis. Fuel can be categorized according to the system's boundary, approach, state, spatial dimension and complexity. This review is organised according to the system's boundary, that is, single cell, stack and system. The single cell model forms the basis of all fuel cell modelling works and can be adopted for stack and system-level modelling.

At cell level, the majority of the models are 3-D, focusing on the durability of the materials used within the cell. These include carbon monoxide poisoning, phosphoric acid leaching, reactant crossover, mechanical and thermal stress of bipolar plates, etcetera. Compared to cell-level models, fewer stack models are found. Physical models of stacks are used to characterise heat-removal techniques such as using high stoichiometric in cathode air, flow-channel configuration and utilising a cooling liquid.

Since the HT-PEM fuel cell is considered best suited to cogeneration application, most of the system-level models are developed to study small-scale cogeneration systems. The

stack models used in system-level modelling are normally based on single cell lumped models due to computational requirements associated with physical models. The fuel cell stack model is coupled to different sub-systems such as a fuel processor, thermal management, power conditioning and oxidant supply. These system-level models are utilised for the investigation of operational characteristics and optimisation studies.

Since high computational power is a requirement for mathematical modelling of the PEM fuel cell stack, lumped parameter models are normally utilised when studying PEM fuel cell-based micro-cogeneration systems. These models only describe the current-voltage characteristics of the fuel cell without taking account of local characteristics and, as such, they tend to over-predict the performance of a fuel cell. In this work, a simplified two-dimensional mathematical model for a HT-PEM fuel cell, which does not require heavy computational, time is utilised. This is done by developing a quasi-two-dimensional (1D + 1D) model that does not only consider current-voltage characteristics but also takes into account local characteristics within the fuel cell.

The remaining chapters of this thesis present in detail the development and application of models for a HT-PEM fuel cell-based micro-cogeneration system. The next chapter includes the model development and simulation results of the HT-PEMFC micro-cogeneration system. The model predictions are validated against experimental and numerical data. Also, the system performance is analysed with emphasis on fuel-processing parameters and performance.

Chapter 4

Parametric Analysis of a High-Temperature PEM Fuel Cell-Based Micro-Cogeneration System

4.1 Introduction

Owing to of the inefficiency and pollution associated with centralised power generation, there has been a growing interest in shifting to distributed (decentralised) power-generation systems. Cogeneration (or Combined-Heat-and-Power [CHP]) is seen to have the potential for primary energy savings and greenhouse gas emission reductions when compared with large power stations (Angrisani *et al.*, 2012; Sonar *et al.*, 2014). Cogeneration is the combined production of electrical and thermal energy from a single primary energy source. In residential applications, cogeneration provides electricity and heat (for hot water and space heating) for the household. Fuel cells, specifically the polymer electrolyte membrane (PEM) fuel cell and the solid oxide fuel cell (SOFC), are considered as an alternative to combustion-based technologies utilised to meet heating requirements.

This is because PEM fuel cells and SOFC exhibit high efficiencies, low emissions and noise levels, modularity and a low heat-to-power ratio (De Melo Furtado *et al.*, 2010). The low-temperature PEM (LT-PEM) fuel cell is the most developed and widely studied type of PEM fuel cell, operating at relatively low temperatures (<80 °C) having a Nafion-based membrane. Micro-cogeneration systems based on LT-PEM fuel cells have been widely demonstrated and have enjoyed some commercialisation success (Carter *et al.*, 2012). There are, however, disadvantages associated with this stack technology. For instance, the proton conduction mechanism of the Nafion membrane requires water management systems to prevent MEA flooding/drying. The low-operating temperature makes the LT-PEM fuel cell susceptible to carbon monoxide poisoning and thus requires 99.99% hydrogen-rich gas.

The development of a high-temperature PEM (HT-PEM) fuel cell which operates at a higher temperature (120-200 °C) has overcome these issues because the proton conduction mechanism in the polybenzimidazole (PBI)-based HT-PEM fuel cell is dependent on the phosphoric acid content and not on the membrane water content (Xiao *et al.*, 2005; Zhang *et al.*, 2013). The need for complex water management systems is eliminated, thus simplifying the system design. The high-temperature operation improves the PEM fuel cell performance and has operational advantages, such as tolerance to carbon monoxide (CO) levels (Qingfeng *et al.*, 2001; Li *et al.*, 2003; Jalani *et al.*, 2006; Qi & Buelte, 2006). The HT-PEM fuel cell has a tolerance of CO of up to 3% in hydrogen at 0.8 A cm^{-2} and 200 °C as reported by Li *et al.* (2003). The improved tolerance to CO allows use of a synthetic gas from various fuel sources without the need for complex CO clean-up systems (Authayanun *et al.*, 2013b; Gardemann *et al.*, 2014; Maximini *et al.*, 2014; Samsun *et al.*, 2016).

There are a number of HT-PEMFC based micro-cogeneration systems' modelling studies in literature as outlined in Chapter 3. In these studies, researchers investigated methane steam reforming based systems. In their analysis, they typically consider parameters such as steam-to-carbon ratio and reforming temperature when evaluating the fuel processor performance. Modelling of the combustion of fuels for heat supply to the reformer is almost universally limited to calculating the adiabatic flame temperature without considering the combustion reactions rate equations.

This chapter focuses on the effects of combustion parameters on the performance of the micro-cogeneration system by modelling a fuel processor, accounting for reaction kinetics in the steam reformer and catalytic combustor. Firstly, varying the fuel ratio from 0.75 to 0.95 and the equivalence ratio from 0.45 to 0.75 on the performance of the fuel processor is investigated. Subsequently, the effects of the combustion parameters on the micro-cogeneration system are evaluated by choosing four operating points that present combinations of fuel ratio and equivalence ratio. Their effect on the system performance is evaluated at different steam-to-carbon ratios, fuel cell stack operating temperatures and anode stoichiometry. The fuel processor results are summarised as contour plots of reactor temperatures, species mole fractions at reactor outlets, fuel-processing efficiency and fuel consumption. On the other hand, the system results are presented as the plot of stack voltage, electrical and cogeneration efficiencies. The remainder of the chapter is organised as follows: Section 4.2 presents the model's development and validation; Section 4.3 discusses the simulation result; finally, the summary of the results are presented in Section 4.4.

4.2 Modelling of the cogeneration system

The fuel cell cogeneration system consist of the following subsystems and components shown in the process flow diagram in Figure 4.1 as follows:

- Fuel processing sub-system for hydrogen-rich reformate gas production from natural gas;

- HT-PEM fuel cell stack for electricity generation;

- Catalytic combustor to supply heat required in the methane steam reformer;

- Balance of plant units: heat exchangers to maintain the desired temperatures and for cogeneration purpose.

The fuel-processing sub-system consists of methane steam reforming (MSR) reactor, a single stage water-gas shift (WGS) reactor and a catalytic combustor. Methane and water are fed to the MSR where they are converted to a reformate gas mixture of H_2, CO, CO_2 and un-reacted H_2O and CH_4 through steam-reforming reactions. In the second
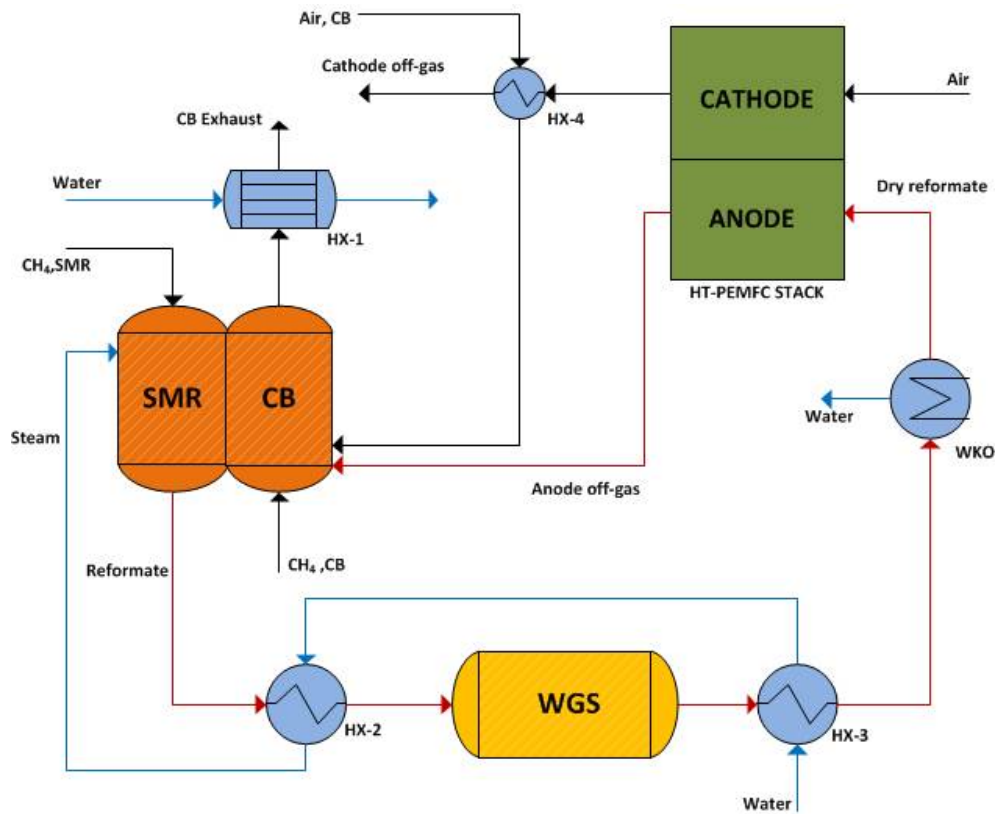
Figure 4.1: Schematic representation of the HT-PEM fuel cell cogeneration system.

stage of the fuel processor, the reformate gas from the MSR is fed into the WGS reactor, where CO and H_2O are converted into CO_2 through the shift reaction. This is to ensure that the CO levels in the reformate gas are within acceptable levels to avoid carbon monoxide poisoning in the fuel cell stack. The now H_2 rich reformate goes through a water knockout stage where excess water in the gas is removed before it enters the fuel cell stack. In the anode of the HT-PEM fuel cell stack, the hydrogen is consumed through electrochemical reactions to produce electricity. The anode off-gas, which contains some un-reacted H_2 and CH_4, is fed to the catalytic combustor (CB) to provide energy required by the endothermic reactions in the MSR and subsequently used to heat hot water for cogeneration purposes.

4.2.1 Methane-steam reformer (MSR)

The model presented can be applied to any kinetic model appropriate for the type of catalyst used. In this work, the intrinsic kinetic expressions reported by Xu and Froment (1989) for nickel-alumina catalysts, that have been widely used in literature, are adopted. The reaction kinetics are based on the Langmuir-Hinshelwood reaction mech-

anism, consisting of the steam-reforming reaction and the water-gas shift reaction. Two global reaction schemes are considered and are expressed as follows:

$$CH_4 + H_2O \longrightarrow CO + 3H_2 \qquad \Delta H_{298} = 206.1 \text{ kJ mol}^{-1} \qquad \text{(MSR)} \qquad (4.1)$$

$$CO + H_2O \longrightarrow CO_2 + H_2 \qquad \Delta H_{298} = -42.1 \text{ kJ mol}^{-1} \qquad \text{(WGS)} \qquad (4.2)$$
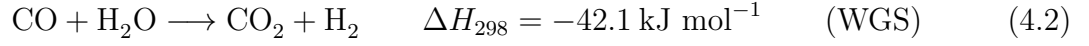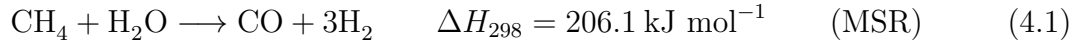
Their respective rate equations are:

For methane steam reforming:

$$r_1 = \frac{\frac{k_1}{P_{H_2}^{2.5}} \left[P_{CH_4} P_{H_2O} - \frac{P_{H_2}^3 P_{CO}}{K_1} \right]}{DEN^2} \qquad (4.3)$$

For water-gas-shift:

$$r_2 = \frac{\frac{k_2}{P_{H_2}} \left[P_{CO} P_{H_2O} - \frac{P_{H_2} P_{CO_2}}{K_2} \right]}{DEN^2} \qquad (4.4)$$

$$DEN = 1 + K_{CO} P_{CO} + K_{H_2} P_{H_2} + K_{CH_4} P_{CH_4} + K_{H_2O} \frac{P_{H_2O}}{P_{H_2}}$$

The rate constants and adsorption constants are determined by the Arrhenius and Vant Hoff relations:

$$k_i = A(k_i) \, exp \left(-\frac{E_{a,i}}{RT} \right)$$

$$(4.5)$$

$$K_j = A(K_j) \, exp \left(-\frac{\Delta H_j}{RT} \right)$$

$$(i = 1, 2) \qquad (j = H_2, H_2O, H_2O, CO, CO_2, CH_4)$$

4.2.2 Water-gas shift (WGS)

The reformate gases leaving the steam reformer are a mixture of mainly hydrogen (H_2), carbon dioxide (CO_2), water vapour (H_2O), carbon monoxide (CO) and small traces of methane (CH_4). The platinum catalyst used in the fuel cell stack is prone to CO poisoning in the temperature range at which it operates. Thus, to reduce the CO content in the reformate gas, the gas is fed to a shift reactor where the CO reacts with H_2O to produce more H_2. In the WGS reactor, the CO content should be reduced to an acceptable level (for the fuel cell stack) of less than 2%. The kinetic model of the WGS reactor is described in detail in Kim *et al.* (2005), and the global reaction considered is expressed as follows:

$$CO + H_2O \longrightarrow CO_2 + H_2 \qquad \Delta H_{298} = -42.1 \, \text{kJ mol}^{-1} \qquad \text{(WGS)} \qquad (4.6)$$
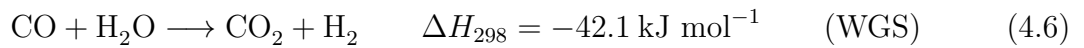
$$r_3 = k_o \exp\left(\frac{-E_a}{RT}\right) P_{CO} P_{H_2} \left(1 - \frac{P_{CO_2} P_{H_2}}{P_{CO} P_{H2O} K_{eq}}\right) \qquad (4.7)$$

$$K_{eq} = 9.543 \times 10^{-3} \exp\left(\frac{39.876}{RT}\right) \qquad (4.8)$$

4.2.3 Catalytic combustor

The steam-reforming reaction is highly endothermic and needs to be supplied with heat for it to proceed. The anode off-gas is fed to the catalytic combustor, where the unreacted H_2, CH_4 and CO are burned with air to supply the required heat to the steam reformer. Additional CH_4 is also supplied to the combustor because the anode off-gas is not sufficient to maintain the required temperature in the steam reformer. The reactions occurring in the combustor are:

$$CH_4 + 2O_2 \longrightarrow 2H_2O \qquad \Delta H_{298} = -802 \, \text{kJ mol}^{-1} \qquad \text{(methane combustion)} \qquad (4.9)$$

$$H_2 + 0.5O_2 \longrightarrow H_2O \qquad \Delta H_{298} = -242 \, \text{kJ mol}^{-1} \qquad \text{(hydrogen combustion)} \quad (4.10)$$

$$CO + 0.5O_2 \longrightarrow CO_2 \qquad \Delta H_{298} = -283 \, \text{kJ mol}^{-1} \qquad \text{(carbon monoxide combustion)} \tag{4.11}$$
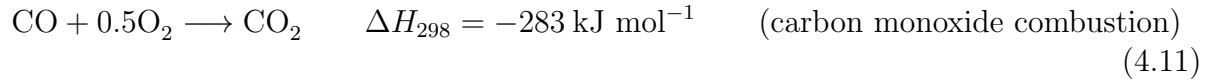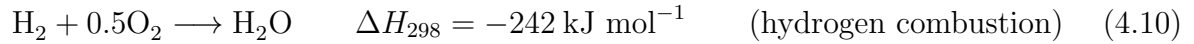
The reaction kinetics of hydrogen (Schefer, 1982), methane (Song *et al.*, 1991) and carbon monoxide (Cant *et al.*, 1978) combustion on a platinum catalyst are used. For methane combustion:

$$r_4 = 1.3 \times 10^{11} \exp\left(-\frac{134,700}{RT}\right) y_{CH_4} \sqrt{y_{O_2}} \tag{4.12}$$

For hydrogen combustion:

$$r_5 = 1.4 \times 10^3 \exp\left(-\frac{14979}{RT}\right) c_{H_2} \tag{4.13}$$

For carbon monoxide combustion:

$$r_6 = 2.25 \times 10^5 \exp\left(-\frac{28850}{RT}\right) \frac{p_{CO}}{(p_{O_2})^{0.5}} \tag{4.14}$$

4.2.4 HT-PEM fuel cell stack

The fuel cell stack model was developed using a modular approach in which each component (flow channel, gas diffusion layer and catalyst layer) was individually modelled and the connectivity equations at the boundaries used to connect the adjacent layers. Figure 4.2 shows the schematic diagram of the modelling domain considered in the fuel cell model.
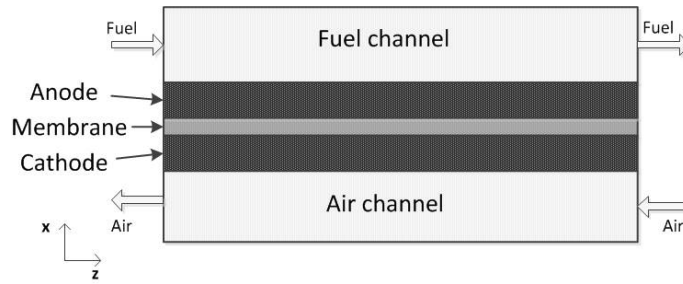
Figure 4.2: Modelling domain of the HT-PEM fuel cell.

4.2.4.1 Basic assumptions

The following basic assumptions hold when developing the fuel cell model:

1. All chemical components of working fluid are considered ideal incompressible gases, and fully developed laminar flow is considered.

2. Single phase operation.

3. Isothermal operation.

4. There is no reactant crossover in the electrolyte.

5. The concentration polarisation loss is neglected.

6. A steady-state operation is assumed.

7. Heat loss to surroundings is negligible.

4.2.4.2 Gas channel sub-domain

In the gas channels, the consumption of hydrogen and oxygen (O_2) due to electrochemical reactions occurs and water vapour is produced. The conservation of the mass in the presence of electrochemical reactions leads to a set of ordinary differential equations for the rate of change of molar concentration with respect to axial positions within the flow channel. The conservation of mass is solved along the axial coordinate (Z) for the anode and cathode as follows:

$$c_{t,k}\, u_k\, \frac{\partial y_{i,k}}{\partial z} = S_i \qquad (k = a, c) \tag{4.15}$$

where c_t is the total gas concentration in the channel, u the gas velocity and y_i represents

the species molar fractions. The source terms S_i represents the species reaction. The source terms of the species taking part in the reactions (hydrogen, oxygen and water) are calculated as:

$$S_{H_2} = j\frac{M_{H_2}}{2F}$$

$$S_{O_2} = j\frac{M_{O_2}}{4F} \tag{4.16}$$

$$S_{H_2O} = -j\frac{M_{H_2}}{2F}$$

where j is the exchange current density and M_i is the molecular mass of each species. The mass conservation equations are complemented with the associated boundary. The boundary conditions dictate that the molar concentration of each species at the channel inlet, is equal to those of the respective feed stream. A first order finite difference method (BFDM) was used to solve the conservation equation in the gas channel with 20 discrete points.

4.2.4.3 MEA sub-domain

In MEA, five components are included in the model: the anode and cathode GDLs, the anode and cathode electrodes and the membrane. Only mass transport due to diffusion is considered in the MEA direction. Mass transport in the gas diffusion layer is considered to be 1-D along the diffusion flux direction X ϵ [0,1]. The Stefan-Maxwell equation is to describe the mass transfer in the GDL:

$$\frac{\partial y_{i,k}}{\partial X} = \sum \frac{y_i N_i - y_j N_j}{c_{t,k} D_{ij}^{eff}} \tag{4.17}$$

where D_{ij}^{eff} is the effective binary diffusion coefficient between species i and j, N_i represents the molar flux of species i. The correlation proposed by Jiao *et al.* (2011) was used to determine the binary diffusion coefficients (equation 4.18), which were subsequently corrected using Bruggeman's correlation to account for the tortuosity and porosity of

porous media (equation 4.19). A second order centre finite difference method with five discrete points is employed to solve the equations:

$$D_{ij}|_{T,P} = D_{ij}|_{T_{ref},P_{ref}} \left(\frac{T}{T_{ref}}\right)^{1.5} \left(\frac{P_{ref}}{T}\right) \tag{4.18}$$

$$D_{ij}^{eff} = \varepsilon^{1.5} D_{ij}|_{T,P} \tag{4.19}$$

4.2.4.4   Electrochemical Model

The electrochemical reactions in the HT-PEMFC occur in the thin catalyst zones which are close to the electrode and membrane. In this work, it is assumed that electrochemical reactions only occur at the GDL/CL interface and, as such, the catalyst layers are modelled as interfaces. This simplification has been widely used in cell-level and system-level analysis. The concentrations of the reacting species (hydrogen and oxygen) at the catalyst interface are determined using Ficks law of diffusion (Scott & Mamlouk, 2009):

$$\frac{N_{i,k}}{S_{Pt,k}} = \frac{-D_{i,k}^{H_3PO_4}(C_{i,k}^{Pt} - C_{i,k}^{eq})}{\delta_k} \tag{4.20}$$

The $C_{i,k}^{Pt}$ represents the species concentration on the catalyst surface, $C_{i,k}^{eq}$ is the equilibrium concentration in the acid thin film at the studied temperature and δ_k is the film thickness. The concentrations of the species dissolving at the thin film boundary $C_{(i,dissolved)}$ are calculated from their solubility (Scott & Mamlouk, 2009):

$$C_{i,k}^{eq} = C_{i,k}^{dissolved} y_{i,k} P_k \tag{4.21}$$

where y_i is the species model fraction at the electrode/electrolyte interface. The correlations employed by Cheddie and Monroe (2007) are used to calculate the solubility and diffusivity of O_2 in phosphoric acid, whereas the diffusivity and solubility of H_2 are assumed to be twice and four times those of O_2, respectively. The activation over voltage due to electrochemical reactions is calculated using the ButlerVolmer equation for the

Oxygen Reduction Reaction in the cathode,(c) and Hydrogen Oxidation Reaction in the anode, (a).

$$j_c = i_{o,c} \left[exp \left(\frac{-\alpha_{Rd,c}F}{RT} \eta_c \right) - exp \left(\frac{\alpha_{Ox,c}F}{RT} \eta_c \right) \right]$$

$$j_a = i_{o,a} \left[exp \left(\frac{-\alpha_{Rd,a}F}{RT} \eta_a \right) - exp \left(\frac{\alpha_{Ox,a}F}{RT} \eta_a \right) \right]$$

(4.22)

where the exchange current density is approximated by:

$$i_{o,c} = i_o^{ref} a_c L_c \left(\frac{C_{O_2}}{C_{O_2}^{ref}} \right)^{\gamma} exp \left[-7900 \left(1 - \frac{T}{T_{ref}} \right) \right]$$

$$i_{o,a} = i_o^{ref} a_a L_a \left(\frac{C_{H_2}}{C_{H_2}^{ref}} \right)^{\gamma} exp \left[-1400 \left(1 - \frac{T}{T_{ref}} \right) \right]$$

(4.23)

Owing to of a reformate gas operation, the effect of CO poisoning on the anode catalyst layer is accounted for by using a modified exchange current density (j_a^{CO}) (Sousa *et al.*, 2010*a*):

$$j_a^{CO} = j_{o,a}(1 - \theta_{CO})^2$$

(4.24)

where the temperature dependence of the surface coverage of the reaction site by CO θ_{CO} is obtained by correlation employed by Dhar *et al.* (1986):

$$\theta_{CO} = 19.9 \, exp(-7.69 \times 10^{-3}T) - 0.085 \, ln \left[\frac{CO}{H_2} \right]$$

(4.25)

The ohmic loss follows Ohm's law and is caused by a resistance of ions in the electrolyte through the membrane. The proton conductivity κ as a function of temperature and acid-doping level W follows the Arrhenius law as obtained from Cheddie and Munroe (2007).

$$\kappa = \frac{100}{T} exp \left[8.0129 - \frac{2605.6 - 70.1W}{T} \right] \quad (4.26)$$

The total cell voltage U_{cell} is given by:

$$U_{cell} = E_{ocv} - \eta_{act} - \eta_{ohm} \quad (4.27)$$

where the thermodynamic equilibrium potential E_{ocv} is determined using the Nernst equation:

$$E_{ocv} = 1.1669 - 0.24 \times 10^{-3}(T - 373.15) \quad (4.28)$$

The values of the paramaters used in the fuel cell model are listed in Table 4.1.

Table 4.1: **Values of parameters used in HT-PEMFC model**

Parameter	Value
GDL porosity	0.6
Membrane thickness (m)	4×10^{-5}
Anode film thickness (m)	2.5×10^{-9}
Cathode film thickness (m)	1.48×10^{-9}
Anode reference exchange current density (A m^{-2})	1440
Cathode reference exchange current density (A m^{-2})	0.0004
Anode catalyst surface area (m^2 g^{-1})	64
Cathode catalyst surface area (m^2 g^{-1})	32.25
Anode catalyst loading (mg cm^{-2})	0.2
Cathode catalyst loading (mg cm^{-2})	0.4
Transfer coefficient at anode	0.5
Transfer coefficient at cathode	0.5
Anode reference concentration (mol cm^{-3})	0.0002
Cathode reference concentration (mol cm^{-3})	0.0004
Anode activation energy (kJ mol^{-1})	16000
Cathode activation energy (kJ mol^{-1})	54066
Anode reference cell temperature (K)	433.15
Cathode reference cell temperature (K)	373.15
Reaction order	1

4.2.5 Heat exchangers

The thermal analysis of the heat exchangers is based on the number of transfer units (NTU) method, based on the concept of heat exchanger effectiveness (ε). The effectiveness of a heat exchanger is the ratio of the actual heat transfer rate to the thermodynamically limited maximum possible heat transfer rate if an infinite heat transfer surface area were available. For a cross-flow compact heat exchanger with both fluids unmixed, the ε-NTU function is:

$$\varepsilon = 1 - exp\left\{ \left(\frac{1}{C_r}\right) NTU^{0.22}[exp(-C_r NTU^{0.78})] - 1 \right\} \tag{4.29}$$

4.2.6 System performance parameters

The objective functions that are used in the analysis of the system performance are the fuel processor efficiency η_{FP}, fuel consumption γ_{CH_4}, electrical efficiency η_{el} and cogeneration efficiency η_{cogen}. The fuel processor efficiency is defined as the ratio of hydrogen produced in the fuel-processor and the amount of chemicals available in the input gas (methane) entering the system:

$$\eta_{FP} = \frac{\dot{m}_{H_2 anode} LHV_{H_2}}{\dot{m}_{CH_4 system} LHV_{CH_4}} \tag{4.30}$$

where $\dot{m}_{H_2 anode}$ is the mass flow rate of hydrogen at the anode inlet and $\dot{m}_{CH_4 system}$ is the total mass flow rate of methane which is consumed. The fuel conversion/consumption rate is one of the most widely used parameters in evaluating fuel processor performance defined as:

$$\gamma_{CH_4} = \left(1 - \frac{\dot{m}_{CH_4,MSRoutlet}}{\dot{m}_{CH_4,MSRinlet}}\right) \times 100 \tag{4.31}$$

where $\dot{m}_{CH_4,MSRoutlet}$ is the methane flow rate at the MSR outlet and $\dot{m}_{CH_4,MSRinlet}$ is methane the flow rate at the MSR inlet. The electrical efficiency is defined as the ratio

of the electrical power output from the fuel cell stack divided by the chemical energy of the hydrogen from the fuel processor:

$$\eta_{el} = \frac{P_{el}}{(\dot{m}_{CH_4,in}LHV_{CH_4})_{systeminlet}} \tag{4.32}$$

where P_{el} represents the electrical power produced in the fuel cell stack. The system cogeneration efficiency is defined as the sum of the thermal and electrical power divided by the amount of methane which is consumed:

$$\eta_{cogen} = \frac{P_{el} + P_{th}}{(\dot{m}_{CH_4,in}LHV_{CH_4})_{systeminlet}} \tag{4.33}$$

where P_{th} is the thermal energy recoverable from the cogeneration heat exchanger. The system model was implemented in a commercial application, the gPROMS Model Builder version 3.6.0 from Process Systems Enterprise Ltd (PSE (Process Systems Enterprise)., n.d.). The computation station consists of a 64-bit Windows platform, 8GB RAM and an Intel(R) Core^{TM}i5 3.20 GHz processor. The gPROMS DASolver is used to solve numerical functions during simulation.

4.2.7 Models Validation

In order to determine whether the physical/chemical model correctly describes the behaviour occurring in each component and if the model represents a realistic system and the component characteristics, a model validation with experimental or numerical data must be undertaken. This section presents the validation of the components/system with such data. The fuel cell current-voltage characteristics obtained from the model and experimental results from Bujlo *et al.* (2013) at different operating conditions are compared in Figure 4.3. The experimental data from Bujlo *et al.* (2013) were obtained in a $1\,\mathrm{kW_e}$ HT-PEMFC stack operated at 140 °C with an anode feed gas composition of H_2 mixed with different CO concentrations (0.1, 0.3, 0.5 and 1%). As can be noted in Figure 4.3, there is an acceptable agreement between the model and the experiment's results, which verifies the validity of the model.
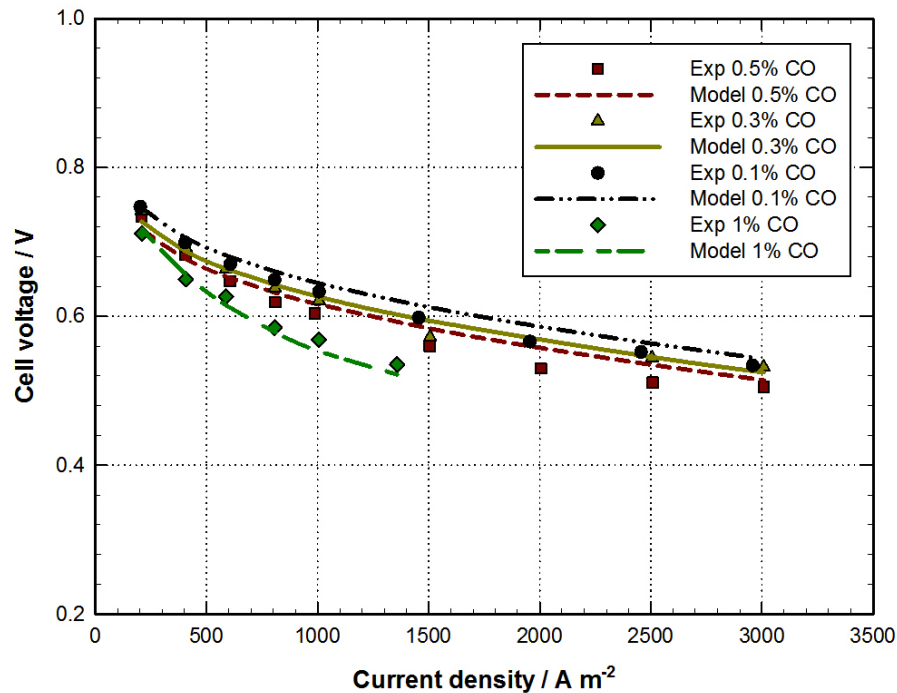
Figure 4.3: Validation of the voltage characteristics of the HT-PEM fuel cell stack.

Kinetic models of a methane steam reformer by Xu and Froment (1989) over a nickel-based catalyst and of a water-gas shift by Kim *et al.* (2005) over a copper-based catalyst, were used to model the MSR and shift reactors, respectively. Therefore, the validation of the fuel-processor model is conducted with experimental and numerical data sets in which the same types of catalyst were used for both reactors. Accordingly, two set of data were selected for this purpose, experimental data by Di Bona *et al.* (2011) and numerical data by Jung *et al.* (2014). Figure 4.4 compares the simulation, experimental and numerical results of the dry-gas composition at the outlet of the WGS reactor. The simulation results from this work agree well with these data sets.
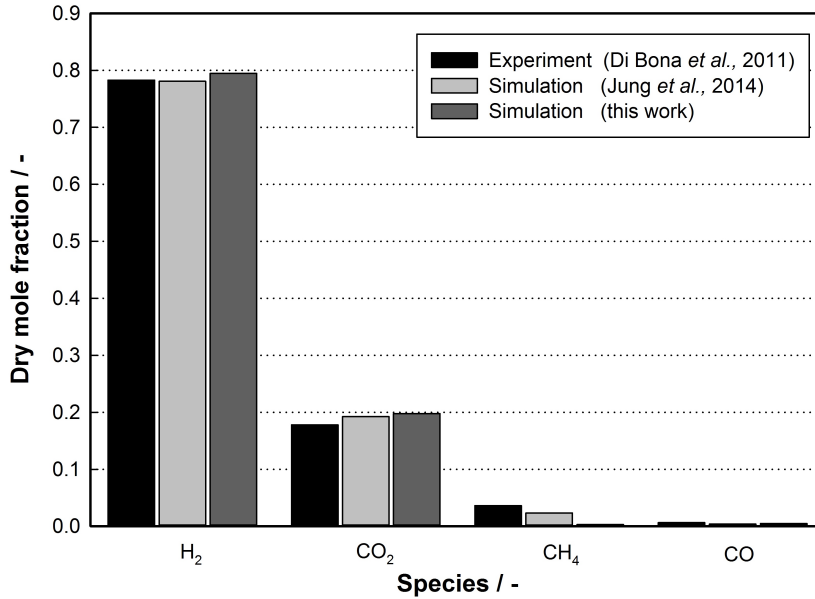
Figure 4.4: Comparison of the experimental and numerical dry reformate gas from the fuel processor.

Similar to the fuel-processor validation, the cogeneration system developed in this chapter is validated using numerical and experimental data from the literature of HT-PEM (Zuliani & Taccani, 2012) and LT-PEM (Briguglio *et al.*, 2011) based systems. In Zuliani and Taccani (2012), commercial software Aspen Plus^{TM}is employed to simulate the performance of a natural gas-fuelled system using energy balances. Briguglio *et al.* (2011) conducted experiments to explore the effects using direct water injection in the cathode of an LT-PEM system operating at 73 °C as a heat recovery strategy from the stack and its suitability for cogeneration application. The input parameters and the results are shown in Table 4.2. The model shows a voltage deviation of 10% from the HT-PEM system. This can be attributed to the chosen operating current density which leads to a high voltage. There is significant voltage deviation (25.7%) in the model output compared to the LT-PEM system. This is due to two factors: the lower operating current density and pure hydrogen operation in the LT-PEM system results in a higher voltage. In terms of electrical efficiency, the model produces a similar efficiency to the HT-PEM with a deviation of 3.7%, while there is a big deviation (37%) from the LT-PEM system. The high deviation from the LT-PEM system is due to the higher operating voltage and the use of pure hydrogen which has a higher calorific value than methane. The model cogeneration efficiency compares well with both the HT-PEM and LT-PEM system with deviations of 1.8% and 0.8%, respectively. From the analysis it can be concluded that the

model developed in this study can accurately predict the performance of a fuel cell-based micro-cogeneration system.

Table 4.2: Validation of cogeneration system

Variable	HT-PEM[a]	HT-PEM[b]	LT-PEM[c]
Operating conditions			
Current density (A m^{-2})	3000	4200	2000
Operating temperature (K)	423	433	347
Steam-carbon-ratio	3	3.5	-
Fuel stoichiometry	1.25	1.2	1
Air stoichiometry	2	2	-
System outputs			
Power (W$_e$)	1000	1000	4800
Cell voltage (V)	0.55	0.5	0.74
Fuel processor efficiency (LHV)	80.9	78	-
Electrical efficiency (LHV)	27.7	26	44[*]
Thermal efficiency (LHV)	51.7	52	36[*]
Cogeneration efficiency (LHV)	79.4	78	80[*]
Fuel Type	NG	NG	Hydrogen

[*] Values based on HHV
[a] Numerical data by authors
[b] Numerical data of a HT-PEM system (Zuliani & Taccani, 2012)
[c] Experimental data of a LT-PEM system (Briguglio *et al.*, 2011).

4.3   Simulation results

A parametric study was conducted to investigate the effect of different operating parameters on the system's performance. Accordingly, to study the behaviour of the fuel processor, the mixed effect of a variation of combustor equivalence ratio and the fuel ratio on the performance of the systems were considered first. Based on this, a case study in which four operating points, based on the combination of the two parameters were chosen. In the four points chosen, the required constraints, such as the CO concentration

in the fuel cell anode inlet, were met. From a design perspective, to maintain realistic dimensions of the cogeneration system, the fuel cell stack design parameters as shown in Table 4.3, and all the heat exchangers' geometries were kept constant in each of the cases considered.

Table 4.3: Parameters kept constant during the simulation.

Parameters	Value
Stack operation temperature (K)	423
Current density (A m^{-2})	3000
No of cells in a stack	65
Fuel cell active area (m^2)	0.01

4.3.1 Combustor operating parameters

As an initial investigation, the effect of the variation of the combustion parameters (fuel ratio and equivalence ratio) on the fuel processor performance was investigated. The combustion of the fuel and air is a chemical reaction that strongly depends on the composition of the fuel and air fed to the combustor. The fuel ratio (FR) was defined as the ratio of the combined flow rate of combustion fuel (auxiliary CH_4 and combustible gases in the anode off-gas) to that of the CH_4 flow rate into the reformer. It was varied by increasing the auxiliary CH_4 flow rate into the combustor. The equivalence ratio (φ) was defined as the actual fuel/oxidant (air) ratio normalised by the stoichiometric fuel/oxidant ratio into the combustor (Lee et $al.$, 2014).

$$\varphi = \frac{(FA)_{actual}}{(FA)_{stoich}} \tag{4.34}$$

Figure 4.5 presents the contour plots of the simulated cases carried out for fuel with a ratio range of 0.75 - 0.95 and equivalence ratios range of 0.45 - 0.75. The results of combined effect of the fuel ratio and equivalence ratio are summarized by plots of the temperature of the MSR and WGS reactors, fuel processor efficiency and fuel consumption rate. Figures
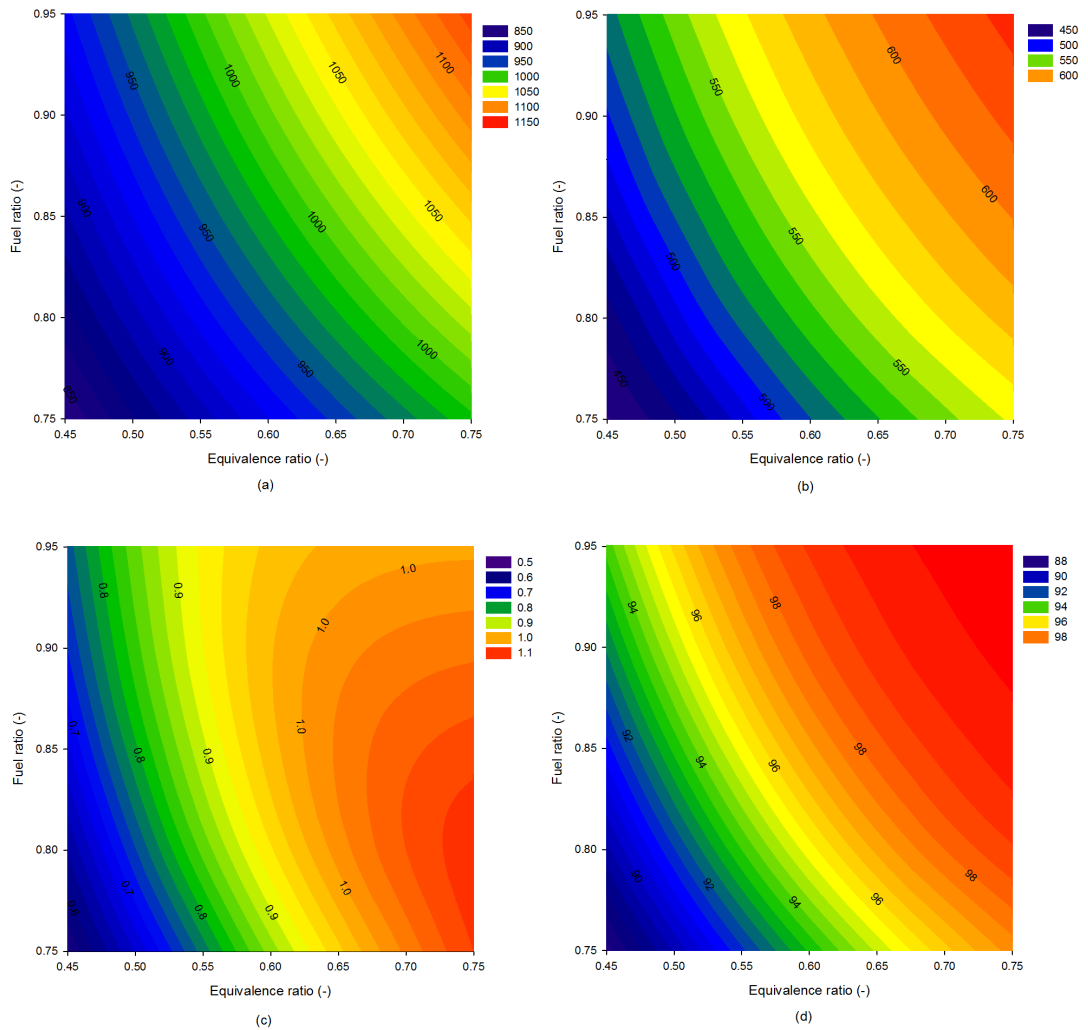
Figure 4.5: Effects of combination of equivalence ratio and fuel ratio. (a) Contours of MSR outlet temperature. (b) Contours of WGS outlet temperature. (c) Contour of fuel processor efficiency. (d) Contour of fuel consumption.

4.5a and b show the temperature at the outlet of the MSR and WGS reactors. It can be seen that increasing the equivalence ratio and fuel ratio results in a rise of reactor outlet temperatures. The simulation shows that the temperatures of the reactor outlets are highest when the φ approaches unity for all fuel ratios considered. This is caused by the increase in the heat of combustion due to increased fuel conversion in the combustor which raises the heat transferred to the reforming reactor. Figure 4.5c shows that for equivalence ratio less 0.56 the fuel processor efficiency increases with increased fuel ratios (a similar trend to the reactor temperatures). However, a peak of the efficiency is visible at different fuel ratios for equivalence ratios greater than 0.56. If the fuel ratio is higher than the peak fuel ratio the fuel processor efficiency decreases. This implies that when the reforming temperature rises above 1020 K, the fuel processor efficiency drops.

The fuel processor efficiency depends on the H_2 production rates from both the MSR and WGS reactor. The increased steam-reforming temperature increases the rates of the MSR reaction and decreases the WGS reaction. Since the magnitude of the reaction rate of the WGS reaction is lower in the steam reformer, H_2 production is expected to be high in the steam reformer reactor at high temperatures. In the WGS reactor, the effects of the high-temperature operation on the WGS reaction are visible. The higher temperature results in less CO being converted to H_2, reducing the H_2 production rate from the fuel processor, which explains the peak observed in the fuel processor efficiency at fuel ratios above 0.65. Another important variable with which to measure the performance of the fuel processor is the fuel consumption/conversion.

Figure 4.5d shows the relationship between the fuel consumption and the two fuel processor parameters (equivalence and fuel ratio). As the fuel consumption and the fuel processor efficiency are related, they are expected to exhibit the same trend. However, the results show that the fuel consumption does not reach a peak like the fuel processor efficiency. Unlike the fuel processor efficiency, the fuel consumption only depends on the CH_4 reforming in the MSR reactor. As mentioned above, increasing the reforming temperature results in an increase in CH_4 conversion towards H_2 and CO. This explains the similar trend of the fuel consumption and the MSR reactor temperature when the fuel and equivalence ratios are varied.

It is important to consider how the fuel processor parameters affect the quality of the reformate gas produced. Lee *et al.* (2014) showed that to maximise the synthesis gas production from a steam reformer for use in a SOFC and MCFC, the fuel ratio should not exceed 80%. In this work, the effect of varying the fuel ratio and equivalence ratio on the reformate gas composition is considered. Figure 4.6 presents the concentration (on a dry basis) of the reformate species entering the fuel cell stack. It can be noted in Figure 4.6a that the CH_4 concentration decreases with increased equivalence ratio for a range of fuel ratios. This is consistent with what was shown in Figure 4.5d, illustrating the increased temperature effects on CH_4 consumption. Figure 4.6c depicts an increasing trend in the H_2 concentration when the fuel ratio is increased at every equivalence ratio. The highest value for the H_2 concentration of 79.3% was obtained at high fuel and equivalence ratios. Figure 4.6d shows the carbon monoxide concentration in the fuel processor. For fuel ratios

between 0.75 - 0.85, a decrease in the CO concentration is observed when the equivalence ratio is increased. However, when the equivalence ratio reaches 0.56, the CO concentration starts to increase. For fuel ratios above 0.85, the CO concentration has been observed to increase monotonically with the equivalence ratio.
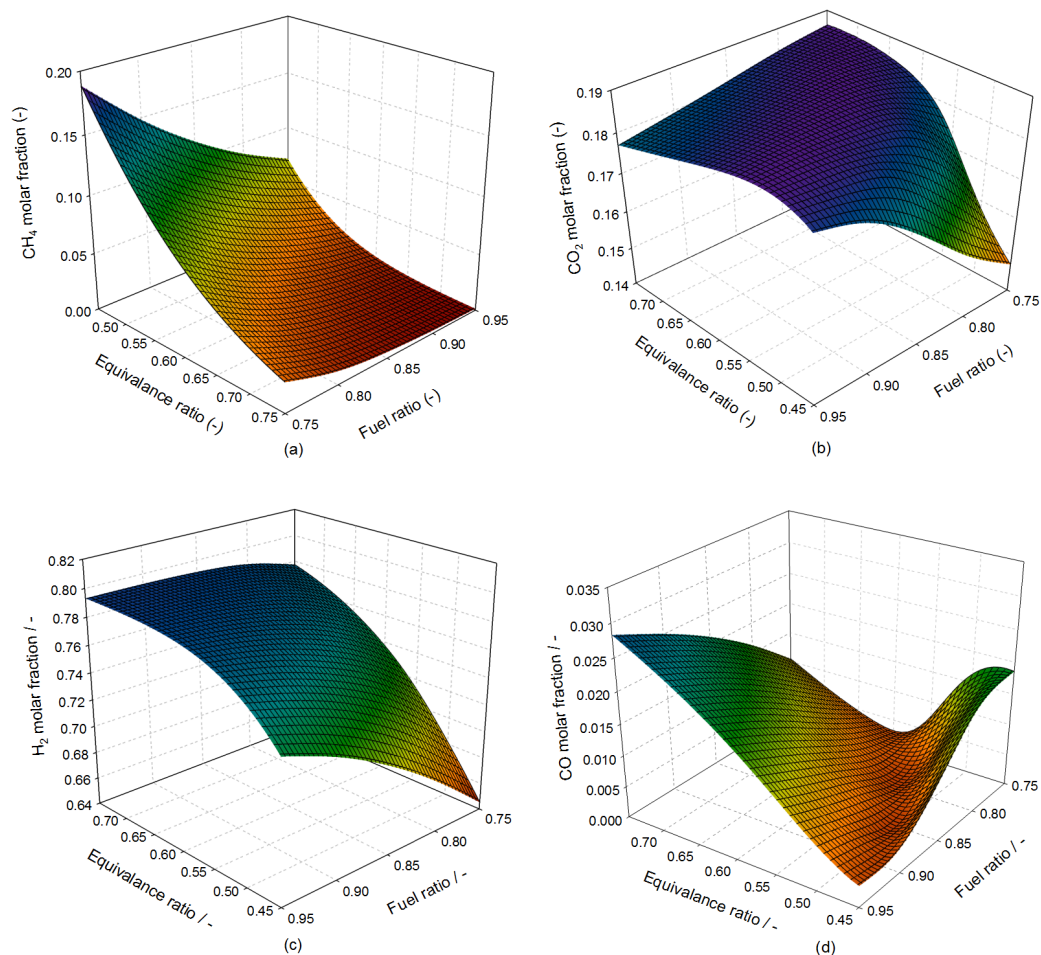
Figure 4.6: Results for reformate gas composition (dry basis) from the fuel processor with respect to equivalence and fuel ratio. (a) methane, (b) carbon dioxide, (c) hydrogen, (d) carbon monoxide.

4.3.2 System operating parameters

To investigate the behaviour of the system with various operating conditions, four operating points, based on different combinations of fuel ratio and equivalence ratio, were chosen and are presented in Table 4.4. The operating points were chosen so that they cover a wide range of CO concentration at the anode inlet that are within the acceptable levels in fuel cell stack.

Table 4.4: Operating conditions of the chosen cases

Parameters	Case A	Case B	Case C	Case D
Equivalence ratio	0.55	0.53	0.51	0.50
Fuel ratio	0.80	0.85	0.90	0.95
Fuel processor efficiency	0.854	0.853	0.854	0.855
CO anode inlet (%)	0.34	0.42	0.57	0.72

The effects of varying the S/C ratio (2.5 - 4) on the performance of the fuel processor are presented in Figures 4.7 and 4.8. It can be seen in Figure 4.7 that, increasing the S/C ratio from 2.5 to 4 results in a 14.67%, 13.92%, 12.49%, and 11.3% increase in the fuel processor efficiency for cases A, B, C, and D respectively. The main reason for this behaviour is that increasing the S/C ratio has a positive effect on the kinetics of the reactors in the fuel processor. It increases the rate of the steam reforming reactions in the MSR (equations 4.1 & 4.2) and the water-gas shift reaction in the shift reactor (equation 4.6) (Najafi et $al.$, 2015a). This leads to a higher conversion of CH_4 towards H_2 in the MSR and CO towards H_2 in the shift reactor for the same amount of methane fed into the system. The net effect of this is increased H_2 concentration (in dry basis) for the four cases in the reformate gas entering the fuel cell stack.
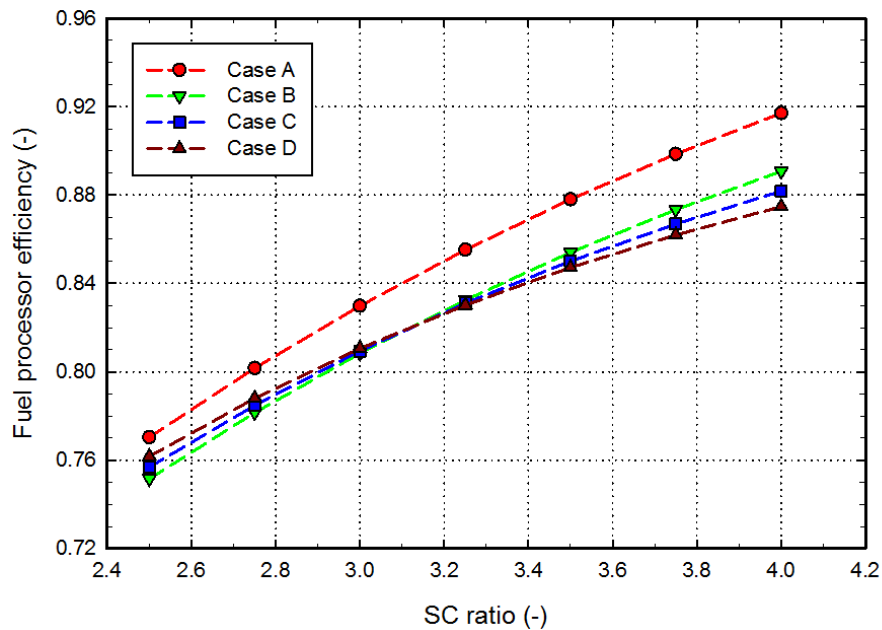
Figure 4.7: Results of fuel processor efficiency with respect S/C ratio.

The calculated carbon monoxide concentration (in dry basis) in the reformate gas entering the fuel cell stack for varying S/C ratio is presented in Figure 4.8. As it would be expected, increasing the S/C ratio from 2.5 to 4 reduces the carbon monoxide concentration by 50.5%, 57.3%, 65.6% and 68.3% for Cases A, B, C and D respectively. The influence of S/C ratio on the CO concentration and the fuel processor efficiency is in agreement with work published by Ersöz and Sayar (2015) for an autothermal reforming based system.
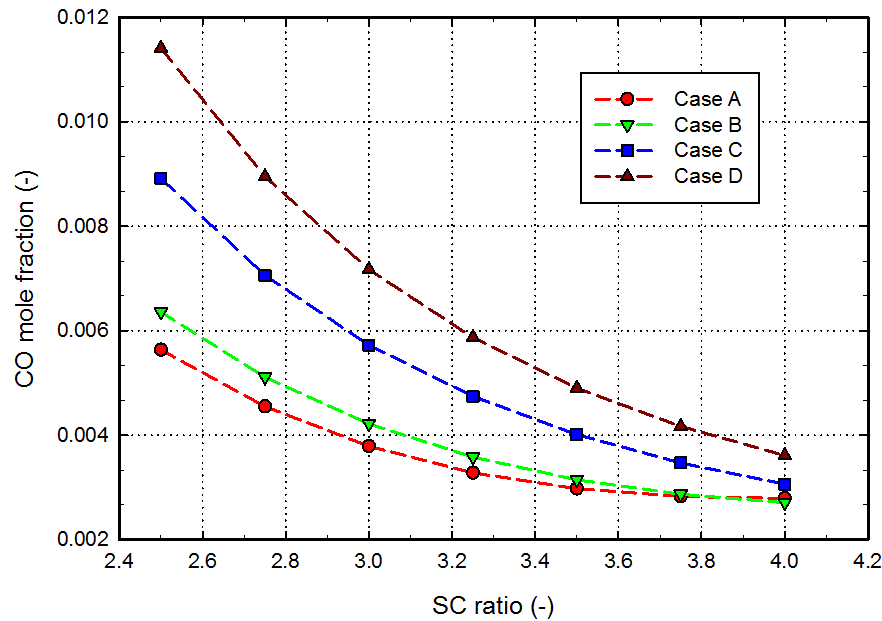
Figure 4.8: Results of carbon monoxide composition with respect S/C ratio.

The effect of varying the fuel cell stack operating temperature on the performance of the system is shown in Figures 4.9 and 4.10. In general, operating at a higher temperature results in high cell voltage as the electrochemical reactions occurring in the fuel cell are favoured in this condition. The characteristics of the membrane determine the upper limit of the operating temperature. For instance, the state-of-the-art phosphoric acid-doped PBI membranes experience acid leaching at temperatures higher than $473\,\mathrm{K}$, resulting in diminishing performance. From Figure 4.9, it is observed that by increasing the stack's operating temperature from $403\,\mathrm{K}$ to $443\,\mathrm{K}$ results in an increase in the stack's average cell voltage from 0.518 to $0.570\,\mathrm{V}$ for case A, 0.517 to $0.568\,\mathrm{V}$ for case B, 0.516 to $0.565\,\mathrm{V}$ for case C and 0.515 to $0.560\,\mathrm{V}$ for case D. This is as a result of improved reaction kinetics in the cell catalyst layer that decreases the associated cell voltage losses (Scott & Mamlouk, 2009). The cases A, B, C and D present different CO concentrations of 0.34%, 0.42%, 0.57% and 0.72% respectively in the reformate gas supplied to the fuel cell stack.
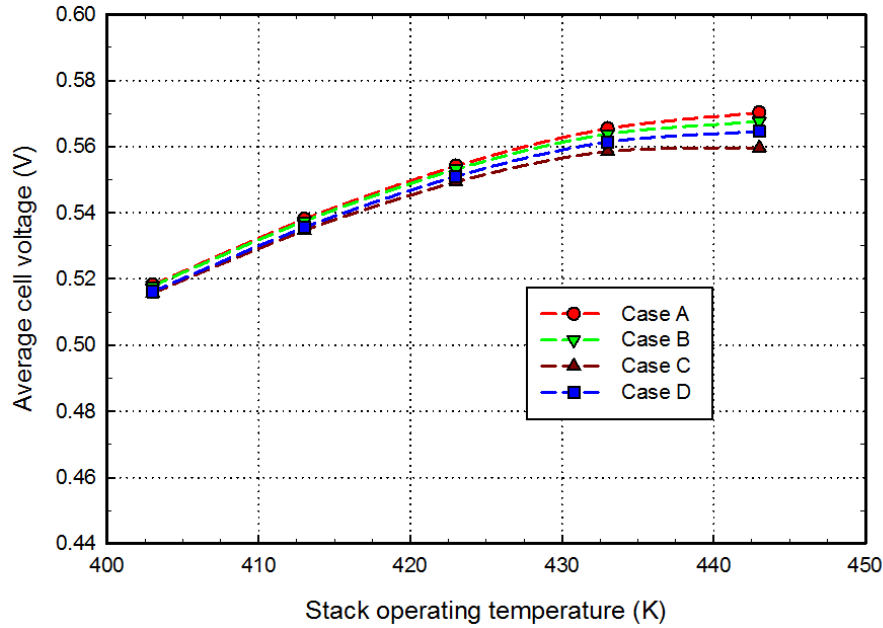
Figure 4.9: Results of temperature on the average stack voltage.

The presence of CO in the reformate gas leads to a surface coverance of active catalyst sites due to the adsorption of CO on the catalyst surface. The incremental presence of CO in the reformate gas from case A to D results in a decreased performance for the same temperature due to the decrease of active catalyst sites. For example, at $423\,\mathrm{K}$ the cell voltage for case A (0.34% CO) is $0.554\,\mathrm{V}$ and for case D (0.72% CO), it is $0.549\,\mathrm{V}$.

To explain the observed behaviour for each case in Figure 4.9, two cases can be considered, namely A and D. The reason for this is because the operating points for each case in Table 4.4 lead to a different carbon monoxide composition in the stack anode inlet, the lowest being in case A (0.32%) and the highest in case D (0.72%). As a result of this, Case A results in the highest cell voltage and Case D in the lowest one for all temperatures. It can also be noted that while there is a small difference in the cell voltage at lower temperatures, Case A and Case B show a better performance at high temperatures because of the low CO content in the anode inlet.

Figure 4.10 presents the variation of the stack's electrical efficiency at different stack operating temperatures. Since the power generated in the stack is proportional to the stack voltage, a trend similar to that of the voltage at different operating temperatures is observed (Najafi *et al.*, 2015a).
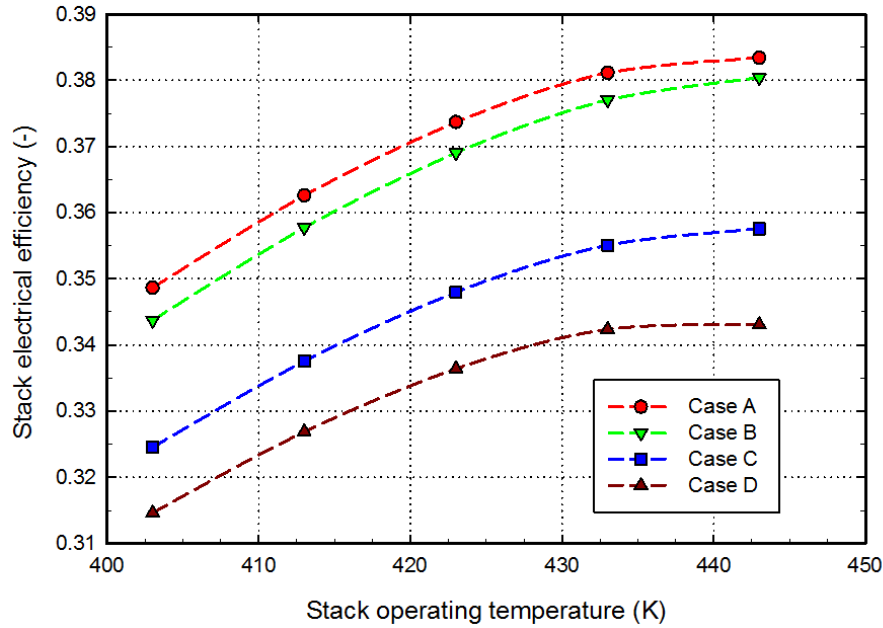
Figure 4.10: Results of temperature on the stack electrical efficiency.

The anode stoichiometric ratio, the ratio between the fuel-flow rate at the anode inlet and the rate of consumption of the fuel inside the fuel cell stack, is an important parameter in the system as it determines the concentration of fuel in the combustor (Arsalis *et al.*, 2011*a*) and operating temperature. Simulations of system performance were conducted at four anode stoichiometric ratios (1.25-1.55) and the results are presented in Figure 4.11.

As the stoichiometric ratio is increased from 1.25 to 1.55, the molar fraction of hydrogen in the anode off-gas is increased. This results in an increased heat of reaction and temperature of combustion gases because of the rise in the mass of fuel fed to the catalytic combustor. As shown in section 4.3.1, the temperature of the combustor is coupled with the reformer operating temperature and, as a result, the reforming temperature rises, thus increasing the fuel processor efficiency and system thermal efficiency. An increased temperature of combustion gases also leads to large amounts of heat available for thermal power generation in a cogeneration heat exchanger (HX-1). An increasing trend was observed in the cogeneration efficiency from 79% to 82% as a result of an increment (from 1.25 to 1.55) in the anode stoichiometric ratio for Case C. Although increasing the stoichiometric ratio results in better cogeneration efficiency, this is to the detriment of the stack's electrical efficiency as it decreases. The higher heat transferred to the
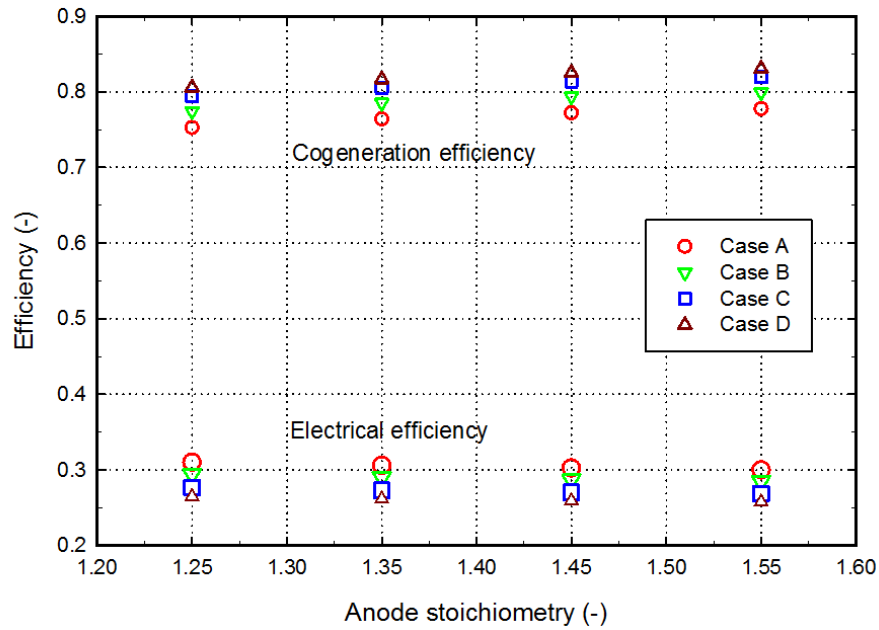
Figure 4.11: Results of electrical and cogeneration efficiency with respect to anode stoichiometry.

reformer leads to increased CO levels in the anode inlet, which subsequently results in decreased cell voltage. The effect of the stoichiometric ratio on the electrical efficiency is also shown in Figure 4.11 and a slight decreasing trend can be observed for all the cases considered.

Surface plots were generated in order to investigate the sensitivity of the electrical and cogeneration efficiency to the changes in the three parameters (S/R, stack temperature and anode stoichiometry). In doing so, the effect of changing two parameters within one simulation can be determined. For this analysis, Case C has been considered. Figures 4.12 and 4.13 present the sensitivity of the electrical and cogeneration efficiencies of the system. The system's optimal point for maximum electrical efficiency can be defined in Figure 4.12 (a,b,c). It corresponds to a high S/C ratio, high temperature and lower anode stoichiometry.
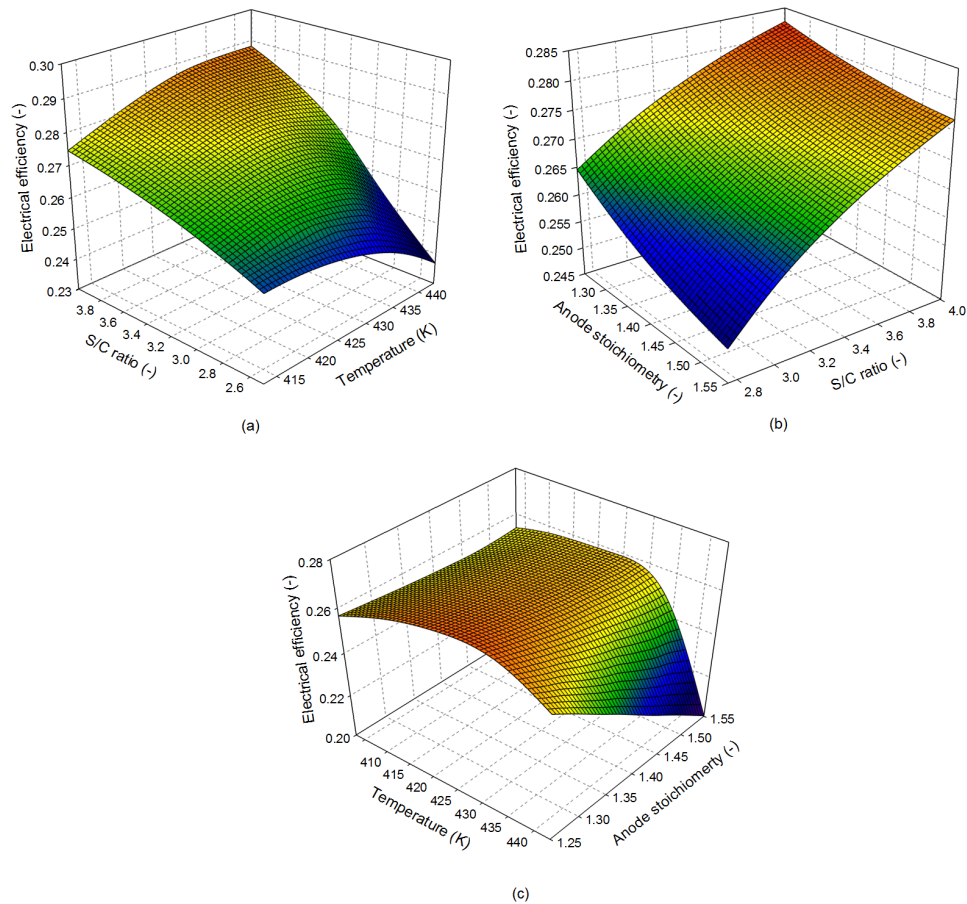
Figure 4.12: Sensitivity of the electrical efficiency with respect to (a) temperature and S/C ratio, (b) anode stoichiometry and S/C ratio, (c) temperature and anode stoichiometry.

In a similar manner, surface plots depicting the sensitivity of the cogeneration efficiency to the three parameters are presented in Figure 4.13 (a,b,c). For maximizing cogeneration efficiency high anode stoichiometry, high S/C ratio and high temperature present the optimal point. The selection of maximizing electrical or cogeneration efficiency depends on the operation strategy selected by the end user (Kupecki, 2015). The two commonly used strategies are the electrical load driven and thermal load driven operations. For electricity load driven operation where the system is operated to meet the electrical demand, operating point which maximizes the electrical efficiency would be considered as optimal. Similarly for a user with high thermal load demand, maximizing the cogeneration efficiency would be preferred.
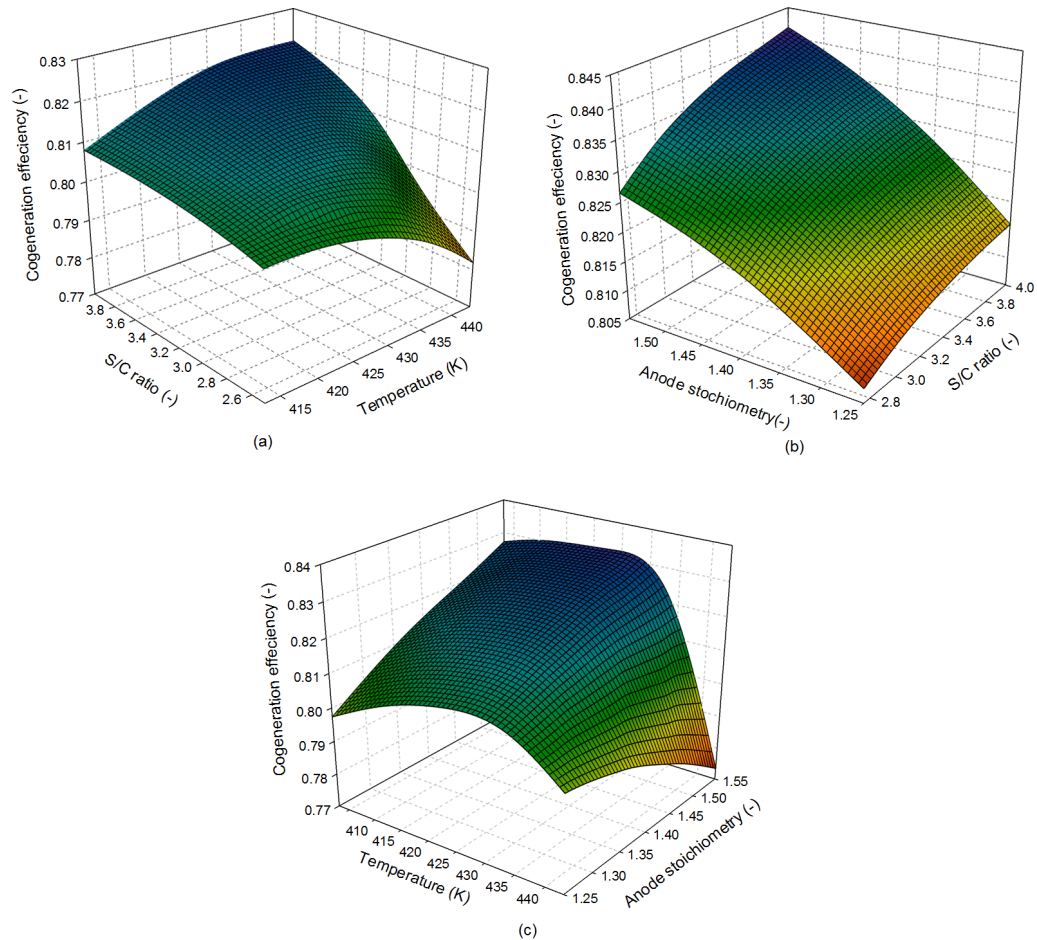
Figure 4.13: Sensitivity of the cogeneration efficiency with respect to (a) temperature and S/C ratio, (b) anode stoichiometry and S/C ratio, (c) temperature and anode stoichiometry.

4.4 Summary

In this work, a model for a $1\,kW_e$ HT-PEM fuel cell cogeneration system suitable for residential application is presented. In the first part of the investigation, a parametric study of the combustor parameters (fuel ratio and equivalence ratio) was conducted. It is shown that while a higher fuel ratio and equivalence ratio lead to high fuel processor efficiencies, they result in high levels of CO content in the reformate gas that are not acceptable to the fuel cell stack. Using four operating points that represent the combination of fuel ratio and equivalence ratio, a parametric study of the cogeneration system was conducted. A variation of the steam-carbon ratio, stack operating temperature and anode stoichiometric ratio on the system performance was considered. Increasing the SC ratio (2.5 - 4.0) resulted in increased fuel-processor performance, reducing the anodic CO molar fraction

to less than 0.4% for all the cases. The stack average cell voltage was shown to increase as a result of lower CO molar fraction in the anode inlet. It was shown that increasing the stack operating temperature (403 - 443 K) increased the electrical efficiency from 34.84% to 38.34% for Case A. It was also shown that while high-temperature operation results in increased voltage for all cases, better performance for cases with a lower CO content is obtained at high temperatures. Increasing the anode stoichiometric ratio from 1.25 to 1.55 has a positive impact on the cogeneration efficiency while the electrical efficiency drops, showing that the anode stoichiometry can be useful in regulating the system load demands.

Chapter 5

System Modelling and Analysis of a HT-PEM Fuel Cell Cogeneration System for Residential Application

5.1 Introduction

The residential sector consumes more energy than any other sector, with a worldwide average energy consumption of approximately 30% (Swan & Ugursal, 2009). This makes it an attractive target for the use of non-conventional energy conversion technologies that are efficient, renewable and environmentally friendly. These include a distributed power-generation (DG) system from renewable/sustainable primary energy resources (wind power, photovoltaic energy and biomass energy) or conventional energy resources (natural gas) (Donadel *et al.*, 2015). Among the drivers for the uptake of DG are the reduction in greenhouse gas emissions, energy resource optimisation, increased dependence on alternative energy sources, energy security, and so on (Lazarou *et al.*, 2013). Renewable energy systems may not always be practical as they might require large areas of land and are intermittent. On the other hand, a distributed fossil fuel solution (such as natural gas), together with zero emission power-generation technology (such as fuel cells), can provide a continuous energy supply at a high efficiency and a reduced environmental impact. This efficiency can be further enhanced when utilised in cogeneration technology.

Cogeneration systems generate electrical and thermal power (hot water and space heating) from a single source of fuel. These systems have gained interest in the residential sector because they offer a higher efficiency compared to the traditional production of electricity by a centralised utility operator and thermal power (hot water) production through a gas-fired boiler or by heating using electrical power. Due to the anticipated commercialisation of fuel cell-based cogeneration systems, agencies, such as the U.S. Department of Energy (DOE), have set technical performance targets in order for the systems to be acceptable to customers (Spendelow *et al.*, 2012). For instance, for the year 2015, the DOE expects the electrical and cogeneration efficiency to be more than 42.5% and 87.5% respectively. The work found in the literature for HT-PEM fuel cell cogeneration does not aim to reach these minimum performance criteria, which makes the results of not much use in a commercial application without more thorough validation and optimisation. One of the goals of South Africa, in their research on hydrogen energy and fuel cell technology, is to manufacture cogeneration systems to augment the drive towards cleaner and distributed power systems for remote households under the prevailing climatic conditions.

This chapter focuses on the off-design performance of a HT-PEMFC based micro-cogeneration system. The system's optimal operating point is determined through a parameter shift analysis. It is shown that by using this simple parametric analysis, the system can reach the desired technical performance of a fuel cell-based cogeneration system. The remainder of the chapter is organised as follows: Section 5.2 presents the model used to evaluate the micro-cogeneration system; in Section 5.3, the validation of the fuel cell stack, fuel processor and integrated system is presented followed by a discussion of the result of varying decision variables (fuel ratio, fuel-flow rate, current density and fuel utilisation) on the performance of the system; and the summary of the results are presented in Section 5.4.

5.2 Methodology

In this section, a steady-state model of the micro-cogeneration system contained within the boundary shown in Figure 5.1, which follows in 5.2.1, is developed. The system model is implemented in gPROMS® Model Builder (PSE (Process Systems Enterprise)., n.d.), an

equation-oriented environment for simulation and optimisation of a steady and dynamic process. Separate models for system components (fuel cell stack, methane steam reformer, water gas shift, catalytic combustor and heat exchangers) are developed separately and connected within a flow-sheet environment.

5.2.1 Description of the micro-cogeneration unit

The cogeneration system proposed in this work comprises of a two-stage fuel-processing unit (FPU) and a power unit (PU) and is presented in Figure 5.1. The first stage of the FPU is a high-temperature endothermic conversion in a methane-steam reforming reactor (MSR), where the natural gas is converted to a reformate gas mixture of H_2, CO, CO_2, CH_4 and un-reacted H_2O. The heat required by the endothermic reactions occurring in the MSR is supplied by a combustor fuelled with auxiliary natural gas and the anodic off-gas from the power unit. In the second stage, a low temperature, slightly exothermic, conversion of CO and H_2O towards H_2 and CO_2 takes place in a water-gas shift reactor (WGS). The HT-PEMFC stack does not require humidified reactant gases to operate and, as such, the water content in the reformate gases exiting the WGS is removed in a water-knock-out stage. The steam required for the reforming reactions in the MSR is produced by recovering heat from the reformate gas using three heat exchangers, HX-II, HX-III, HX-IV. The exhaust gases from the catalytic burner supply the heat needed to preheat the natural gas to the temperature required for the MSR and heating up the air to the temperatures required in the fuel cell stack, prior to entering the recuperator where it is used to heat water for thermal demand. This process can be seen in Figure 5.1
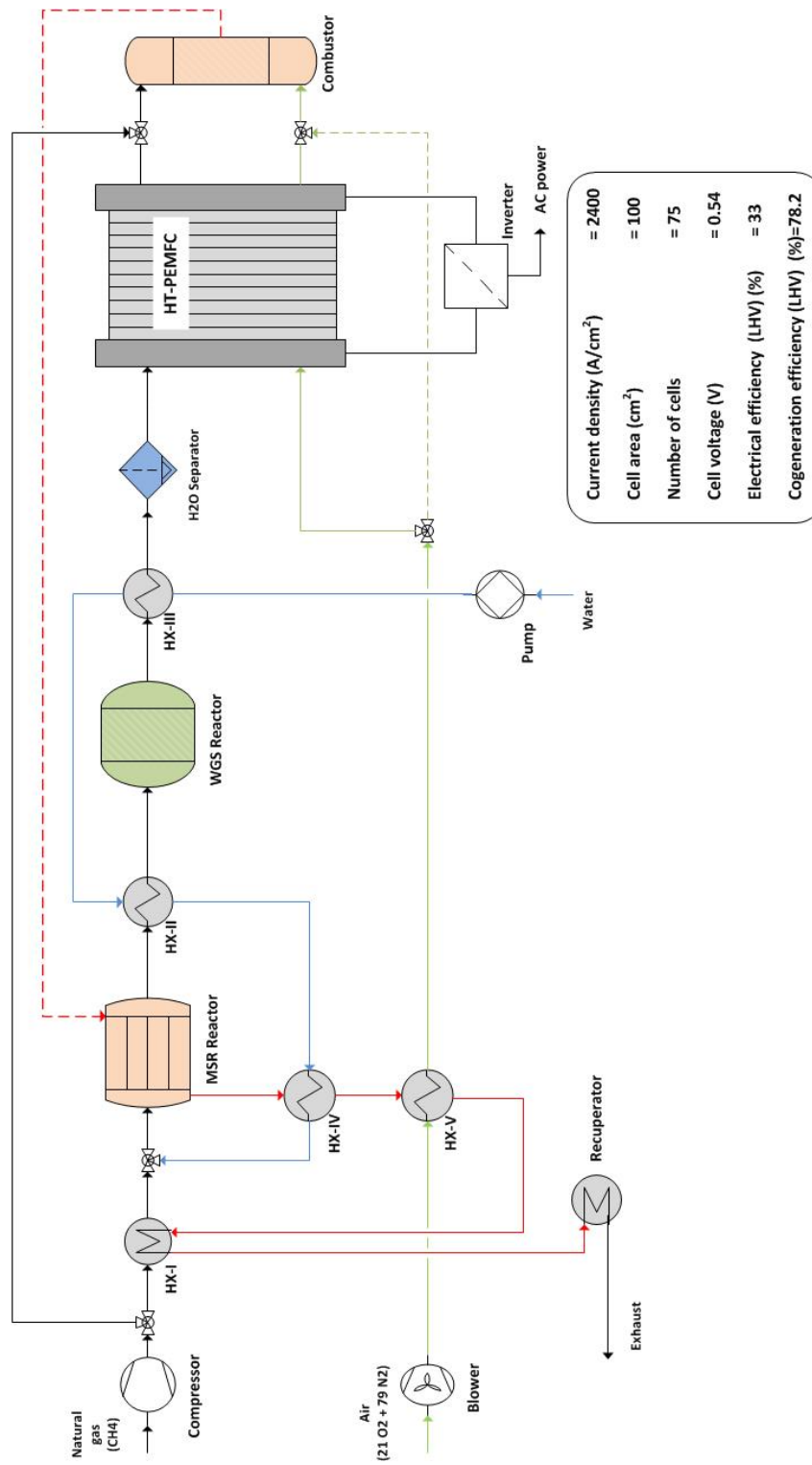
Figure 5.1: A process flow diagram of the residential cogeneration system.

5.2.2 Model of components

5.2.2.1 HT-PEMFC stack

The fuel cell stack model developed in Chapter 4 is used in this system's model. The fuel cell stack model was developed using a modular approach in which each component (flow channel, gas diffusion layer and catalyst layer) was individually modelled and the connectivity equations at the boundaries used to connect the adjacent layers. Figure 5.2 shows the schematic representation of the modelling domain considered in the fuel cell model development. The gas channels are considered as one-dimensional in the flow direction (Z) and one-dimensional through the MEA direction (X). Within the gas channel, H_2 and O_2 are gradually consumed due to the electrochemical reactions while H_2O is formed. Furthermore, the mass conservation is used in order to calculate the profiles of the species concentration along the gas channels. Mass transport within the GDL is modelled considering multi-component gas diffusion using the Stefane-Maxwell law. To account for the electrochemical reaction in the electrode, the Bulter-Volmer equations are employed. Details of the model governing equations can be found in Chapter 4.
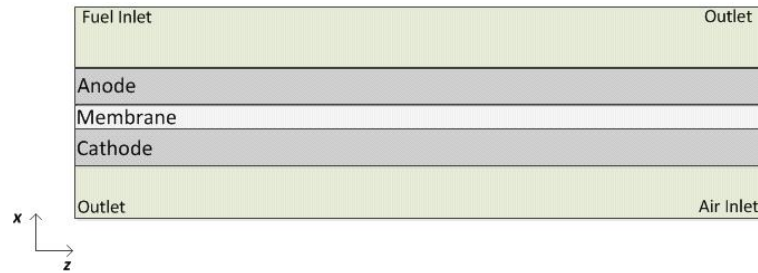
Figure 5.2: Modelling domain of the HT-PEM fuel cell.

The total cell voltage V_{cell} is given by:

$$V_{cell} = V_{ocv} - \eta_{act} - \eta_{ohm} \qquad (5.1)$$

where the thermodynamic equilibrium potential V_{ocv} is determined using the Nernst equation as a function of operating temperature, T (K) (Chippar & Ju, 2013):

$$V_{ocv} = 1.1669 - 0.24 \times 10^{-3}(T - 373.15) \tag{5.2}$$

The total electrical power produced by the fuel cell stack is:

$$P_{stack} = V_{cell}I_{cell}N_{cell} \tag{5.3}$$

where I_{cell}, and, N_{cell}, represent the single cell current and number of cell in the stack.

5.2.2.2   Power management system

The power management subsystem is needed to deliver the electrical power produced by the fuel cell stack to the end-user. It also modifies the fuel cell stack's electrical power so that it matches the load requirements in terms of voltage, type of current and power quality (Barbir, 2012). Furthermore, the subsystem coordinates the power from the system with that imported/exported from the utility grid. The electrical power output from the fuel cell stack given by equation 5.3, is a DC power. As appliances in households use AC, a DC/AC inverter is necessary to convert the DC power from the fuel cell stack to AC power suitable for household appliances. Part of this electrical power is also used for parasitic loads such as the compressors and pumps within the system. The inverter efficiency, η_{inv}, in this work is assumed to be 95% (Larminie & Dicks, 2003). Therefore, the net electrical power output of the system is (Larminie & Dicks, 2003):

$$P_{net} = \eta_{inv}P_{stack} - P_{prs} \tag{5.4}$$

where, P_{prs} is the parasitic power which includes the methane, $P_{CH_4,comp}$, and air, $P_{O_2,comp}$, compressors and the water pump, P_{pump}.

$$P_{prs} = P_{pump} + P_{CH_4,comp} + P_{O_2,comp} \tag{5.5}$$

$$P_{pump} = \frac{64.8 \times Hd \times SG}{367\eta_{pump}} M_w \tag{5.6}$$

where Hd is the head, SG the specific gravity and M_w the molecular weight of water.

$$P_{i,comp} = \frac{cp \times T_{i,in}}{\eta_c \eta_m} \left[\left(\frac{P_{out}}{P_{in}} \right)^{0.286} - 1 \right] \dot{m} \tag{5.7}$$

where cp is the specific heat capacity, $T_{i,in}$ the gas inlet temperature, η_c and η_m represent the compressor and mechanical efficiency respectively. P_{in} is the gas inlet pressure and P_{out} is the outlet pressure. $\dot{m}$ is the mass flow rate and the constant 0.286 represents the heat capacity ratio (Larminie & Dicks, 2003).

5.2.2.3 Steam-reforming reactor

Steam reforming is still one of the main stream hydrogen production technologies and accounts for more than 50% of the global hydrogen production (Holladay *et al.*, 2009). The steam-reforming reactor has been modelled as a homogenous 1-D steady state, non-isothermal compact heat exchanger. Two separate passages are considered, namely, the cold and hot passage. The steam-reforming reaction and the water-gas shift reaction proceed in the cold passage over a Nickel catalyst. The kinetic expressions developed by Xu and Froment (1989) have been employed. In the hot passage, the catalytic combustion gases pass through, providing the energy required for the endothermic reforming reactions. The reactions and kinetic equations employed in the modelling of the steam reformer are given in Table 5.1.

5.2.2.4 Water-gas shift reactor

The state-of-the-art HT-PEMFC can tolerate up to 3% (mole basis) of carbon monoxide content (>160 °C) (Chandan *et al.*, 2013) in the reformate gas supplied in the anode. The reformate gas exiting the MSR normally has somewhere between 8-11% CO content. In the water-gas shift reactor, this amount of CO is reduced to acceptable levels that will not

lead to poisoning of the catalyst in the fuel cell anode. The developed model for the shift reactor is based on the kinetic model (see Table 5.1) for high temperature WGS reaction presented in Kim et $al.$ (2005).

5.2.2.5 Catalytic combustor

The steam-reforming reaction is a highly endothermic reaction and requires energy to proceed. The anode off-gas is fed to the catalytic combustor, where the un-reacted hydrogen, methane and carbon monoxide are oxidised to supply the required energy to the MSR. Auxiliary methane is supplied to the combustor because the anode off-gas is not sufficient to maintain the required temperature in the steam reformer. The reactions occurring in the combustor and the associated kinetics on a platinum catalyst used in the combustor model are given in Table 5.1.

Table 5.1: Reactions and rates used in the fuel processor model.

Reaction	Rate expression	
Methane Steam Reforming		
(i) $CH_4 + H_2O \longrightarrow CO + 3H_2$	$r_1 = \dfrac{\frac{k_1}{P_{H_2}^{2.5}}\left[P_{CH_4}P_{H_2O} - \frac{P_{H_2}^3 P_{CO}}{K_1}\right]}{DEN^2}$	(5.8)
(ii) $CO + H_2O \longrightarrow CO_2 + H_2$	$r_2 = \dfrac{\frac{k_2}{P_{H_2}}\left[P_{CO}P_{H_2O} - \frac{P_{H_2}P_{CO_2}}{K_2}\right]}{DEN^2}$	(5.9)
Water Gas Shift		
(iii) $CO + H_2O \longrightarrow CO_2 + H_2$	$r_3 = k_o \exp\left(\frac{-E_a}{RT}\right)P_{CO}P_{H_2}\left(1 - \frac{P_{CO_2}P_{H_2}}{P_{CO}P_{H2O}K_{eq}}\right)$	(5.10)
Catalytic Combustor		
(iv) $CH_4 + 2O_2 \longrightarrow 2H_2O$	$r_4 = 1.3 \times 10^{11} \exp\left(-\dfrac{134,700}{RT}\right) y_{CH_4}\sqrt{y_{O_2}}$	(5.11)
(v) $H_2 + 0.5O_2 \longrightarrow H_2O$	$r_5 = 1.4 \times 10^3 \exp\left(-\dfrac{14979}{RT}\right) c_{H_2}$	(5.12)
(vi) $CO + 0.5O_2 \longrightarrow CO_2$	$r_6 = 2.25 \times 10^5 \exp\left(-\dfrac{28850}{RT}\right)\dfrac{p_{CO}}{(p_{O_2})^{0.5}}$	(5.13)

5.2.2.6 Heat exchanger analysis

For thermodynamic modelling of heat exchangers, the effectiveness-NTU method is the most generally used method and is appropriate when the output temperature of the hot and cold streams are not defined. A cross-flow compact plate-fin heat exchanger, with both fluids unmixed, is employed to model the characteristics of all the system heat exchangers.

5.2.2.7 Thermodynamic property

In general, the ideal physical properties of the foreign object (IPPFO) database in gPROMS satisfy most of the calculations of gas properties for the fuel cell cogeneration system. However, calculations of other physical properties, for example, the viscosity and conductivity of a multi-component gas mixture, can be calculated more accurately using related literature. The Wassiljewas equation (Equation 5.14) and Lindsaye-Bromley equation (Equation 5.15) (Todd & Young, 2002) are employed to estimate the thermal conductivity and viscosity of the multi-component gas mixture.

$$\lambda_m = \sum_{i=1}^{n} \frac{y_i \lambda_i}{\sum_{j=1}^{n} y_i \Phi_{ij}} \tag{5.14}$$

$$\Phi_{ij} = \frac{\varepsilon[1 + (\lambda_i/\lambda_j)^{0.5}(M_i/M_j)^{0.33}]^2}{[8(1 + M_i/M_j)]^{0.5}} \tag{5.15}$$

where, λ_m, represents the viscosity/thermal conductivity of the gas mixture, λ_i the viscosity/thermal conductivity of pure component, y_i is the mole fraction of the component, M the molecular mass of the components i and j, ε the numeric constant near unity and Φ_{ij} the interaction parameter for the gas mixture.

5.2.2.8 System metrics

The performance of the system is defined by thermal efficiency, electrical efficiency and cogeneration efficiency as shown in Equations 5.16 - 5.18. These efficiencies are defined at a lower heating value (LHV). The thermal efficiency, η_{th}, is defined by the total heat that can be recovered in the system, Q_{th} and the chemical energy input into the system. The system electrical efficiency, η_{elec}, is defined in terms of the net electrical power, P_{net}, and the chemical energy input into the system. The cogeneration efficiency, η_{cogen}, is defined in terms of the net power of system, P_{net}, the total heat that can be recovered in the system, Q_{th}, and the chemical energy input into the system.

$$\eta_{th} = \frac{Q_{th}}{(\dot{m}_{fuel}LHV_{fuel})_{inlet}} \tag{5.16}$$

$$\eta_{el} = \frac{P_{net}}{(\dot{m}_{fuel}LHV_{fuel})_{inlet}} \tag{5.17}$$

$$\eta_{cogen} = \frac{P_{net} + Q_{th}}{(\dot{m}_{fuel}LHV_{fuel})_{inlet}} \tag{5.18}$$

5.3 Results and discussion

5.3.1 System-model validation

The fuel cell stack's characteristics obtained from the model are validated by comparing with experimental results of Bujlo *et al.* (2013) at different operating conditions. In Bujlo *et al.* (2013), a performance measurement of a 1 kW$_e$ stack operating at 413 K was conducted using a fuel mixture containing H$_2$ with various CO concentrations (0.1, 0.3, 0.5 and 1%) as a feed gas. The comparison, demonstrated in Figure 5.3, shows that the model can sufficiently predict the polarisation characteristic of the HT-PEM fuel cell with an error of less than 6.4% and thus can be used to simulate its behaviour.
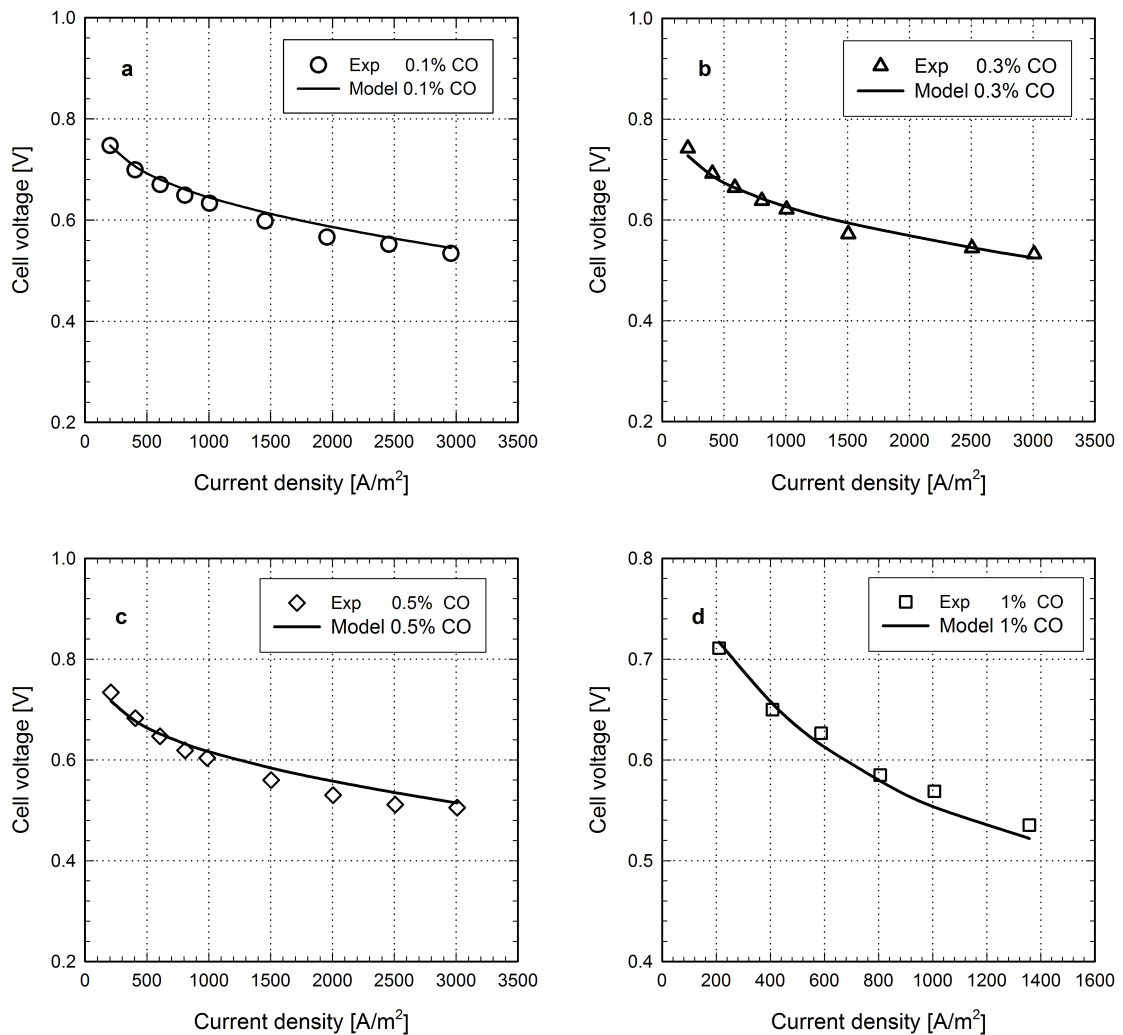
Figure 5.3: Validation of the model for the HT-PEM fuel cell stack.

The results obtained from the fuel processor were validated against the results from literature so as to evaluate the accuracy of the model. Two sets of data, one experimental and the other numerical, from fuel processors used for PEM fuel cell syngas production, were utilised in this process. The dry syngas composition produced in the fuel processor from the model, based on the numerical data of Arsalis *et al.* (2011*b*) and the experimental data from Di Bona *et al.* (2011), are compared in Table 5.2.

Table 5.2: Validation of the fuel processing sub-system.

Variable	HT-PEM	Arsalis *et al.* (2011*b*)	Di Bona *et al.* (2011)
Operating conditions			
Fuel feed (kg s^{-1})	3.51E-05	5.53E-05	8.4 (Nlmin^{-1})
Water feed (kg s^{-1})	1.38E-04	2.03E-04	22 (ccmin^{-1})
Combustor temperature (K)	1060	1093	1073
MSR temperature (K)	960	875.5	955
WGS temperature (K)	533.8	569.6	472
SC ratio	3	3.3	2.6
Syngas composition (vol)			
CH_4(%)	2.9	4.3	3.87
H_2 (%)	77.5	76.4	75.1
N_2 (%)	-	-	3.14
CO_2(%)	19	18.7	17.9
CO (%)	0.5	0.5	<10 ppm

Moreover, the outlet temperature at the exit of the reformer, WGS and the combustor are also compared for the three fuel processors. Taking into account the slightly different operating conditions, such as the S/C ratio and combustor temperature, the syngas composition from the model developed in this work, shows minor discrepancies from the numerical model of Arsalis *et al.* (2011*b*). When compared to the experimental data of Di Bona *et al.* (2011), the model shows a higher CO content. This is because the fuel processor is designed for an LT-PEMFC system which requires no CO in the stack feed. Overall, the fuel processor model developed in this work can accurately predict the per-

formance of a fuel processor for both numerical and experimental data. This shows the validity of the model for nickel-based reformer catalyst and copper-based water-gas shift catalyst.

The cogeneration system is validated by the analytical results from Zuliani and Taccani (2012) and Ersöz and Sayar (2015) and the performance is compared in Table 5.3. In Zuliani and Taccani (2012), a 1 kW$_e$ system that utilises a steam reformer, is analysed at different load conditions and efficiency plots presented. The system performance at design load is 26% and 78% electrical and cogeneration efficiencies, respectively.

Table 5.3: Validation of the cogeneration system

Variable	HT-PEM[a]	HT-PEM[b]	H-TPEM[c]
Operating conditions			
Current density (A m^{-2})	2400	4200	-
Operating temperature (K)	423	433	453
Steam-carbon-ratio	3	3.5	3
Fuel utilisation	80	83	80
Air stoichiometry	50	50	50
System outputs			
Power (W$_e$)	865	1000	1000
Cell voltage (V)	0.54	0.5	0.5
Fuel processor efficiency (%)	87.3	78	88.6
Electrical efficiency (%)	33.0	26	28.7
Thermal efficiency (%)	45.2	52	49.5
Cogeneration efficiency (%)	78.2	78	78.2
Fuel Type	NG	NG	NG

[a] Data by authors
[b] Data of an MSR-based HT-PEM system (Zuliani & Taccani, 2012)
[c] Data of an ATR-based HT-PEM system (Ersöz & Sayar, 2015)

In Ersöz and Sayar (2015), an auto-thermal reformer based 1 kW$_e$ system is evaluated to determine the characteristics of the fuel-processor (fuel flow rate, steam/carbon ratio, and reactor temperatures) on the performance of the system. While their system performance

varied, at optimal conditions it had an electrical efficiency of 28.7%, fuel processor of 88.6% and cogeneration efficiency of 78.2%. The characteristics of these systems are shown in Table 5.3 and are compared with the proposed model. The cogeneration system presented in this work shows a higher electrical and lower thermal efficiency whilst the cogeneration efficiency is equal to the models in the literature. The higher electrical efficiency can be attributed to the high operating voltage. The high operating current density for Zuliani and Taccani (2012) is due to the fuel cell stack characteristics of their system (cell active area $= 50 \, \text{cm}^{-2}$, number of cells $= 100$ and operating voltage $= 0.5 \, \text{V}$) and thus requiring a higher current density for 1kW_e power output.

5.3.2   Performance targets

The U.S. Department of Energy (DOE) has set some technical targets for 2015 for fuel cell-based cogeneration systems, some of which are presented in Table 5.4 (Spendelow *et al.*, 2012). For acceptance by customers, the DOE suggests a minimum electrical and cogeneration efficiency of 42.5% and 87.5%, respectively. Table 5.4 also compares the performance of the cogeneration system presented in this work as seen above in Table 5.3 (base case). It can be seen that, although the system performance compares well with previously published work, the system performance is below the targets set by DOE for 2015. For instance, the electrical efficiency is 33%, which is 9.5% below the DOE target. The cogeneration efficiency, on the other hand, is 78% at the design point which is also 9.5% below the DOE target.

Table 5.4: Technical targets of natural gas fuel cogeneration system compared to performance of those obtained for the base case.

Performance, cost, durability	Units	DOE target	Base case
Electrical efficiency	%	42.5	33
Cogeneration efficiency	%	87.5	78
Cost (2 kW$_\text{e}$ systems)	$/kW$_\text{e}$	1200	-
Start-up time (from 20°C)	min	20	-
Operating lifetime (time until >20% net power degradation)	hour	40,000	-
Degradation (with cycling)	%/1000-h	0.5	-

5.3.3   System performance

In the following section, the developed model is employed to conduct a parametric analysis in order to gain insight into the influence of the main variables in the system and to investigate off-design performance. The effects of varying equivalence-ratio, fuel-input flow rate and current density and fuel utilisation on the cogeneration system's performance were investigated.

5.3.3.1   Equivalence ratio

Figure 5.4 describes the influence of the equivalence ratio (φ) at different fuel ratios (FR) on the combustor and reforming temperatures. These two variables influence the combustion gas temperature and, by extension, the reforming temperature, thus the composition of the reformate gas entering the fuel cell stack. The equivalence ratio was varied from 0.5 to 0.66. These values are chosen such that the combustor temperature does not exceed a temperature of 1100 K and does not go below 950 K. The 1100 K limit is to ensure no damage is caused to the MSR and the 950K limit to ensure that the MSR temperature does not go below 850 K. The increase of φ increases the combustor temperature by 12% for all fuel ratios, which increases the heat transfer between the combustor and results in a 9% rise of the reformer temperature.
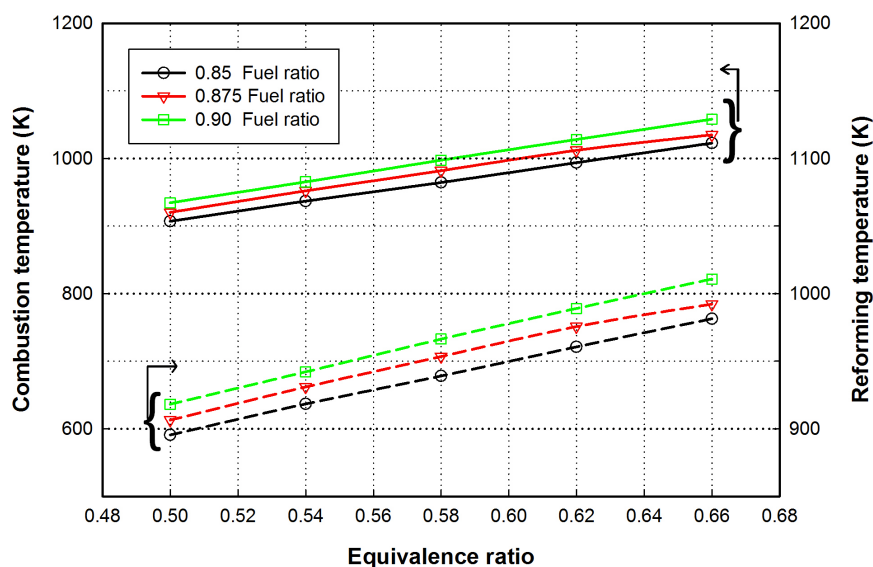
Figure 5.4: **Effect of equivalence ratio on combustor and reformer temperature.**

Figure 5.5a shows the electrical power output as a function of equivalence ratio. From this diagram, it can be noted that, at a low equivalence ratio ($\varphi = 0.5$), the power output is 795 W for a fuel ratio of 0.85, 828 W for a fuel ratio of 0.88 and 851 W for a fuel ratio of 0.90. This indicates that operating at a lower equivalence ratio requires high fuel ratios for better performance. However, when the equivalence ratio is increased, the performance of the FR = 0.9 declines, whereas that of FR = 0.85 and 0.875 rises first and then declines. The observed behaviour is attributed to the variation in the combustion gas temperature caused by the change in the equivalence ratio for the different fuel ratios.
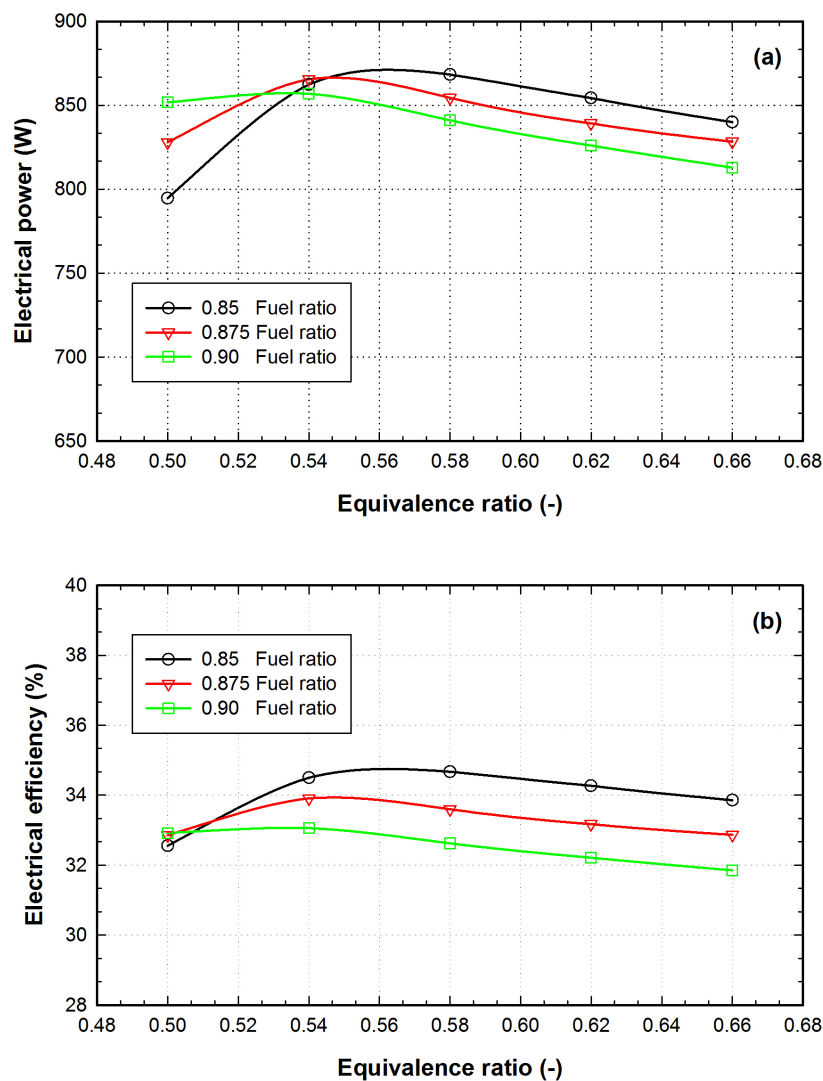
Figure 5.5: Effect of equivalence ratio on (a) electrical power and (b) electrical efficiency

Increasing the equivalence ratio, results in an increased combustor temperature (Figure 5.4). This, in turn, increases the fuel conversion in the reformer leading to a higher hydrogen yield. However, the elevated temperature of the syngas exiting the reformer

reduces the rate of the water-gas shift reaction in the shift reactor. This results in a reduction of the total hydrogen yield from the fuel processor, thus leading to a decline in electrical power generated in the fuel stack. It was noted that the maximum electrical power generation was achieved when a combination of fuel and equivalence ratios resulted in a combustor temperature of 960K. The maximum power generated was: $857\,\text{W}$ for φ = 0.90 & FR = 0.53; $866\,\text{W}$ for φ = 0.875 & FR = 0.55; and $872\,\text{W}$ for φ = 0.850 & FR = 0.56.

The system's electrical efficiency as a function of the equivalence ratio is shown in Figure 5.5b. It can be noted that the efficiency follows a similar trend with the electrical power output showing the highest efficiency when the power output is maximum. From these results it can be concluded that for optimal electrical power, the temperature of the combustor should be kept at 960 K. Figure 5.6 illustrates the thermal and cogeneration efficiency as functions of fuel and equivalence ratio. The thermal efficiency displays an inverse trend compared to the electrical efficiency. For fuel ratios 0.85 and 0.875, the thermal efficiency drops initially when equivalence ratio is increased until a value of 0.55. When the equivalence ratio is increased beyond this point there is no significant change in the thermal efficiency. The cogeneration efficiency is less sensitive to the variations in the fuel and equivalence ratio as a small decline of 1% is observed when the equivalence ratio is increased.
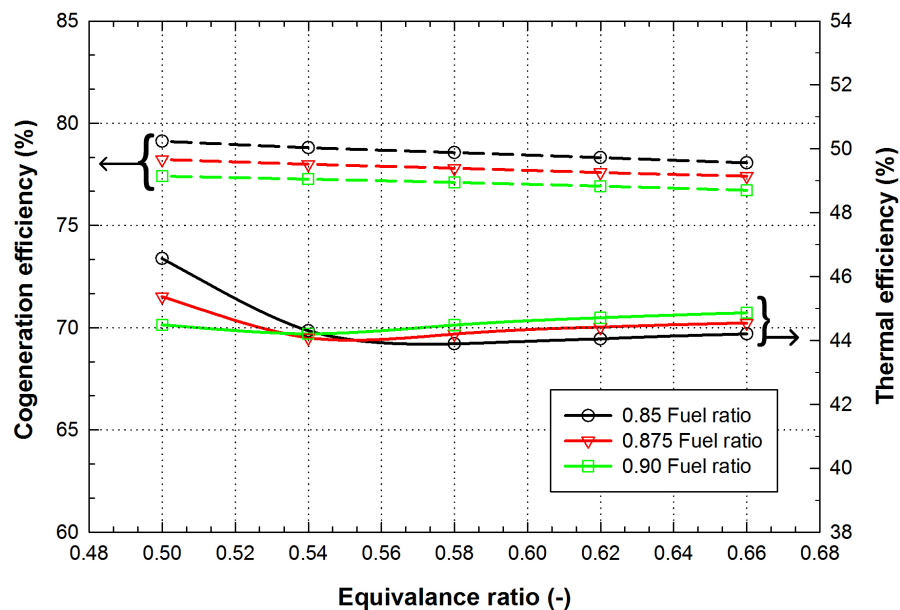
Figure 5.6: Thermal and cogeneration efficiency as functions of equivalence ratio

5.3.3.2 Input fuel flow rate

Simulations of the system's performance were conducted when the inlet fuel flow rate is changed. Kazempoor *et al.* (2009) showed that for a methane-fuelled SOFC system, increasing the fuel flow rate at a constant fuel utilisation, resulted in a drop of the voltage due to higher activation and ohmic over-potential. In this section, the influence was evaluated of varying the fuel flow rate from 0.14 to 0.22 kg h^{-1} for a constant voltage operation of 0.54 V and fuel utilisation of 80%. The results show that the current density rises by 5.2% when increasing the fuel flow rate from 0.14 to 0.22 kg h^{-1} in Figure 5.7. This is because, when the system's inlet flow rate goes up, more methane will be reformed into hydrogen, resulting in an increase of the rate of electrochemical reaction in the fuel cell stack which leads to the rise in the current density.
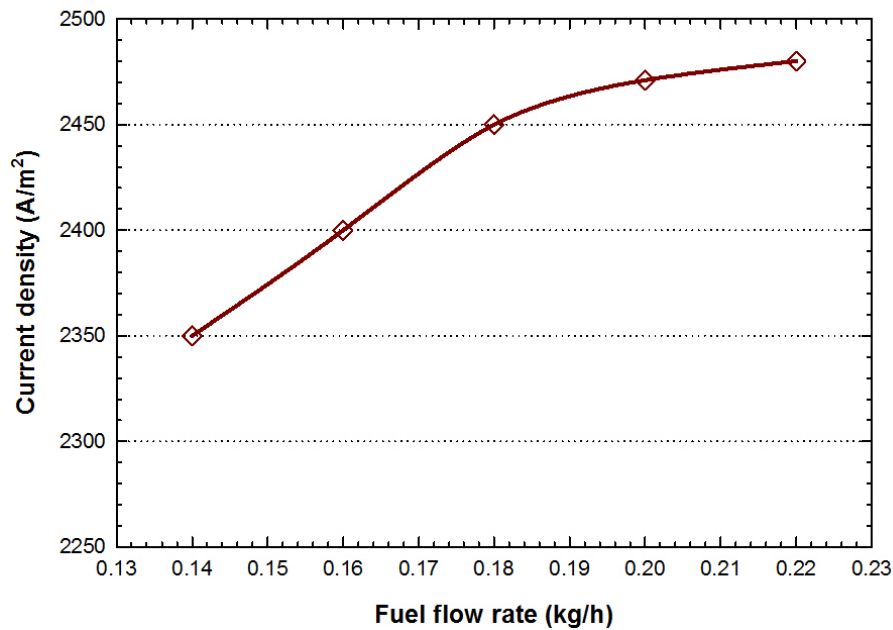
Figure 5.7: Effects of fuel flow rate on the current density.

Figure 5.8 shows the variation of the electrical and thermal power generation when the fuel flow rate is changed. Both the electrical and thermal power generation are observed to increase. The electrical power generated rises from 835 W to 858 W, corresponding to a 2.6% increase. It should be noted that when the fuel flow rate is increased, additional power from the methane and air compressor and the water pump are required. As a result, the parasitic power demand of the system rises. However, the effect of increased current density is more dominant, hence the observed electrical power increase. The thermal power, on the other hand, was found to be more sensitive to a variation in fuel flow rate, increasing from 1048 W to 1271 W. The noted gain in the thermal power can be attributed to the rise in the low heating value (LHV) of the anode off-gas into the combustor, which surpasses the energy requirements of the reformer, resulting in increased energy that is recoverable from the thermal cogeneration heat exchanger.
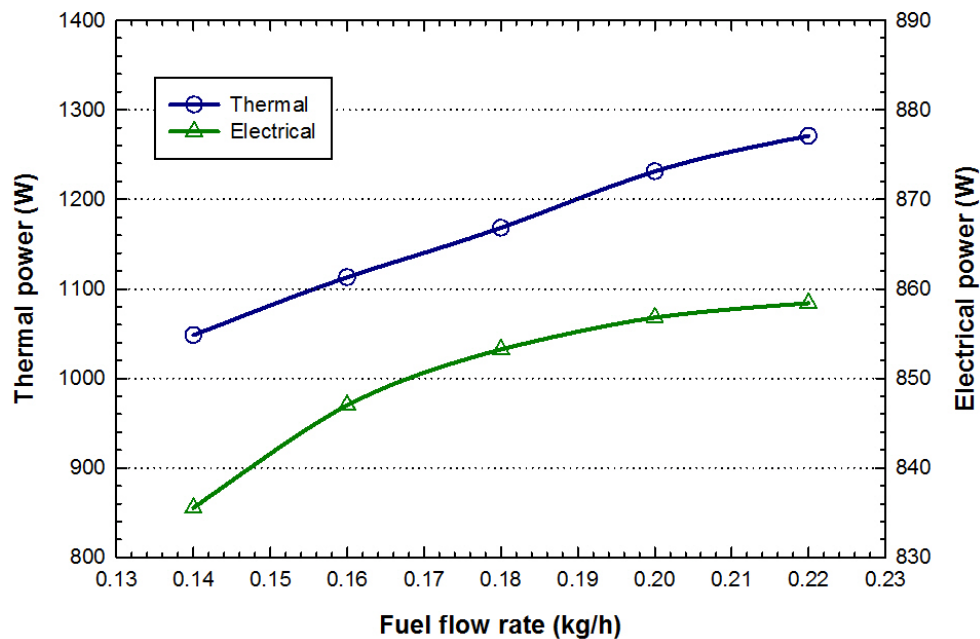
Figure 5.8: Effects of fuel flow rate on the energy outputs.

Figure 5.9 shows that varying the fuel inlet flow rate has a significant influence on the system's efficiency, indicating a 30%, 18% and 24% decline in the electrical, thermal and cogeneration efficiency. The diminishing efficiency shows that when increasing the fuel flow rate, more energy is lost with the mass flow of the exhaust gas due to the limits imposed by the fuel utilisation in the fuel stack and the area of the cogeneration heat exchanger. It can be noted in these results that operating with a high fuel-flow rate can increase the energy outputs. It may be undesirable to do so from an operating cost perspective.
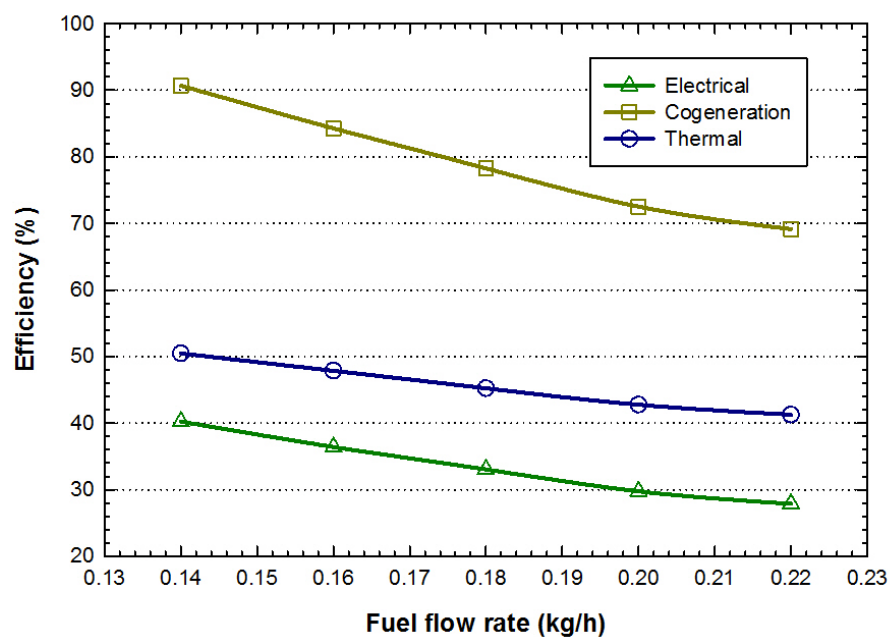
Figure 5.9: Effects of fuel flow rate on the system's efficiency.

5.3.3.3 Operating current density

The effects of varying the load on the system performance are presented in Figures 5.10 and 5.11. During the investigation, the current density from the stack was varied from $1000\,\text{A}\,\text{m}^{-2}$ to $2500\,\text{A}\,\text{m}^{-2}$. From the cell's current-voltage characteristics, operating at a lower current density is expected to lead to higher fuel cell stack efficiencies as the voltage of the stack increases (Barbir, 2012). Figure 5.10 shows the electrical and thermal power generated as the operating current of the system changes. It can be observed in this diagram that both the electrical and thermal power generation are improved when the operating current is increased. The electrical power rises from $388\,\text{W}$ to $838\,\text{W}$ (53.7%) and the thermal power increases from $390\,\text{W}$ to $1096\,\text{W}$ (64.4% rise).
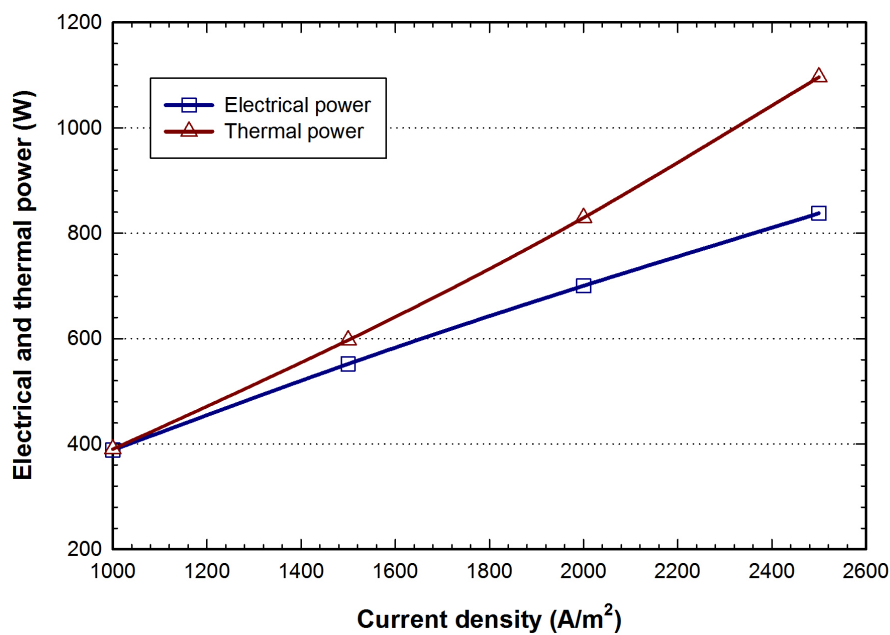
Figure 5.10: Effects of current density on the system power outputs.

The corresponding efficiencies are plotted in Figure 5.11, indicating an 11% decline in both the electrical efficiency and cogeneration efficiency, while the thermal efficiency remains unchanged. The decrease of the electrical and cogeneration efficiencies can be attributed to lower stack voltage and increased parasitic power (fuel and air compressors). Operating at the lowest current density ($1000\,\text{A}\,\text{m}^{-2}$) is shown to display the highest system efficiencies (Figure 5.11) and lowest energy outputs (Figure 5.10). This indicates higher efficiencies can be obtained when a higher voltage is chosen as an operating point. Operating at

a lower current density would be desirable when considering operational cost (Doherty *et al.*, 2010) because of higher system efficiencies. However, this would require the use of a larger cell stack (larger area or increased number of cells) to maintain the required electrical output, which will not be desirable when considering the capital cost of the system. This suggests that there must be a trade-off between voltage, power output and efficiency when choosing an operating point of the cogeneration system.
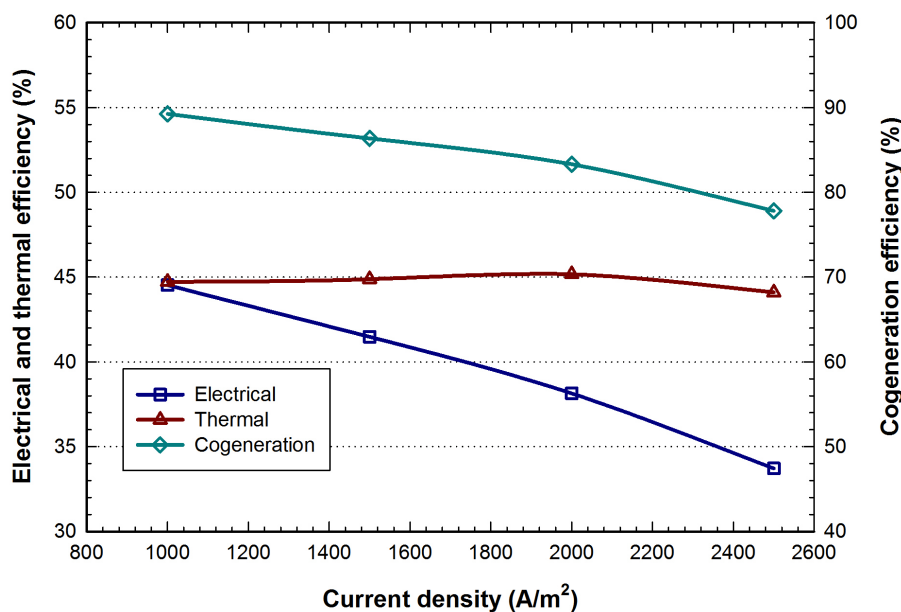
Figure 5.11: Effects of current density on the system efficiencies.

5.3.3.4 Fuel utilisation factor (Uf)

The fuel utilisation, defined as the ratio between the fuel consumed and the fuel supplied in the fuel cell stack, is a key parameter that influences the system's performance. Lower fuel utilisation in the stack improves the fuel processor performance due to increased combustion and reforming temperatures which results in a decreased CO content at the stack inlet (Najafi *et al.*, 2015a; Romero-Pascual & Soler, 2014). However, from the analysis in section 5.3.3.1, it has been shown that, for this particular design, the optimal combustor temperature is 960 K. As such, it is desirable to keep the combustor temperature constant at 960 K. To achieve this, the auxiliary methane and the excess air supplied to the combustor are adjusted accordingly during the simulations. This is expected to result in an unchanged reformate composition in the stack inlet. Figure 5.12 illustrates the effects of

the fuel utilisation on the system's energy outputs when it is varied from 65 to 80%.
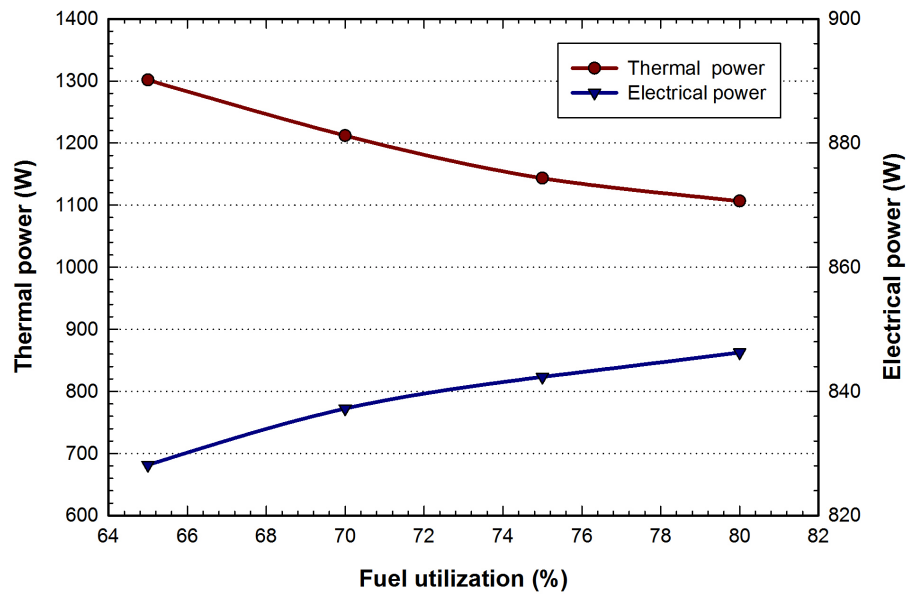
Figure 5.12: Effects of load on the system efficiencies

The electrical power output rises by 2% from 828 W to 846 W when the utilisation is varied. Bujlo *et al.* (2013) demonstrated that varying fuel utilisation (between 40% - 80%) has no influence on the voltage of a HT-PEM fuel cell stack. Therefore, the noted rise in the electrical power in this work can be attributed to the reduced parasitic power caused by the decreased excess air and auxiliary methane required in the combustor in order to keep the required reforming temperature. Low fuel utilisation results in an increase of the un-reacted hydrogen in the anode off-gas and increased heating value of the stream. The calculated H_2 mole fraction in the anode off-gas was 0.51 for Uf=65% and 0.35 for Uf=80% (dry mass basis). As a result of the higher concentration of H_2 at low Uf, the amount for auxiliary methane required in the combustor is reduced. The excess energy of the combustion gases and the energy recovered from this stream in the cogeneration heat exchanger rise. Consequently, the thermal power generated is 1300 W when the Uf=65%, presenting the highest value.

The net effect of lower auxiliary methane and higher thermal energy is reflected in the efficiencies presented in Figure 5.13. It can be observed in this diagram that increasing the Uf lowers the thermal efficiency by 9% and cogeneration efficiency by 10%. Minimal effect is observed in the electrical efficiency when the Uf is changed. Similar observations have been made by other authors (Arsalis *et al.*, 2011*b*).
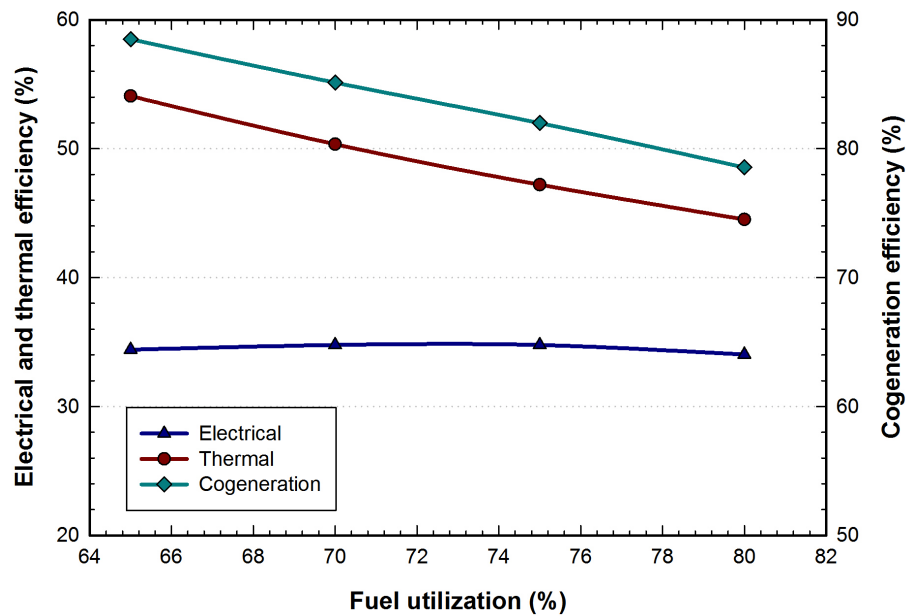
Figure 5.13: effects of fuel utilization on the system efficiencies

5.3.3.5   Approaching performance targets

Following the parametric analysis in the previous section, it can be seen that by selecting a combination of parameters, the efficiencies could be improved to meet the target efficiencies set out in Table 5.4 in Section 5.3.2. From the four parameters considered, the maximum electrical and the cogeneration efficiencies are 34.6% and 79.1%, respectively when the combustor temperature is varied. Both values are below the required targets. When varying the flow rate and the voltage, the set targets can be met for both the electrical and cogeneration efficiencies. On the other hand, changing the fuel utilisation is only beneficial in reaching only the cogeneration efficiency. Thus, when selecting an operating point, a combination that includes the fuel flow rate, voltage and fuel utilisation is desirable.

Table 5.5 compares some of the inputs and outputs from the base to the revised operating point. Revising the operating parameters results in an improved electrical efficiency at 42.8%, which meets the target value of 42.5%. The cogeneration efficiency is improved to 89% when the operating parameters have been improved. This value also exceeds the target set at 87.9% in Table 5.4.

Table 5.5: Improved performance with revised parameters

Variable	Base case	Revised case
Operating conditions		
Current density ($A\ m^{-2}$)	2400	2100
Operating temperature (K)	423	423
Steam-carbon-ratio	3	3.5
Fuel utilisation	80	76
Fuel flow rate ($kg\ h^{-1}$)	0.179	0.133
System outputs		
Power (W_e)	865	785
Cell voltage (V)	0.54	0.56
Fuel processor efficiency (%)	87.3	90.1
Electrical efficiency (%)	33.0	42.8
Thermal efficiency (%)	45.2	47.2
Cogeneration efficiency (%)	78.2	89

5.4 Summary

A model of a natural gas-fuelled cogeneration system, based on the HT-PEMFC, was developed for an investigation of the performance characteristics for a $1\,kW_e$ residential application. The cogeneration system model is employed to conduct a sensitivity analysis in order to evaluate the influence of the main variables on the system. The effects of varying catalytic combustor temperature, fuel input flow rate, and current density and fuel utilisation on cogeneration system performance were investigated, the results of which

reveal the following:

- There must be a trade-off between the electrical and thermal efficiency with respect to combustor temperature. Higher combustion temperatures generally increase the thermal efficiency whilst it decreases the electrical efficiency.

- Electrical and thermal power outputs are highest when the fuel flow rate is high. This is, however, at the expense of the system efficiencies which experience a 30%, 18% and 24% decline in net electrical, thermal and cogeneration efficiency respectively.

- From an operating perspective, the efficiency loss with increasing current density outweighs the reduction in power and therefore the stack should be operated at a lower current density.

- Operating at a lower fuel utilisation (65%) was shown to improve the thermal energy output by 15% and the cogeneration efficiency by 10%.

- The design conditions with regard to the DOE requirements for the cogeneration system developed in this work were identified as: voltage = 0.54 V, fuel utilisation = 76%, fuel flow rate = 0.133 kg h^{-1}, combustion temperature = 960 K and SCR = 3.5.

This chapter has shown that the HT-PEM fuel cell-based micro-cogeneration system can meet the technical performance requirements. In the following chapter, the system when operating in South Africa home, using energy consumption data, is evaluated. The performance of the system is used to estimate the environmental and economic benefit that could be made by utilising the system in a single family home.

Chapter 6

Application of a fuel cell cogeneration system in a South African single family residence

6.1 Introduction

The global problem of climate change has been key in the development of national energy policies for many countries. Decentralising power generation to districts and individual buildings presents one of the alternatives, especially with the utilisation of sustainable energy technologies. In particular, small-scale cogeneration and tri-generation systems which provide electricity, heating and cooling are amongst the technologies that are attractive in the reduction of primary energy consumption and carbon emissions. The proton exchange membrane (PEM) fuel cell is one of the most promising technologies for clean electricity generation for the built-environment environment (Upreti *et al.*, 2012; Maghanki *et al.*, 2013; Rosato & Sibilio, 2013; Staffell & Green, 2013; Elmer *et al.*, 2015). This is due to the ability to generate electricity with little or no carbon emissions depending on the fuel used. Moreover, in the process of generating electricity, the PEM produces heat which can be utilised further for heating (hot water and space) and cooling in cogeneration and tri-generation applications, respectively.

Beaussoleil-Morrison and Lombardi (2009) stated that utilisation of a fuel cell cogeneration system (FCCS) in an individual building could reduce the primary energy consumption and carbon dioxide (CO_2) emissions compared to a conventional system. The reduction is however dependent on the reference system being replaced and its energy consumption and rated CO_2 emissions. For instance, Pade *et al.* (2013) note that, in Denmark, the utilisation a FCCS will lead to reduced primary energy consumption and CO_2 emissions. On the other hand, for countries like France, a FCCS will replace power generation from nuclear energy. This will result in increasing natural gas consumption and CO_2 emissions (Pade *et al.*, 2013).

There is a potential of greater CO_2 emission reduction by utilising FCCS in South Africa as 90% of electricity is generated from coal-fired power stations. In this chapter, an analysis of a household's integrated micro-cogeneration system, based on a HT-PEM fuel cell, is investigated. The cogeneration unit is considered for a single family middle-class South African home (3-4 occupants) for the production of electricity and hot water for use on-site. The rest of the chapter is structured in the following way: Section 6.2 describes the fuel cell-based micro-cogeneration system and the energy demand profiles of the residential building; in Section 6.3, the simulation results are presented and the discussion of the three operating strategies, in terms of system power output performance, CO_2 emissions reduction and economic analysis, follows; and Section 6.4 is the conclusion.

6.2 Methodology

6.2.1 Fuel cell system

Figure 6.1 shows the superstructure of the FCCS considered for the household cogeneration system, which shows the process flow diagram of the main components. The FCCS consists of a two-stage fuel-processing subsystem (steam reformer and water-gas shift) which converts methane into a hydrogen-rich gas, a power-generating unit (HT-PEMFC) that converts the chemical energy from the gas into DC electrical power, a thermal management system for energy storage and a power conditioning unit (inverter) which converts the DC power from the power unit into AC power that is suitable for consumption in the

household. The $1\,\mathrm{kW_e}$ FCCS model, previously developed in Chapter 4, has been used in this study. Each subsystem/unit model was developed and integrated in the gPROMS Model Builder® platform. The system's model includes and physically resolves steady-state governing equations of a HT-PEM fuel cell stack, methane-steam reformer reactor, water-gas shift reactor, catalytic combustor, heat exchangers and inverter. The details of the system and components modelling can be found in Chapter 4.
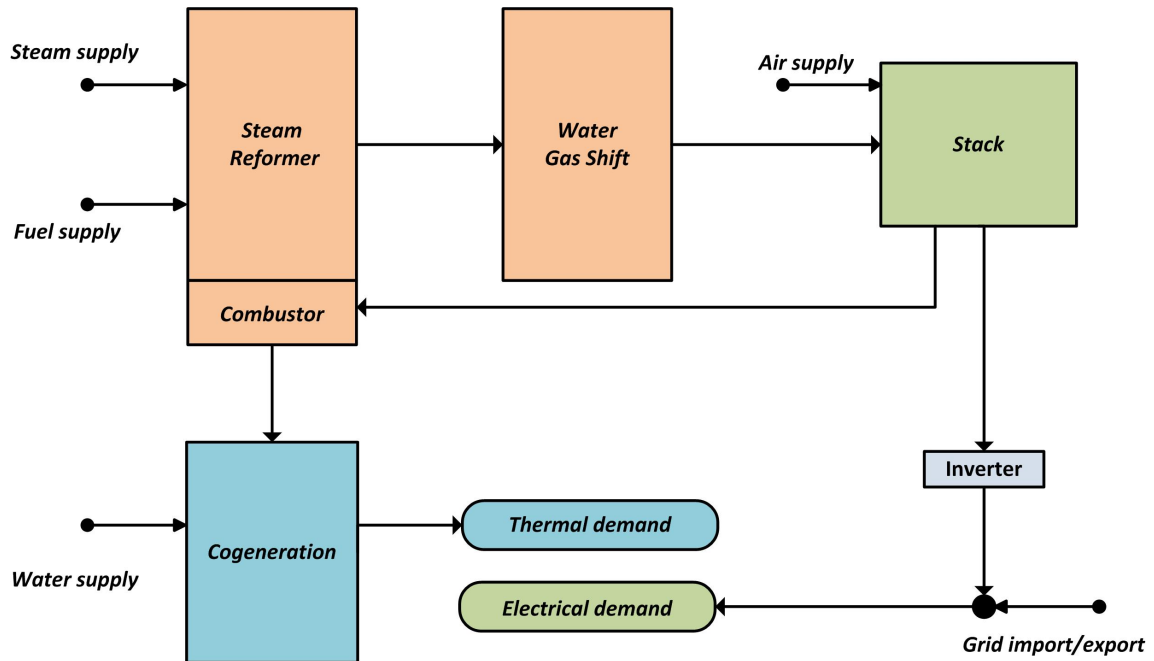
Figure 6.1: Super structure of the fuel cell cogeneration unit

Table 6.1 summarises the main specifications of the cogeneration system.

Table 6.1: Properties of the fuel cell cogeneration unit

Component	Parameter	Value
Fuel cell stack	Cell active area	$100\,\mathrm{cm}^{-2}$
	No of cell	65
	Membrane	PBI
	Current density	$0.2\,\mathrm{A\ cm}^{-2}$
	Stack Voltage	$35\,\mathrm{V}$
	Temperature	$150\,^\circ\mathrm{C}$
	Maximum power	$1.2\,\mathrm{kW_e}$
Reformer	Steam-carbon-ratio	3.5
	Temperature	974 K
Water-gas-shift	Temperature	523 K
Inverter	Efficiency	0.95

6.2.2 Energy demands

The household energy demand is divided into electrical and thermal demand. The electrical demand represents the electrical requirements of the household for electrical appliances and air-conditioning. The thermal demand represents the hot water requirements for the household. The energy-demand data can either be obtained by direct measurement on site or through a building simulation software, like TRNSYS, EnergyPlus, Flexisim, and others.

In this work, energy-demand data collected by the Energy Research Centre (Davis *et al.*, 2011) in the period between 2008 and 2010, was used. The data consist of electrical and hot water (thermal) consumption, which was collected in 10-minutes time intervals for a single family household in South Africa. Normalised daily electrical and thermal demand patterns for a representative day are shown in Figure 6.2 for the specific household as measured by Davis *et al.* (2011).
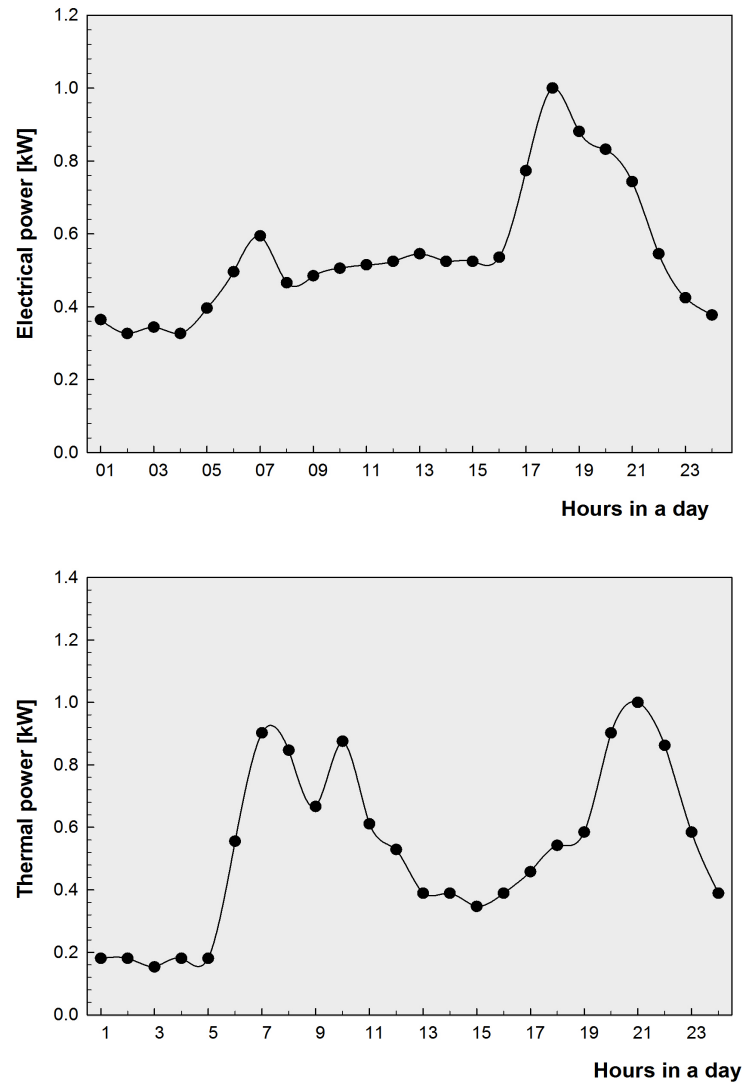
Figure 6.2: Energy demands of a household for a representative day's (a) electrical power, (b) thermal power. (Davis *et al.*, 2011)

6.3 Simulation results

6.3.1 Operating strategies

In the following section, three operational strategies, based on operating intervals of the cogeneration system during the representative day, have been proposed. These strategies are used to investigate the system's ability to meet the energy demands of the residence. For this purpose, two rated power-output units (0.6 and 0.4 kW$_e$) from the cogeneration system are considered in order to evaluate the effect of size on the performance. Furthermore, it is assumed that the size of the thermal storage tank is able to cover the periods

in which the cogeneration system is not operational because of the higher thermal power generated when in operation. Unlike previous work on operating strategies of HT-PEM based systems, the power demand of the user are taken into consideration in this work, instead of an assumed constant power demand.

6.3.1.1 Continuous mode

The first strategy presents a simple operating mode where the system is designed to operate at the same rated power output without any need to modulate/control so as to follow the demand-profile of the residence. In this mode, the FCCS is considered to be operating at a single point for each power output throughout the representative day.

Figure 6.3 shows the interaction of the FCCS's, residential demand and the grid. The electrical power demand is shown by the black plot. For the $0.6\,\mathrm{kW_e}$ rated power unit, all of the residence's electrical demand is supplied by the FCCS. It can also be noted that there is a substantial amount of electricity that is exported to the grid for this rated power output. The total power generated by the system during the representative day is $15.4\,\mathrm{kW_e}$ of which 53.5% ($8.24\,\mathrm{kW_e}$) is used within the residence and 46.5% ($7.17\,\mathrm{kW_e}$) is exported.

For the $0.4\,\mathrm{kW_e}$ unit, the power generated by the FCCS is able to meet the residence demand for the most part of the operating period. During operation, 94.5% of the residence's demand is met by the FCCS. However, between 17:00 to 22:00 the residence's power demand exceeds the power generated by the FCCS. During this period, the residence imports $0.45\,\mathrm{kW_e}$ from the grid. During the hours when the residential demand is smaller than the rated power, $2.87\,\mathrm{kW_e}$ is exported.
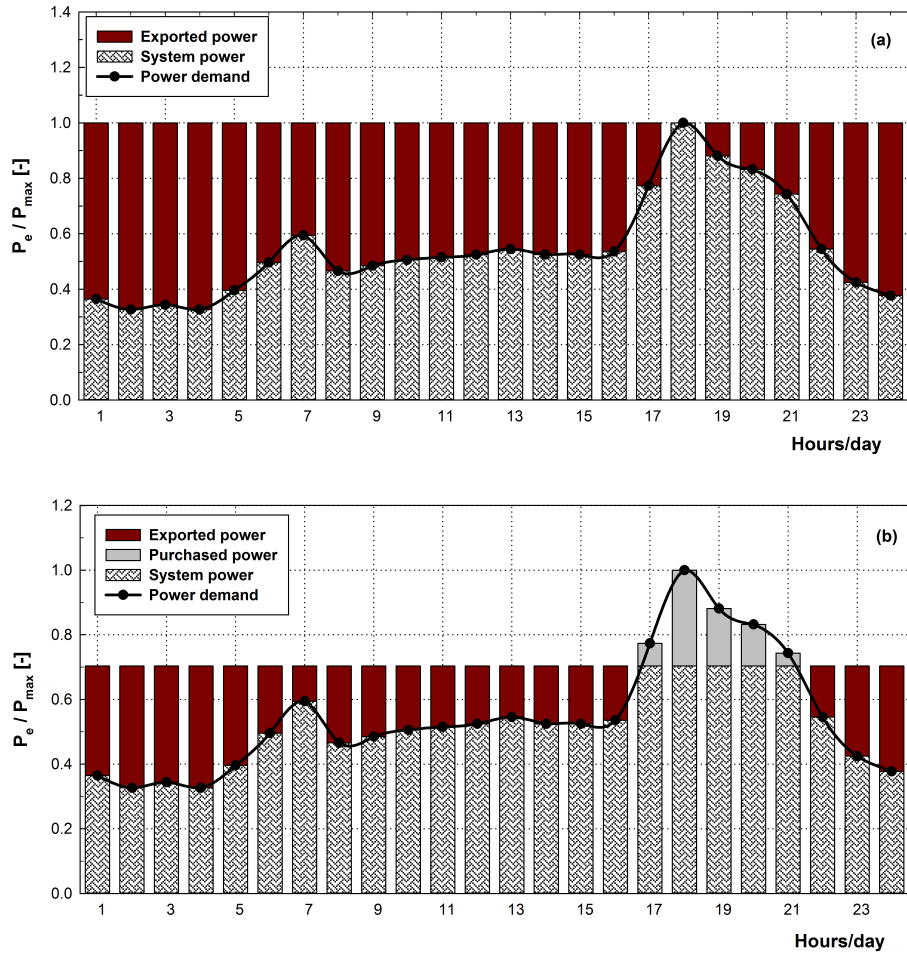
Figure 6.3: **Normalised hourly residential loads (a)** $0.6\,\mathrm{kW_e}$ **unit (b)** $0.4\,\mathrm{kW_e}$ **unit for continuous running.**

6.3.1.2 Day-night segmented mode

The second strategy is to have the FCCS operation divided into two segments: a day operation and a night operation. The day-operation mode covers the residence's power demand during peak and mid-peak hours of the representative day between 05:00 and 23:00. The night-operation mode covers the rest of the night, from 23:00 to 05:00. Owing to the low electrical demand during this period, the FCCS is switched off in this mode and all the electrical power demand is met by imported electricity from the grid. For this scenario, the electrical operation pattern for the $0.6\,\mathrm{kW_e}$ and $0.4\,\mathrm{kW_e}$ units are shown in Figure 6.4.

Similarly to the continuous mode, the $0.6\,\mathrm{kW_e}$ unit is able to cover all of the residence's power demand for the day-operation mode. For this rated power output, the FCCS covers
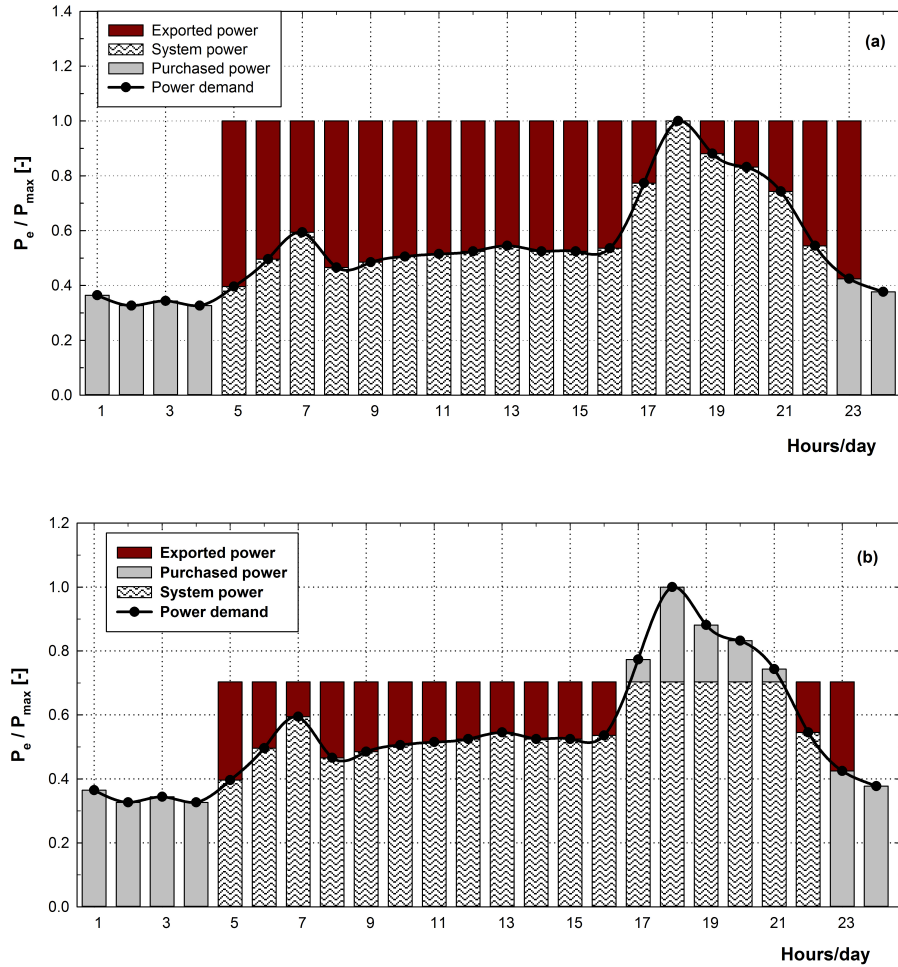
Figure 6.4: Normalised hourly residential loads (a) $0.6\,\mathrm{kW_e}$ **unit (b)** $0.4\,\mathrm{kW_e}$ **unit for day-night segmented mode.**

83.4% ($6.87\,\mathrm{kW_e}$) of the residence's total demand and exports 40.4% ($4.67\,\mathrm{kW_e}$) of the total power generated. For the night-operation mode, 16.6% ($1.37\,\mathrm{kW_e}$) of the power demand is imported. For the $0.4\,\mathrm{kW_e}$ rated power unit, the imported electricity increases to 22.0% ($1.81\,\mathrm{kW_e}$) of the total demand. The increase is due to the FCCS lower electricity output, which only cover 78% ($6.42\,\mathrm{kW_e}$) of the electricity demand of the residence during the operation.

6.3.1.3 Restricted-time mode

The third operating mode considered is the restricted-time mode, wherein the FCCS is operated periodically when there is a high electricity demand. In this scenario, the system is switched on for two time-periods, from 5:00 to 10:00 and again from 17:00 to 22:00. Figure 6.5 shows the residential load profiles for the restricted running-time mode. As the

FCCS is only available at specific periods, it is expected that the total power generated by the system will decrease. The total power produced during this mode is 8.33 kW$_e$ and 5.3 kW$_e$ which corresponds to 63.2% and 53.9% of the total residential demand covered by the 0.6 and 0.4 kW$_e$ systems, respectively. A substantial increase is noted in electricity import when operating in a restricted running time and when compared to continuous and day-night modes. The imported electricity accounts for about 36.7% of the residential demand for the 0.6kW$_e$ unit, while for the 0.4kW$_e$ unit, this value is 46.1%. Tables 6.2 and 6.3 summarised the characteristics of each operating strategy used.
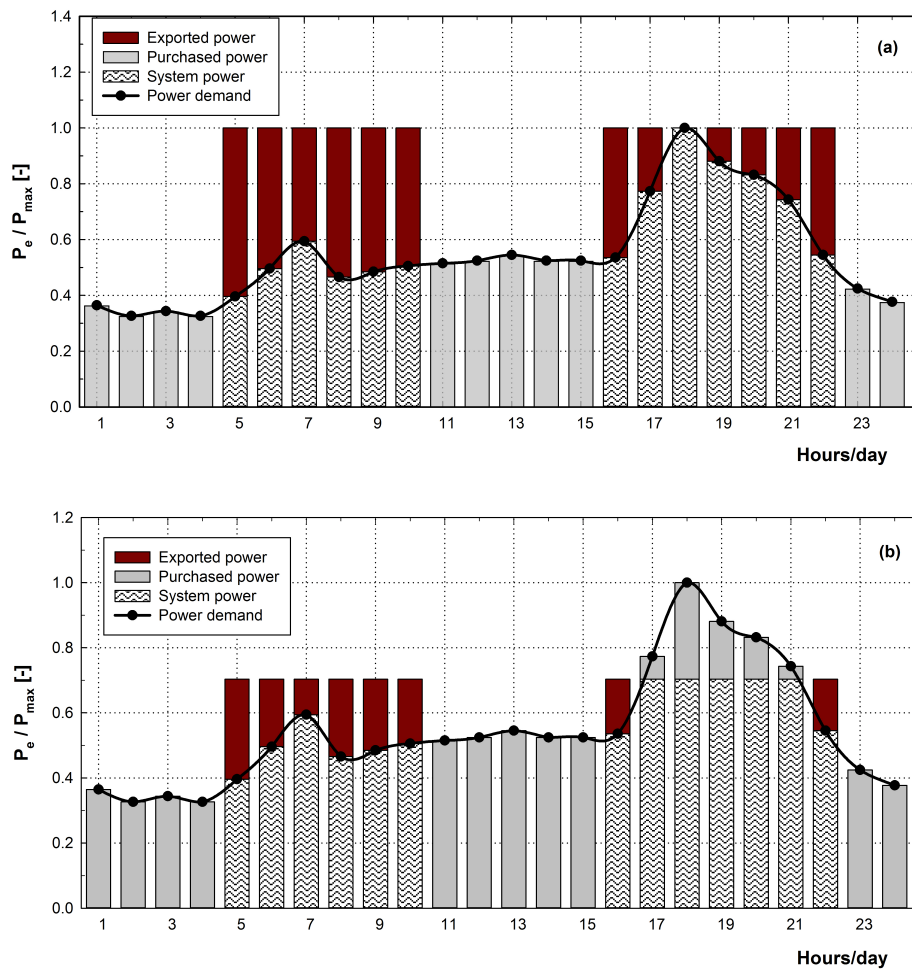
Figure 6.5: Normalised hourly residential loads (a) $0.6\,\mathrm{kW_e}$ **unit (b)** $0.4\,\mathrm{kW_e}$ **unit for restricted running time.**

Table 6.2: Electrical utilisation characteristic of the 0.6 kW$_e$ unit.

Operating mode	Period	Electricity generated (kWh)	Electricity imported (kWh)	Electricity exported (kWh)	Portion of demand met by FCCS (%)
Continuous	-	15.4	0	7.17	100
Constant output	05:00 - 22:00	11.5	1.37	4.67	83.4
Restricted running time	05:00 - 10:00 & 18:00 - 22:00	8.33	3.03	3.12	63.2

Table 6.3: Electrical utilisation characteristic of the 0.4 kW$_e$ unit.

Operating strategy	Period	Electricity generated (kWh)	Electricity imported (kWh)	Electricity exported (kWh)	Portion of demand met by FCCS (%)
Continuous running	-	10.7	0.45	2.87	94.5
Constant output	05:00 - 22:00	7.99	1.81	1.57	78.0
Restricted running time	05:00 - 10:00 & 18:00 - 22:00	5.3	3.80	0.89	53.9

6.3.2 Environmental assessment

The environmental benefit of utilising a fuel cell cogeneration system is one of the incentives for their introduction to residential sector. This section presents the assessment of the environmental benefits of the FCCS operating within a South African energy system framework. The environmental assessment compares the $0.6\,kW_e$ and $0.4\,kW_e$ unit to the traditional energy supply from the utility grid. To evaluate the environmental performance, the CO_2 emission reduction ratio (Ren & Gao, 2010) is used. It is defined by the difference between CO_2 emissions from the centralised power generation and from the micro-cogeneration as:

$$EER = \frac{E_{grid} - E_{fccs}}{E_{grid}} \times 100 \qquad (6.1)$$

where EER is the emission reduction ratio, E_{grid} and E_{fccs} represent annual CO_2 emission from the electricity production from the utility grid and emissions from the fuel cell cogeneration system, respectively. The CO_2 emission index from the centralised electricity production is $0.925\,kg_{CO2}$ kWh^{-1} (Spalding-Fecher, 2011). Table 6.4 presents the annual CO_2 emission results of the FCCS for the three operating strategies used.

Table 6.4: Environmental assessment of the cogeneration system.

Operating mode	Annual CO_2 emission (kg CO_2)	
	0.4 kW (ERR - %)	0.6 kW (ERR - %)
Continuous	3887 (52.0)	3735 (53.9)
Day-night	3414 (57.9)	3262 (59.7)
Restricted time	3305 (59.2)	3045 (62.4)

Firstly, it is noted that adapting the cogeneration system results in the reduction of carbon dioxide emissions for both the $0.6\,kW_e$ and $0.4\,kW_e$ units. The extent of CO_2-emission savings is, however, dependent on the operating strategy and the amount of electricity imported from the utility. Since the continuous running mode operates for longer peri-

ods, it results in high CO_2 emissions when compared to the day-night modulation and restricted-time operating modes.

For instance, when operating on continuous mode, the annual CO_2 emission is reduced to 3735 kg CO_2 and 3887 kg CO_2 for the $0.6\,kW_e$ and $0.4\,kW_e$ units, respectively. The restricted-time operating mode, even though it imports more electricity from the grid, seems to be more environmentally friendly for both the $0.6\,kW_e$ and $0.4\,kW_e$ units. This is because of the lower CO_2 emission when the cogeneration system is switched on which leads to a total reduction of 62.4% for the $0.6\,kW_e$ and 59.2% for the $0.4\,kW_e$ units. From an environmental emission perspective, the continuous operating mode should be avoided. Even though it leads to CO_2 emission saving, it is still more than what the day-night modulation and restricted-time mode can offer.

6.3.3 Economic evaluation

In this section, the economic evaluation of the fuel cell cogeneration system operating in the South African context is presented. The economic evaluation of the $0.6\,kW_e$ unit is limited to the cost benefits of introducing a fuel cell cogeneration system. Using the net present value (NPV), the payback period of investing in a cogeneration system can be determined from the initial cost C_o, running cost savings C_{rcs} and the inflation rate r (Fong & Lee, 2016).

$$NPV = \frac{log\left(1 - r\frac{C_o}{C_{rcs}}\right)}{log\left(\frac{1}{1+r}\right)} \tag{6.2}$$

A fuel cell-based cogeneration system's costs are still high, so much so that government subsidies are used to bring them down. The subsidies are expected to lower the purchase (investment) cost incurred by the customer (Staffell & Green, 2013). The US Department of Energy (DOE) has set cost targets of US$1000 per kW for small-scale fuel cell cogeneration systems by 2020. However Staffell & Green (2013) argue that this target is not feasible in the short term and a more reasonable target of US$3000-5000 per kW for 1-2

kW$_e$ systems is realistic and attainable by 2020. Therefore, the initial investment cost in the economic analysis is assumed to be US\$ 5000.

In table 6.5, a summary of the economic assessment using the 0.6 kW$_e$ unit for all operating strategies is given. The annual running-cost saving is the difference between the cost of utilising electricity from the grid to satisfy the electrical and hot water demands, and the cost of running the cogeneration system. Table 6.5 indicates the time it takes for the NPV to reach zero, which is 8.4, 9.7 and 11.1 for the continuous, day-night modulation and restricted-time operating strategies, respectively. The continuous mode has the lowest payback period because of the high amount of electricity that is exported to the grid, which generates income for the household. The payback period for all operating modes can be considered acceptable in lieu of the expected lifetime of a PEM fuel cell stack of 12 years (Elmer *et al.*, 2015).

Table 6.5: Economic assessment of the micro-cogeneration system

	Continuous	Day-night	Restricted
Initial cost of system (US\$)	5000	5000	5000
Installation cost (US\$)	1200	1200	1200
Energy cost of conventional (US\$)	1004.8	1004.8	1004.8
Energy cost of micro cogeneration (US\$)	471.6	423.5	410.1
Selling cost (US\$)	465.3	302.8	202.7
Extra maintenance (US\$)	33.7	25.3	18.2
Running cost saving (US\$)	964.7	858.9	779.1
Inflation	0.06	0.06	0.06
NPV (Year)	8.4	9.7	11.1

6.4 Conclusion

In this work, three operating strategies have been used to analyse the energy, environmental and economic performance of a fuel cell cogeneration system operating in the domestic

built-environment. A case study, involving a residential household in South Africa, has been used as an illustrative example to evaluate the performance of the FCCS. From the simulation results the following conclusions can be made:

- From an energy point of view, the 0.6 kW unit, operating in the continuous running mode, presents the best option. This is because it meets all the electrical requirements of the customer, resulting in no need to import electricity.

- Generally, introducing the FCCS results in large CO_2 emission reductions. However the restricted running time mode of the 0.6 kW unit presents the best CO_2 reduction.

- The ecnonomic appraisal of the system in the context of a South African household has shown that the continuous operating mode lead to the lowest payback period of 8.4 years.

Chapter 7

Conclusions and recommendations

7.1 Conclusions

This thesis investigates the performance of a HT-PEM fuel cell-based micro-cogeneration system. A mathematical model of the system was developed and implemented in gPROMS Model Builder. It consisted of a quasi-two-dimensional model of a HT-PEMFC stack, a methane-steam reformer, water-gas shift reactor and balance-of-plant components. The fuel cell stack model was validated with experimental data, whilst the fuel processor and system model were validated against numerical and experimental data from literature. The component and system models showed good agreement with these data sets, highlighting their validity.

In Chapter 4, the system model is used in a parametric study to investigate the performance of the fuel processor. The fuel processor efficiency, fuel consumption and species composition are determined as a function of combustor-fuel ratio and the equivalence ratio to find the optimal condition for a suitable composition of reformate gas feed to the fuel cell stack. It was found that an equivalence ratio of less than 0.56 and a fuel ratio of between 0.9-0.95, favour acceptable levels of CO in the reformate gas from the fuel processor. Subsequently, a combination of different fuel and equivalence ratios (representing a range of CO in the reformate gas) and system-operating parameters (steam-to-carbon ratio, stack temperature and fuel stoichiometry) are used to examine the system's performance.

During these simulations, the objective function was the stack electrical and cogeneration efficiency. It was shown that for a high electrical efficiency, a higher steam-to-carbon ratio and a high hydrogen stoichiometry are desired. In addition, for maximising the cogeneration efficiency, a high hydrogen stoichiometry is suitable.

In Chapter 5, the micro-cogeneration model is used to select the operating point, taking into account the technical requirements set for the system to compete well with traditional technologies. Four decision variables (equivalence ratio, fuel flow rate, current density and fuel utilisation) were considered for examining the system output objectives. Simulations of the model show that to meet the performance targets set by the DOE for fuel cell systems in the 1-5 kW_e range, an operating voltage of 0.54V, fuel utilisation of 76%, fuel flow rate of $0.133 \, \mathrm{kg} \, \mathrm{h}^{-1}$, combustion temperature of $960 \, \mathrm{K}$ and steam-carbon ratio of 3.5 present the optimal operating conditions.

An application of the micro-cogeneration system model to evaluate its operation within a South African domestic energy demand context was presented in Chapter 6. Three operating strategies, namely continuous-output, constant-output and restricted-time running mode were utilised to evaluate (i) the interaction between the system and utility grid; (ii) the environmental performance of introducing the micro-cogeneration system; and (iii) the economic benefits of introducing the micro-cogeneration system. Overall, the continuous-output mode was shown to cover most of the household's electrical need of more than 90%, while the constant-output and restricted-time operating covered up to 83.4% and 63.2%, respectively. The restricted-time operating mode appeared to be the most environmentally friendly, as it led to the highest carbon savings of up to 62.4%. Whilst all the operating modes resulted in payback periods that fall within the life-time of the fuel cell stack, the continuous operating mode showed to be most economical as it resulted in the lowest payback period of 8.4 years.

7.2   Recommendations

- The models developed in this work have been able to define a set of operating and design points that best describe the system's performance. The models can be

further utilised in a systematic optimisation to explore the design space to find a unique set of parameters that would inform the best performance of the system.

- Methane-steam reforming was selected as the hydrogen-production method in this work. There is a trend to move towards green hydrogen production and, as such, an evaluation of a cogeneration system with a renewable hydrogen-production method is recommended.

- The models can be further developed to include the degradation characteristics of the system's components (fuel cell stack, fuel processor and power conditioning efficiency) and to evaluate the long-term thermodynamic, environmental and economic performance of the cogeneration system.

References

Adam, A., Fraga, E. S. & Brett, D. J. L. 2013. Modelling and optimisation in terms of CO_2 emissions of a solid oxide fuel cell based micro-CHP system in a four bedroom house in London. *Energy Procedia*, **42**, 201–209.

Andreasen, S. J. & Kær, S. K. 2008. Modelling and evaluation of heating strategies for high temperature polymer electrolyte membrane fuel cell stacks. *International Journal of Hydrogen Energy*, **33**(17), 4655–4664.

Andújar, J. M. & Segura, F. 2009. Fuel cells: History and updating. A walk along two centuries. *Renewable and Sustainable Energy Reviews*, **13**(9), 2309–2322.

Ang, S. M. C., Brett, D. J. L. & Fraga, E. S. 2010. A multi-objective optimisation model for a general polymer electrolyte membrane fuel cell system. *Journal of Power Sources*, **195**(9), 2754–2763.

Ang, S. M. C., Brett, D. J. L., Staffell, I., Hawkes, A. D., Fraga, E. S., Samsatli, N. J. & Brandon, N. P. 2012. Design of fuel-cell micro-cogeneration systems through modeling and optimization. *Wiley Interdisciplinary Reviews: Energy and Environment*, **1**(2), 181–193.

Ang, S. M. C., Fraga, E. S., Brandon, N. P., Samsatli, N. J. & Brett, D. J. L. 2011. Fuel cell systems optimisation - methods and strategies. *International Journal of Hydrogen Energy*, **36**(22), 14678–14703.

Angrisani, G., Roselli, C. & Sasso, M. 2012. Distributed microtrigeneration systems. *Progress in Energy and Combustion Science*, **38**(4), 502–521.

Arsalis, A., Kær, S. K. & Nielsen, M. P. 2015. Modeling and optimization of a heat-pump-assisted high temperature proton exchange membrane fuel cell micro-combined-heat-and-power system for residential applications. *Applied Energy*, **147**, 569–581.

Arsalis, A., Nielsen, M. P. & Kær, S. K. 2011*a*. Modeling and off-design performance of a 1 kWe HT-PEMFC (high temperature-proton exchange membrane fuel cell)-based residential micro-CHP (combined-heat-and-power) system for Danish single-family households. *Energy*, **36**(2), 993–1002.

Arsalis, A., Nielsen, M. P. & Kær, S. K. 2011*b*. Modeling and parametric study of a 1kWe HT-PEMFC-based residential micro-CHP system. *International Journal of Hydrogen Energy*, **36**(8), 5010–5020.

Arsalis, A., Nielsen, M. P. & Kær, S. K. 2012*a*. Modeling and optimization of a 1kWe HT-PEMFC-based micro-CHP residential system. *International Journal of Hydrogen Energy*, **37**(3), 2470–2481.

Arsalis, A., Nielsen, M. P. & Kær, S. K. 2012*b*. Modeling and simulation of a 100kWe HT-PEMFC subsystem integrated with an absorption chiller subsystem. *International Journal of Hydrogen Energy*, **37**(18), 13484–13490.

Arsalis, A., Nielsen, M. P. & Kær, S. K. 2013. Optimization of a high temperature PEMFC micro-CHP system by formulation and application of a process integration methodology. *Fuel Cells*, **13**(2), 238–248.

Asl, S. M., Rowshanzamir, S. & Eikani, M. H. 2010. Modelling and simulation of the steady-state and dynamic behaviour of a PEM fuel cell. *Energy*, **35**(4), 1633–1646.

Authayanun, S., Arpornwichanop, A., Paengjuntuek, W. & Assabumrungrat, S. 2010. Thermodynamic study of hydrogen production from crude glycerol autothermal reforming for fuel cell applications. *International Journal of Hydrogen Energy*, **35**(13), 6617–6623.

Authayanun, S., Mamlouk, M. & Arpornwichanop, A. 2012. Maximizing the efficiency of a HT-PEMFC system integrated with glycerol reformer. *International Journal of Hydrogen Energy*, **37**(8), 6808–6817.

Authayanun, S., Mamlouk, M., Scott, K. & Arpornwichanop, A. 2013*a*. Comparison of high-temperature and low-temperature polymer electrolyte membrane fuel cell systems with glycerol reforming process for stationary applications. *Applied Energy*, **109**, 192–201.

Authayanun, S., Wiyaratn, W., Assabumrungrat, S. & Arpornwichanop, A. 2013*b*. Theoretical analysis of a glycerol reforming and high-temperature PEMFC integrated system: hydrogen production and system efficiency. *Fuel*, **105**, 345–352.

Avasarala, B. & Haldar, P. 2013. Durability and degradation mechanism of titanium nitride based electrocatalysts for PEM (proton exchange membrane) fuel cell applications. *Energy*, **57**, 545 – 553.

Baek, S. M., Yu, S. H., Nam, J. H. & Kim, C.-J. 2011. A numerical study on uniform cooling of large-scale PEMFCs with different coolant flow field designs. *Applied Thermal Engineering*, **31**(8), 1427–1434.

Balat, H. & Kirtay, E. 2010. Hydrogen from biomass - present scenario and future prospects. *International Journal of Hydrogen Energy*, **35**(14), 7416–7426.

Barbir, F. 2012. *PEM Fuel Cells: Theory and Practice*. 2nd edn. Academic Press. California.

Barelli, L., Bidini, G., Gallorini, F. & Ottaviano, A. 2011. Analysis of the operating conditions influence on PEM fuel cell performances by means of a novel semi-empirical model. *International Journal of Hydrogen Energy*, **36**(16), 10434–10442.

Beausoleil-Morrison, I. & Lombardi, K. 2009. The calibration of a model for simulating the thermal and electrical performance of a 2.8 kW_{AC} solid-oxide fuel cell micro-cogeneration device. *Journal of Power Sources*, **186**(1), 67 – 79.

Bergmann, A., Gerteisen, D. & Kurz, T. 2010. Modelling of CO poisoning and its dynamics in HTPEM fuel cells. *Fuel Cells*, **10**(2), 278–287.

Bezmalinović, D., Strahl, S., Roda, V. & Husar, A. 2014. Water transport study in a high temperature proton exchange membrane fuel cell stack. *International Journal of Hydrogen Energy*, **39**(20), 10627–10640.

Blanchette, S. 2008. A hydrogen economy and its impact on the world as we know it. *Energy Policy*, **36**(2), 522–530.

Bolat, P. & Thiel, C. 2014. Hydrogen supply chain architecture for bottom-up energy systems models. Part 2: Techno-economic inputs for hydrogen production pathways. *International Journal of Hydrogen Energy*, **39**(17), 8898–8925.

Boukhanouf, R. 2011. Small combined heat and power (CHP) systems for commercial buildings and institutions. *in* R. Beith, ed., 'Small and Micro Combined Heat and Power (CHP) Systems'. Woodhead Publishing Series in Energy. Woodhead Publishing. pp. 365 – 394.

Breeze, P. 2014. *Power Generation Technologies (Second Edition)*. Newnes.

Briguglio, N., Ferraro, M., Brunaccini, G. & Antonucci, V. 2011. Evaluation of a low temperature fuel cell system for residential CHP. *International Journal of Hydrogen Energy*, **36**(13), 8023–8029.

Brown, L. C., Besenbruch, G. E., Schultz, K. R., Showalter, S. K., Marshall, A. C., Pickard, P. S. & Funk, J. F. 2002. High efficiency generation of hydrogen fuels using thermochemical cycles and nuclear power. *in* 'American Institution of Chemical Engineers (AIChE) Spring Meeting'. New Orleans, March 1014, 2002.

Bujlo, P., Pasupathi, S., Ulleberg, O., Scholta, J., Nomnqa, M. V., Rabiu, A. & Pollet, B. G. 2013. Validation of an externally oil-cooled 1kwel ht-pemfc stack operating at various experimentalconditions. *International Journal of Hydrogen Energy*, **38**(23), 9847–9855.

Candusso, D., Harel, F., De Bernardinis, A., François, X., Péra, M. C., Hissel, D., Schott, P., Coquery, G. & Kauffmann, J. M. 2006. Characterisation and modelling of a 5kW PEMFC for transportation applications. *International Journal of Hydrogen Energy*, **31**(8), 1019–1030.

Cant, N. W., Hicks, P. C. & Lennon, B. S. 1978. Steady-state oxidation of carbon monoxide over supported noble metals with particular reference to platinum. *Journal of Catalysis*, **54**(3), 372–383.

Carter, D., Ryan, M. & Wing, J. 2012. The fuel cell industry review 2012. Technical report. Fuel Cell Today.

Chamra, L. M. & Mago, P. J. 2007. Micro-CHP power generation for residential and small commercial buildings. *Electric Power Research Trends*, pp. 47–101.

Chandan, A., Hattenberger, M., El-kharouf, A., Du, S., Dhir, A., Self, V., Pollet, B. G., Ingram, A. & Bujalski, W. 2013. High temperature (HT) polymer electrolyte membrane fuel cells (PEMFC) - a review. *Journal of Power Sources*, **231**, 264–278.

Chanpeng, W. & Khunatorn, Y. 2011. The effect of the input load current changed to a 1.2kW PEMFC performance. *Energy Procedia*, **9**, 316–325.

Chaubey, R., Sahu, S., James, O. O. & Maity, S. 2013. A review on development of industrial processes and emerging techniques for production of hydrogen from renewable and sustainable sources. *Renewable and Sustainable Energy Reviews*, **23**, 443–462.

Cheddie, D. F. & Munroe, N. D. 2005. Review and comparison of approaches to proton exchange membrane fuel cell modelling. *Journal of Power Sources*, **147**(1), 72–84.

Cheddie, D. F. & Munroe, N. D. 2006. Mathematical model of a PEMFC using a PBI membrane. *Energy Conservation and Management*, **47**(11), 1490–1504.

Cheddie, D. F. & Munroe, N. D. 2007. A two-phase model of an intermediate temperature PEM fuel cell. *International Journal of Hydrogen Energy*, **32**(7), 832–841.

Chen, J., Siegel, J. B., Stefanopoulou, A. G. & Waldecker, J. R. 2013. Optimization of purge cycle for dead-ended anode fuel cell operation. *International Journal of Hydrogen Energy*, **38**(12), 5092–5105.

Chippar, P. & Ju, H. 2013. Numerical modeling and investigation of gas crossover effects in high temperature proton exchange membrane (PEM) fuel cells. *International Journal of Hydrogen Energy*, **38**(18), 7704–7714.

Chippar, P., Oh, K., Kim, D., Hong, T.-W., Kim, W. & Ju, H. 2013. Coupled mechanical stress and multi-dimensional CFD analysis for high temperature proton exchange membrane fuel cells (HT-PEMFCs). *International Journal of Hydrogen Energy*, **38**(18), 7715–7724.

Choi, J., Kim, Y.-H., Lee, Y., Lee, K.-J. & Kim, Y. 2008. Numerical analysis on the performance of cooling plates in a PEFC. *Journal of Mechanical Science and Technology*, **22**(7), 1417–1425.

Conroy, G., Duffy, A. & Ayompe, L. M. 2013. Validated dynamic energy model for a stirling engine CHP unit using field trial data from a domestic dwelling. *Energy and Buildings*, **62**, 18–26.

Crawley, G. 2006. Alkaline fuel cells (AFC). Technical report. Fuel Cell Today.

Crawley, G. 2007. Direct methanol fuel cells (DMFC). Technical report. Fuel Cell Today.

Dara 2012. 'Climate vulnerability monitor: A guide to the cold calculus of a hot planet'. [Online].
URL: *http://daraint.org/climate-vulnerability-monitor/climate-vulnerability-initiative/;2012 Accessed [2013, September 18]*

Darrow, K., Tidball, R., Wang, J. & Hampson, A. 2014. Catalog of CHP technologies. Technical report. U.S. Environmental Protection Agency.

Davis, S., Prier, M., Cohen, B., Hughes, A. & Nyatsanza, K. 2011. Water heating in middle to high income households. Technical report. University of Cape Town.

De Melo Furtado, J., Gatti, G. C., Serra, E. T. & Anibal de Almeida, S. C. 2010. Performance analysis of a 5kW PEMFC with a natural gas reformer. *International Journal of Hydrogen Energy*, **35**(18), 9990–9995.

Dhar, H. P., Christner, L. G., Kush, A. K. & Maru, H. C. 1986. Performance study of a fuel cell Pt-on-C anode in presence of CO and CO2 and calculation of adsorption parameters for CO poisoning. *Journal of the Electrochemical Society*, **133**(8), 1574–1582.

Di Bona, D., Jannelli, E., Minutillo, M. & Perna, A. 2011. Investigations on the behaviour of 2 kW natural gas fuel processor. *International Journal of Hydrogen Energy*, **36**(13), 7763–7770.

Dincer, I. & Acar, C. 2015. Review and evaluation of hydrogen production methods for better sustainability. *International Journal of Hydrogen Energy*, **40**(34), 11094–11111.

Dincer, I. & Rosen, M. A. 2011. Sustainability aspects of hydrogen and fuel cell systems. *Energy for Sustainable Development*, **15**(2), 137–146.

Doherty, W., Reynolds, A. & Kennedy, D. 2010. Computer simulation of a biomass gasification-solid oxide fuel cell power system using Aspen Plus. *Energy*, **35**(12), 4545–4555.

Donadel, C. B., Fardin, J. F. & Encarnaçã, L. F. 2015. Electrical distribution network operation with a presence of distributed generation units in a Pre Smart Grid environment using a clustering-based methodology. *Energy Systems*, **6**(4), 455–477.

Dutta, S. 2014. A review on production, storage of hydrogen and its utilization as an energy resource. *Journal of Industrial and Engineering Chemistry*, **20**(4), 1148–1156.

El-kharouf, A. & Pollet, B. G. 2012. *Gas Diffusion Media and their Degradation*. Academic Press. Boston. pp. 215–247.

Elmer, T., Worall, M., Wu, S. & Riffat, S. B. 2015. Fuel cell technology for domestic built environment applications: State of-the-art review. *Renewable and Sustainable Energy Reviews*, **42**, 913–931.

Ersöz, A. & Sayar, A. 2015. A process simulation study of a newly designed fuel processing system for a high temperature PEM fuel cell unit. *International Journal of Hydrogen Energy*, **40**(42), 14469–14482.

Fong, K. F. & Lee, C. K. 2016. System analysis and appraisal of SOFC-primed micro cogeneration for residential application in subtropical region. *Energy and Buildings*, **128**, 819–826.

Frangopoulos, C. A. & Nakos, L. G. 2006. Development of a model for thermoeconomic design and operation optimization of a PEM fuel cell system. *Energy*, **31**(10), 1501–1519.

Frey, T. & Linardi, M. 2004. Effects of membrane electrode assembly preparation on the polymer electrolyte membrane fuel cell performance. *Electrochimica Acta*, **50**(1), 99–105.

Gardemann, U., Steffen, M. & Heinzel, A. 2014. Design and demonstration of an ethanol fuel processor for HT-PEM fuel cell applications. *International Journal of Hydrogen Energy*, **39**(31), 18135–18145.

Ghadimi, P., Kara, S. & Kornfeld, B. 2014. The optimal selection of on-site CHP systems through integrated sizing and operational strategy. *Applied Energy*, **126**, 38 – 46.

Guy, R. & Sykes, B. 2007. Micro-CHP Accelerator - interim report. Technical report. Carbon Trust.

Haraldsson, K. & Wipke, K. 2004. Evaluating PEM fuel cell system models. *Journal of Power Sources*, **126**(1), 88–97.

Harrison, J. & On, E. 2011. Stirling engine systems for small and micro combined heat and power (CHP) applications. *in* R. Beith, ed., 'Small and Micro Combined Heat and Power (CHP) Systems'. Woodhead Publishing Series in Energy. Woodhead Publishing. pp. 179 – 205.

Hawkes, A. D., Brett, D. & Brandon, N. P. 2009*b*. Fuel cell micro-CHP techno-economics: Part 1 - model concept and formulation. *International Journal of Hydrogen Energy*, **34**(23), 9545–9557.

Hawkes, A., Staffell, I., Brett, D. & Brandon, N. 2009*a*. Fuel cells for micro-combined heat and power generation. *Energy & Environmental Science*, **2**(7), 729–744.

Holladay, J. D., Hu, J., King, D. L. & Wang, Y. 2009. An overview of hydrogen production technologies. *Catalysis Today*, **139**(4), 244–260.

Jalani, N. H., Ramani, M., Ohlsson, K., Buelte, S., Pacifico, G., Pollard, R., Staudt, R. & Datta, R. 2006. Performance analysis and impedance spectral signatures of high temperature PBI-phosphoric acid gel membrane fuel cells. *Journal of Power Sources*, **160**(2), 1096–1103.

Jannelli, E., Minutillo, M. & Perna, A. 2013. Analyzing microcogeneration systems based on LT-PEMFC and HT-PEMFC by energy balances. *Applied Energy*, **108**, 82–91.

Jia, F., Guo, L. & Liu, H. 2015. A study on current overshoot during start-ups and optimal start-up strategy of proton exchange membrane fuel cells. *International Journal of Hydrogen Energy*, **40**(24), 7754–7761.

Jiao, K., Alaefour, I. E. & Li, X. 2011. Three-dimensional non-isothermal modeling of carbon monoxide poisoning in high temperature proton exchange membrane fuel cells with phosphoric acid doped polybenzimidazole membranes. *Fuel*, **90**(2), 568–582.

Jiao, K. & Li, X. 2010. Athree-dimensionalnon-isothermal model of high temperature proton exchange membrane fuel cells with phosphoric acid doped polybenzimidazole-membranes. *Fuel Cells*, **10**(3), 351–362.

Jiao, K., Zhou, Y., Du, Q., Yin, Y., Yu, S. & Li, X. 2013. Numerical simulations of carbon monoxide poisoning in high temperature proton exchange membrane fuel cells with various flow channel designs. *Applied Energy*, **104**, 21–41.

Jung, U. H., Kim, W., Koo, K. Y. & Yoon, W. L. 2014. Genuine design of compact natural gas fuel processor for 1-kWe class residential proton exchange membrane fuel cell systems. *Fuel Processing Technology*, **121**, 32–37.

Kalinci, Y., Hepbasli, A. & Dincer, I. 2009. Biomass-based hydrogen production:a review and analysis. *International Journal of Hydrogen Energy*, **34**(21), 8799–8817.

Kazempoor, P., Dorer, V. & Ommi, F. 2009. Evaluation of hydrogen and methane-fuelled solid oxide fuel cell systems for residential applications: system design alternative and parameter study. *International Journal of Hydrogen Energy*, **34**(20), 8630–8644.

Kerr, T. M. 2008. CHP - the value of greater global investment. *Power Engineering International*, **16**(4), 38–44.

Kim, G.-Y., Mayor, J. R. & Ni, J. 2005. Parametric study of microreactor design for water gas shift reactor using an integrated reaction and heat exchange model. *Chemical Engineering Journal*, **110**(1), 1–10.

Kim, M., Kang, T., Kim, J. & Sohn, Y.-J. 2014. One-dimensional modeling and analysis for performance degradation of high temperature proton exchange membrane fuel cell using PA doped PBI membrane. *Solid State Ionics*, **262**, 319–323.

Kocha, S. S. 2011. Electrochemical degradation: Electrocatalyst and support durability. *Polymer Electrolyte Fuel Cell Degradation*, pp. 89–214.

Kolb, G. 2008. *Fuel Processing for Fuel Cells*. Wiley. Weinheim.

Kolb, G. 2013. Review: Microstructured reactors for distributed and renewable production of fuels and electrical energy. *Chemical Engineering and Processing: Process Intensification*, **65**(0), 1–44.

Korsgaard, A. R., Refshauge, R., Nielsen, M. P., Banga, M. & Kær, S. K. 2006. Experimental characterization and modeling of commercial polybenzimidazole-based MEA performance. *Journal of Power Sources*, **162**(1), 239–245.

Krumpelt, M., Krause, T. R., Carter, J. D., Kopasz, J. P. & Ahmed, S. 2002. Fuel processing for fuel cell systems in transportation and portable power applications. *Catalysis Today*, **77**(1), 3–16.

Kuhn, V., Klemeš, J. & Bulatov, I. 2008. MicroCHP: Overview of selected technologies, products and field test results. *Applied Thermal Engineering*, **28**(16), 2039–2048.

Kupecki, J. 2015. Off-design analysis of a micro-CHP unit with solid oxide fuel cells fed by DME. *International Journal of Hydrogen Energy*, **40**(35), 12009–12022.

Kvesić, M., Reimer, U., Froning, D., Lüke, L., Lehnert, W. & Stolten, D. 2012. 3D modeling of an HT-PEFC stack using reformate gas. *International Journal of Hydrogen Energy*, **37**(17), 12438–12450.

Lang, S., Kazdal, T. J., Kühl, F. & Hampe, M. J. 2015. Experimental investigation and numerical simulation of the electrolyte loss in a HT-PEM fuel cell. *International Journal of Hydrogen Energy*, **40**(2), 1163–1172.

Larminie, J. & Dicks, A. 2003. *Fuel cell systems explained*. 2nd edn. John Wiley & Sons Ltd.

Lazarou, S., Vita, V., Karampelas, P. & , Ekonomou, L. 2013. A power system simulation platform for planning and evaluating distributed generation systems based on GIS. *Energy Systems*, **4**(4), 379–391.

Lee, C. B., Cho, S. H., Lee, D. W., Hwang, K. R., Park, J. S. & Kim, S. H. 2014. Combination of preferential CO oxidation and methanation in hybrid MCR (microchannel reactor) for CO clean-up. *Energy*, **78**, 421–425.

Lee, H., Bush, J., Hwang, Y. & Radermacher, R. 2013. Modeling of micro-CHP (combined heat and power) unit and evaluation of system performance in building application in United States. *Energy*, **58**, 364–375.

Li, Q., He, R., Gao, J. A., Jensen, J. O. & Bjerrum, N. J. 2003. The CO poisoning effect in PEMFCs operational at temperatures up to 200 °C. *Journal of the Electrochemical Society,,* **150**(12), A1599–A1605.

Li, X. & Sabir, I. 2005. Review of bipolar plates in PEM fuel cells: Flow-field designs. *International Journal of Hydrogen Energy*, **30**(4), 359–371.

Liso, V., Olesen, A. C., Nielsen, M. P. & Kær, S. K. 2011. Performance comparison between partial oxidation and methane steam reforming processes for solid oxide fuel cell (SOFC) micro combined heat and power (CHP) system. *Energy*, **36**(7), 4216–4226.

Lobato, J., Cañizares, P., Rodrigo, M. A., Pinar, F. J., Mena, E. & Úbeda, D. 2010. Three-dimensional model of a 50cm2 high temperature PEM fuel cell. Study of the flow channel geometry influence. *International Journal of Hydrogen Energy*, **35**(11), 5510–5520.

Maghanki, M. M., Ghobadian, B., Najafi, G. & Galogah, R. J. 2013. Micro combined heat and power (MCHP) technologies and applications. *Renewable and Sustainable Energy Reviews*, **28**, 510–524.

Marbán, G. & Valdés-Solís, T. 2007. Towards the hydrogen economy?. *International Journal of Hydrogen Energy*, **32**(12), 1625–1637.

Maximini, M., Engelhardt, P., Brenner, M., Beckmann, F. & Moritz, O. 2014. Fast start-up of a diesel fuel processor for PEM fuel cells. *International Journal of Hydrogen Energy*, **39**(31), 18154–18163.

Meidanshahi, V. & Karimi, G. 2012. Dynamic modeling, optimization and control of power density in a PEMfuel cell. *Applied Energy*, **93**, 98–105.

Mikalsen, R. 2011. Internal combustion and reciprocating engine systems for small and micro combined heat and power (CHP) applications. *in* R. Beith, ed., 'Small and Micro Combined Heat and Power (CHP) Systems'. Woodhead Publishing Series in Energy. Woodhead Publishing. pp. 125 – 146.

Najafi, B., Mamaghani, A. H., Baricci, A. & Rinaldi, F. 2015*a*. Mathematical modelling and parametric study on a 30kWel high temperature PEM fuel cell based residential micro cogeneration plant. *International Journal of Hydrogen Energy*, **40**(3), 1569–1583.

Najafi, B., Mamaghani, A. H., Rinaldi, F. & Casalegno, A. 2015*b*. Long-term performance analysis of an HT-PEM fuel cell based micro-CHP system: Operational strategies. *Applied Energy*, **147**, 582–592.

Napoli, R., Gandiglio, M., Lanzini, A. & Santarelli, M. 2015. Techno-economic analysis of PEMFC and SOFC micro-CHP fuel cell systems for the residential sector. *Energy and Buildings*, **103**, 131–146.

Ngoh, S. K. & Njomo, D. 2012. An overview of hydrogen gas production from solar energy. *Renewable and Sustainable Energy Reviews*, **16**(9), 6782–6792.

Nissilä, M. E., Lay, C. H. & Puhakka, J. A. 2014. Dark fermentative hydrogen production from lignocellulosic hydrolyzates: a review. *Biomass and Bioenergy*, **67**(0), 145–159.

Oh, K., Jeong, G., Cho, E., Kim, W. & Ju, H. 2014. A CO poisoning model for high-temperature proton exchange membrane fuel cells comprising phosphoric acid-doped polybenzimidazole membranes. *International Journal of Hydrogen Energy*, **39**(36), 21915–21926.

Oh, K. & Ju, H. 2015. Temperature dependence of CO poisoning in high-temperature proton exchange membrane fuel cells with phosphoric acid-doped polybenzimidazole membranes. *International Journal of Hydrogen Energy*, **40**(24), 7743–7753.

Onovwiona, H. I. & Ugursal, V. I. 2006. Residential cogeneration systems: review of the current technology. *Renewable and Sustainable Energy Reviews*, **10**, 389–431.

Onovwiona, H. I., Ugursal, V. I. & Fung, A. S. 2007. Modeling of internal combustion engine based cogeneration systems for residential applications. *Applied Thermal Engineering*, **27**(5), 848–861.

Pade, L. L., Schröder, S. T., Münster, M., Birkl, C., Ropenus, S., Morthorst, P. E., Obé, E., Kötter, E., Huber, A., Costa, A. & Kroff, P. 2013. Policy schemes, operational strategies and system integration of residential co-generation fuel cells. *International Journal of Hydrogen Energy*, **38**(7), 3050–3063.

Park, J. & Min, K. 2012. A quasi-three-dimensional non-isothermal dynamic model of a high-temperature proton exchange membrane fuel cell. *Journal of Power Sources*, **216**, 152–161.

Park, J., Oh, H., Ha, T., Lee, Y. I. & Min, K. 2015. A review of the gas diffusion layer in proton exchange membrane fuel cells: durability and degradation. *Applied Energy*, **155**, 866–880.

Parthasarathy, P. & Narayanan, K. S. 2014. Hydrogen production from steam gasification of biomass: Influence of process parameters on hydrogen yield - a review. *Renewable Energy*, **66**, 570–579.

Pehnt, M., Cames, M., Fischer, C., Praetorius, B., Schneider, L. & Schumacher, K. 2006. *Micro Cogeneration: Towards Decentralized Energy Systems*. Springer.

Peng, J. & Lee, S. J. 2006. Numerical simulation of proton exchange membrane fuel cells at high operating temperature. *Journal of Power Sources*, **162**(2), 1182–1191.

Perna, A., Cicconardi, S. P. & Cozzolino, R. 2011. Performance evaluation of a fuel processing system based on membrane reactors technology integrated with a PEMFC stack. *International Journal of Hydrogen Energy*, **36**(16), 9906–9915.

Petrone, R., Hissel, D., Péra, M. C., Chamagne, D. & Gouriveau, R. 2015. Accelerated stress test procedures for PEM fuel cells under actual load constraints: State-of-art and proposals. *International Journal of Hydrogen Energy*, **40**(36), 12489–12505.

Pohl, E., Maximini, M., Bauschulte, A., Vom Schloß, J. & Hermanns, R. T. E. 2015. Degradation modeling of high temperature proton exchange membrane fuel cells using dual time scale simulation. *Journal of Power Sources*, **275**, 777–784.

Pollet, B. G., Pasupathi, S., Swart, G., Mouton, K., Lototskyy, M., Williams, M., Bujlo, P., Ji, S., Bladergroen, B. J. & Linkov, V. 2014. Hydrogen South Africa (*HySA*) Systems Competence Centre: mission, objectives, technological achievements and breakthroughs. *International Journal of Hydrogen Energy*, **39**(8), 3577–3596.

PSE (Process Systems Enterprise). n.d.. 'gPROMS ModelBuilder v3.6'. [Online]. **URL:** *http://www.psenterprise.com/ [Accessed 2015, July 15]*

Qi, Z. & Buelte, S. 2006. Effect of open circuit voltage on performance and degradation of high temperature PBI-H$_3$PO$_4$ fuel cells. *Journal of Power Sources*, **161**(2), 1126–1132.

Qingfeng, L., Hjuler, H. A. & Bjerrum, N. J. 2001. Phosphoric acid doped polybenzimidazole membranes: physiochemical characterization and fuel cell applications. *Journal of Applied Electrochemistry*, **31**(7), 773–779.

Rabiu, A. M., Dlangamandla, N. & Ulleberg, O. 2012. Novel heat integration in a methane reformer and high temperature pem fuel cell-based mCHP system. *APCBEE Procedia*, **3**, 17–22.

Rasheed, A. R. K. & Chan, S. H. 2015. Transient carbon monoxide poisoning kinetics during warm-up period of a high-temperature PEMFC: Physical model and parametric study. *Applied Energy*, **140**, 44–51.

Rasheed, A. R. K., Ehteshami, S. M. M. & Chan, S. H. 2014. Analytical modelling of boiling phase change phenomenon in high-temperature proton exchange membrane fuel cells during warm-up process. *International Journal of Hydrogen Energy*, **39**(5), 2246–2260.

Reddy, E. H. & Jayanti, S. 2012. Thermal coupling studies of a high temperature proton exchange membrane fuel cell stack and a metal hydride hydrogen storage system. *Energy Procedia*, **29**, 254–264.

Reddy, E. H., Jayanti, S. & Monder, D. S. 2014. Thermal management of high temperature polymer electrolyte membrane fuel cell stacks in the power range of 1-10kWe. *International Journal of Hydrogen Energy*, **39**(35), 20127–20138.

Ren, H. & Gao, W. 2010. Economic and environmental evaluation of micro CHP systems with different operating modes for residential buildings in Japan. *Energy and Buildings*, **42**(6), 853–861.

Romero-Pascual, E. & Soler, J. 2014. g. *International Journal of Hydrogen Energy*, **39**(8), 4053–4059.

Rosato, A. & Sibilio, S. 2013. Performance assessment of a micro-cogeneration system under realistic operating conditions. *Energy Conversion and Management*, **70**(0), 149–162.

Rosen, M. A. 2010. Advances in hydrogen production by thermochemical water decomposition: a review. *Energy*, **35**(2), 1068–1076.

Salomov, U. R., Chiavazzo, E. & Asinari, P. 2015. Gas-dynamic and electro-chemical optimization of catalyst layers in high temperature polymeric electrolyte membrane fuel cells. *International Journal of Hydrogen Energy*, **40**(15), 5425–5431.

Samsun, R. C., Krupp, C., Tschauder, A., Peters, R. & Stolten, D. 2016. Electrical start-up for diesel fuel processing in a fuel-cell-based auxiliary power unit. *Journal of Power Sources*, **302**, 315–323.

Samsun, R. C., Pasel, J., Janßen, H., Lehnert, W., Peters, R. & Stolten, D. 2014. Design and test of a 5kWe high-temperature polymer electrolyte fuel cell system operated with diesel and kerosene. *Applied Energy*, **114**, 238–249.

Saxena, R. C., Seal, D., Kumar, S. & Goyal, H. B. 2008. Thermo-chemical routes for hydrogen rich gas from biomass: a review. *Renewable and Sustainable Energy Reviews*, **12**(7), 1909–1927.

Saygili, Y., Kincal, S. & Eroglu, I. 2015. Development and modeling for process control purposes in PEMs. *International Journal of Hydrogen Energy*, **40**(24), 7886–7894.

Schefer, R. W. 1982. Catalyzed combustion of H2/air mixtures in a flat plate boundary layer: II. Numerical model. *Combustion and Flame*, **45**, 171–190.

Scott, K. & Mamlouk, M. 2009. A cell voltage equation for an intermediate temperature proton exchange membrane fuel cell. *International Journal of Hydrogen Energy*, **34**(22), 9195–9202.

Scott, K., Pilditch, S. & Mamlouk, M. 2007. Modelling and experimental validation of a high temperature polymer electrolyte fuel cell. *Journal of Applied Electrochemistry*, **37**(11), 1245–1259.

Shah, A. A., Luo, K. H., Ralph, T. R. & Walsh, F. C. 2011. Recent trends and developments in polymer electrolyte membrane fuel cell modelling. *Electrochimica Acta*, **56**(11), 3731–3757.

Shamardina, O., Chertovich, A., Kulikovsky, A. & Khokhlov, A. 2010. A simple model of a high temperature PEM fuel cell. *International Journal of Hydrogen Energy*, **35**(18), 9954–9962.

Shamardina, O., Kondratenko, M. S., Chertovich, A. V. & Kulikovsky, A. A. 2014. A simple transient model for a high temperature PEM fuel cell impedance. *International Journal of Hydrogen Energy*, **39**(5), 2224–2235.

Shaneb, O. A., Coates, G. & Taylor, P. C. 2011. Sizing of residential mCHP systems. *Energy and Buildings*, **43**(8), 1991–2001.

Siegel, C. 2008. Review of computational heat and mass transfer modeling in polymer-electrolyte-membrane (PEM) fuel cells. *Energy*, **33**(9), 1331–1352.

Singh, L. & Wahid, Z. A. 2015. Methods for enhancing bio-hydrogen production from biological process: a review. *Journal of Industrial and Engineering Chemistry*, **21**(0), 70–80.

Smith, A. D., Mago, P. J. & Fumo, N. 2013. Benefits of thermal energy storage option combined with CHP system for different commercial building types. *Sustainable Energy Technologies and Assessments*, **1**, 3–12.

Sohn, Y.-J., Kim, M., Yang, T.-H. & Kim, K. 2011. Numerical analysis of convective and diffusive fuel transports in high-temperature proton-exchange membrane fuel cells. *International Journal of Hydrogen Energy*, **36**(23), 15273–15282.

Sonar, D., Soni, S. L. & Sharma, D. 2014. Micro-trigeneration for energy sustainability: Technologies, tools andtrends. *Applied Thermal Engineering*, **71**(2), 790–796.

Song, X., Williams, W. R., Schmidt, L. D. & Aris, R. 1991. Ignition and extinction of homogeneous-heterogeneous combustion: CH4 and C3H8 oxidation on PT. *Symposium (International) on Combustion*, **23**(1), 1129–1137.

Sousa, T., Mamlouk, M. & Scott, K. 2010*a*. A dynamic non-isothermal model of a laboratory intermediate temperature fuel cell using PBI doped phosphoric acid membranes. *International Journal of Hydrogen Energy*, **35**(21), 12065–12080.

Sousa, T., Mamlouk, M. & Scott, K. 2010*b*. An isothermal model of a laboratory intermediate temperature fuel cell using PBI doped phosphoric acid membranes. *Chemical Engineering Science*, **65**(8), 2513–2530.

Spalding-Fecher, R. 2011. What is the carbon emission factor for the South African electricity grid?. *Journal of Energy in Southern Africa*, **22**(4), 8–14.

Spendelow, J., Marcinkoski, J. & Papageorgopoulos, D. 2012. Micro CHP fuel cell system targets. Technical report. US Department of Energy (DOE).

Spiegel, C. 2008. *PEM fuel cell modeling and simulation using Matlab*. ELSEVIER.

Staffell, I. 2010. FUEL CELLS FOR DOMESTIC HEAT AND POWER: ARE THEY WORTH IT?. PhD thesis. University of Birmingham.

Staffell, I. 2015. Zero carbon infinite COP heat from fuel cell CHP. *Applied Energy*, **147**, 373 – 385.

Staffell, I. & Green, R. 2013. The cost of domestic fuel cell micro-CHP systems. *International Journal of Hydrogen Energy*, **38**(2), 1088–1102.

Su, A., Ferng, Y. M. & Shih, J. C. 2010. CFD investigating the effects of different operating conditions on the performance and the characteristics of a high-temperature PEMFC. *Energy*, **35**(1), 16–27.

Sun, H., Xie, C., Chen, H. & Almheiri, S. 2015. A numerical study on the effects of temperature and mass transfer in high temperature PEM fuel cells with ab-PBI membrane. *Applied Energy*, **160**, 937–944.

Swan, L. G. & Ugursal, V. I. 2009. Modeling of end-use energy consumption in the residential sector: a review of modeling techniques. *Renewable and Sustainable Energy Reviews*, **13**(8), 1819–1835.

Szklo, A. S., Soares, J. B. & Tolmasquim, M. T. 2004. Energy consumption indicators and CHP technical potential in the Brazilian hospital sector. *Energy Conversion and Management*, **45**(13-14), 2075 – 2091.

Taherian, R. 2014. A review of composite and metallic bipolar plates in proton exchange membrane fuel cell: materials, fabrication, and material selection. *Journal of Power Sources*, **265**, 370–390.

Tanaka, H., Suzuki, A., Yamamoto, K., Yamamoto, I., Yoshimura, M. & Togawa, K. 2011. 'NEW ECOWILL - a new generation gas engine micro-chp'. International Gas Union Research Conference.

Tanksale, A., Beltramini, J. N. & Lu, G. M. 2010. A review of catalytic hydrogen production processes from biomass. *Renewable and Sustainable Energy Reviews*, **14**(1), 166–182.

Tawfik, H., Hung, Y. & Mahajan, D. 2007. Metal bipolar plates for PEM fuel cell: a review. *Journal of Power Sources*, **163**(2), 755–767.

Thomas, B. 2008. Benchmark testing of Micro-CHP units. *Applied Thermal Engineering*, **28**(16), 2049–2054.

Tiss, F., Chouikh, R. & Guizani, A. 2013. Dynamic modeling of a PEM fuel cell with temperature effects. *International Journal of Hydrogen Energy*, **38**(20), 8532–8541.

Todd, B. & Young, J. B. 2002. Thermodynamic and transport properties of gases for use in solid oxide fuel cell modelling. *Journal of Power Sources*, **110**(1), 186–200.
ΩÚbeda *et al.*

Úbeda, D., Pinar, F. J., Cañizares, P., Rodrigo, M. A. & Lobato, J. 2012. An easy parameter estimation procedure for modeling a HT-PEMFC. *International Journal of Hydrogen Energy*, **37**(15), 11308–11320.

Udomsirichakorn, J. & Salam, P. A. 2014. Review of hydrogen-enriched gas production from steam gasification of biomass: the prospect of CaO-based chemical looping gasification. *Renewable and Sustainable Energy Reviews*, **30**, 565–579.

UNEP (United Nations Environmental Programme) 2012. 'Climate change'. [Online].
URL: *http://www.unep.org/climatechange/Introduction.aspx;2012. Accessed [2013, November 10]*

Upreti, G., Greene, D. L., Duleep, K. G. & Sawhney, R. 2012. Fuel cells for non-automotive uses: status and prospects. *International Journal of Hydrogen Energy*, **37**(8), 6339–6348.

Varsano, F., Murmura, M. A., Brunetti, B., Padella, F., La Barbera, A., Alvani, C. & Annesini, M. C. 2014. Hydrogen production by water splitting on manganese ferrite-sodium carbonate mixture: Feasibility tests in a packed bed solar reactor-receiver. *International Journal of Hydrogen Energy*, **39**(36), 20920–20929.

Veerapen, J. & Beerepoot, M. 2011. Co-generation and renewables: Solutions for a low-carbon energy future. Technical report. The International Energy Agency.

Wang, M., Wang, Z., Gong, X. & Guo, Z. 2014*a*. The intensification technologies to water electrolysis for hydrogen production: a review. *Renewable and Sustainable Energy Reviews*, **29**, 573–588.

Wang, Y., Sauer, D. U., Koehne, S. & Ersoez, A. 2014*b*. Dynamic modeling of high temperature PEM fuel cell start-up process. *International Journal of Hydrogen Energy*, **39**(33), 19067–19078.

Xiao, L., Zhang, H., Jana, T., Scanlon, E., Chen, R., Choe, E. W., Ramanathan, L. S., Yu, S. & Benicewicz, B. C. 2005. Synthesis and characterization of pyridine-based polybenzimidazoles for high temperature polymer electrolyte membrane fuel cell applications. *Fuel Cells*, **5**(2), 287–295.

Xu, J. & Froment, G. F. 1989. Methane steam reforming, methanation and water-gas shift: 1. intrinsic kinetics. *AIChe Journal*, **35**(1), 88–96.

Yin, Y., Wang, J., Yang, X., Du, Q., Fang, J. & Jiao, K. 2014. Modeling of high temperature proton exchange membrane fuel cells with novel sulfonated polybenzimidazole membranes. *International Journal of Hydrogen Energy*, **39**(25), 13671–13680.

Yu, S. & Jung, D. 2010. A study of operation strategy of cooling module with dynamic fuel cell system model for transportation application. *Renewable Energy*, **35**(11), 2525–2532.

Zamfirescu, C. & Dincer, I. 2014. Assessment of a new integrated solar energy system for hydrogen production. *Solar Energy*, **107**, 700–713.

Zhang, G. & Kandlikar, S. G. 2012. A critical review of cooling techniques in proton exchange membrane fuel cell stacks. *International Journal of Hydrogen Energy*, **37**(3), 2412–2429.

Zhang, J., Zhang, H., Wu, J. & Zhang, J. 2013. *Pem Fuel Cell Testing and Diagnosis*. Elsevier. Amsterdam. chapter Chapter 10 - High-Temperature PEM Fuel Cells, pp. 243–282.

Ziogou, C., Voutetakis, S., Papadopoulou, S. & Georgiadis, M. C. 2011. Modeling, simulation and experimental validation of a PEM fuel cell system. *Computers & Chemical Engineering*, **35**(9), 1886–1900.

Zuliani, N. & Taccani, R. 2012. Microcogeneration system based on HTPEM fuel cell fueled with natural gas: performance analysis. *Applied Energy*, **97**, 802–808.